Reduced Order Controllers for Distributed Parameter Systems

Katie Allison Evans

Dissertation submitted to the Faculty of the
Virginia Polytechnic Institute and State University
in partial fulfillment of the requirements for the degree of

Doctor of Philosophy
in
Mathematics

Belinda B. King, Chair
Jeffrey T. Borggaard
John A. Burns
Terry L. Herdman
Robert C. Rogers
Lizette Zietsman

November 21, 2003
Blacksburg, Virginia

Keywords: Balanced Truncation, LQG Balancing, Cable Mass System, Klein-Gordon Equation, Euler-Bernoulli beam, Central Control Design

Reduced Order Controllers for Distributed Parameter Systems

Katie Allison Evans

(ABSTRACT)

Distributed parameter systems (DPS) are systems defined on infinite dimensional spaces. This includes problems governed by partial differential equations (PDEs) and delay differential equations. In order to numerically implement a controller for a physical system we often first approximate the PDE and the PDE controller using some finite dimensional scheme. However, control design at this level will typically give rise to controllers that are inherently large-scale. This presents a challenge since we are interested in the design of robust, real-time controllers for physical systems. Therefore, a reduction in the size of the model and/or controller must take place at some point. Traditional methods to obtain lower order controllers involve reducing the model from that for the PDE, and then applying a standard control design technique. One such model reduction technique is balanced truncation. However, it has been argued that this type of method may have an inherent weakness since there is a loss of physical information from the high order, PDE approximating model prior to control design. In an attempt to capture characteristics of the PDE controller before the reduction step, alternative techniques have been introduced that can be thought of as controller reduction methods as opposed to model reduction methods. One such technique is LQG balanced truncation. Only recently has theory for LQG balanced truncation been developed in the infinite dimensional setting. In this work, we numerically investigate the viability of LQG balanced truncation as a suitable means for designing low order, robust controllers for distributed parameter systems. We accomplish this by applying both balanced reduction techniques, coupled with LQG, MinMax and central control designs for the low order controllers, to the cable mass, Klein-Gordon, and Euler-Bernoulli beam PDE systems. All numerical results include a comparison of controller performance and robustness properties of the closed loop systems.

Dedication

To Mom,
With Love and Appreciation

Acknowledgements

To my advisor, Dr. Belinda B. King: Thank you for your endless patience, support, and enthusiasm. You have exposed me to much science about which I would have otherwise known nothing, and you have opened my eyes to possibilities I never imagined. Both have allowed me to learn about my interests, my aspirations, and myself. Thank you for the opportunities and for your friendship.

To my committee members: Whether it has been in a classroom, through research discussions, or both, I appreciate the impact each of you has had on my academic career. Thank you for your time and patience. On a personal note, I have not only gained an education, but also friendships. Thank you.

To my professors in the math department at Morehead State University: Thank you for helping me become involved in undergraduate research programs and encouraging me to attend graduate school.

To Eileen Shugart: Thank you for the preparation I received before entering the classroom, your continued support after I started teaching, and your friendship.

To my friends and family: Thank you for your support and understanding.

To Dot: Thank you for helping me keep my sanity. You are a treasure.

To Mom: Thank you for always being my biggest fan. The sacrifices you have made for me are immeasurable, and I am deeply grateful. Perhaps I should have studied poetry instead of math since I do not have the words to express how instrumental you have been in my achievements and how important you continue to be in my life. Thank you.

To Brian: Thank you for your support and your love. I think we make quite a team, and I look forward to all of our adventures together. I love you.

Above all, I give thanks to God, who has made this possible.

Contents

List of Figures

List of Tables

Chapter 1

Introduction

Standard techniques for robust controller design for partial differential equation (PDE) systems in the state space yield controllers that are themselves defined by PDEs. Our interest is in the design of robust, real-time, implementable controllers for physical systems, meaning we often approximate the PDE and the PDE controller using some finite dimensional scheme. However, control design at this level will typically give rise to controllers that are inherently large-scale, thus presenting a challenge in the design of controls in which we are interested. Often a reduction in the size of the finite dimensional controller is necessary at some point. We organize reduction techniques into one of two categories, namely "reduce-then-design" and "design-then-reduce" methods. Traditional methods to obtain lower order controllers involve reducing the model from that for the PDE, and then applying a standard control design technique. We term such approaches as "reduce-then-design" techniques. In several recent papers [2, 4, 26, 30, 32, 34], the proper orthogonal decomposition (POD) has been applied in this fashion to obtain reduced order models. Clearly, there is a loss of physical information prior to control design. In [2], it was argued that reduce-then-design methods may have an inherent weakness in that some of the essential "physics" in the PDE model may be lost in model reduction. Consequently, more robustness is demanded from the low order controller.

We summarize our reduce-then-design techniques for this research using the diagram in Figure 1.1. We begin with the plant, or original system we would like to control. From there, we develop a PDE model that represents the dynamics of the plant as closely as possible. Note that we change shapes between the plant and PDE model in the diagram to represent that the plant and PDE model may not necessarily be the same thing, and there will typically be a loss of information at this step. At this stage, existence of a PDE controller can be proven but not written analytically. Next we think about computing a controller numerically, so we develop a finite dimensional approximation to the PDE. In particular, we choose a

stable, consistent, and thus convergent, approximation scheme such that we know the finite dimensional model will converge to the PDE model as we take larger order approximations. Certainly, there is a loss of information at this step since we are transitioning from an infinite dimensional model to a finite dimensional one. Therefore, we show a different shape in the diagram at this stage. In order to achieve real-time, implementable control, we next reduce the approximation to arrive at a low order finite dimensional approximation to the PDE. Again, we have a loss of information. It is on this low order approximation which we design the controller. This controller is guaranteed to stabilize the low order approximation, thus the double directional arrow at this step in the diagram.

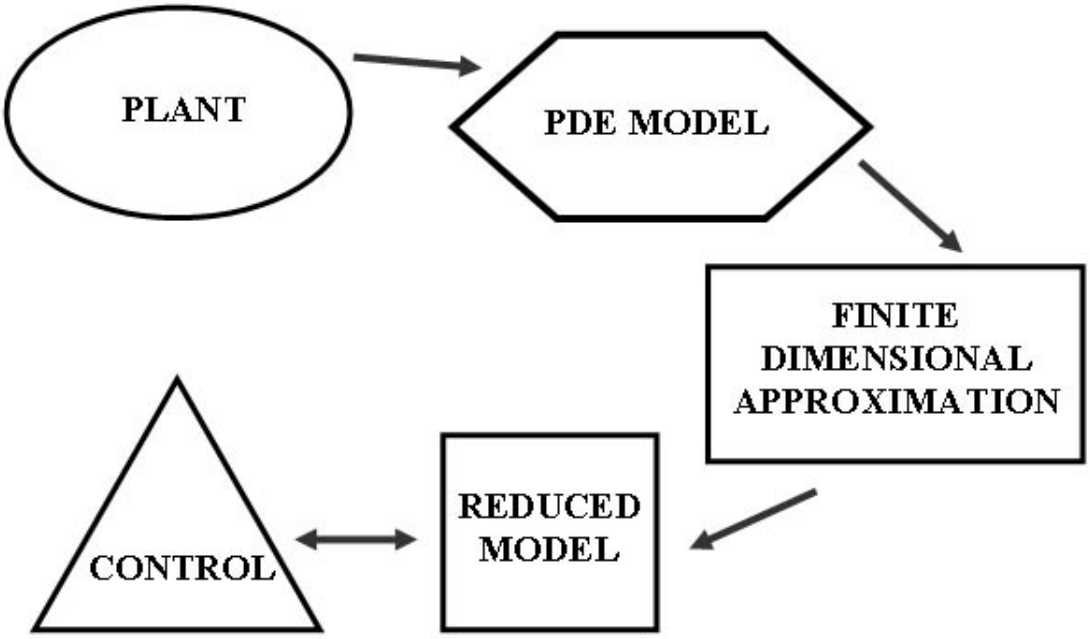

Figure 1.1: "Reduce-then-Design Diagram"

In an attempt to capture characteristics of the PDE controller before the reduction step, an alternative to reduce-then-design was suggested in [2, 8]. In [2], the approach involved using the POD for controller reduction. This is an example from the other group of reduction techniques we term as "design-then-reduce" methods. That is, a finite dimensional, large-scale controller, known to converge to the PDE controller, is designed using a high-order approximation to the PDE. This large-scale controller is then reduced to obtain a low-order controller. This class of methods has the advantage of using the physics of control design before information is lost in the reduction process.

We describe our design-then-reduce techniques to be employed in this research using the diagram in Figure 1.2. We begin the same way as with the reduce-then-design method. We

have a plant, or original system we would like to control, and we develop a PDE model to represent the plant dynamics. Here we have two branches. On one hand, we can prove the existence of an infinite dimensional controller for the PDE model. On the other hand, we want to numerically compute this controller, so we develop a finite dimensional approximation to the PDE in the manner described above. We design the controller on this high order approximation, which is guaranteed to stabilize the high order approximation. Additionally, we know this controller converges to the theoretical controller designed on the PDE model. At this stage, we have a high order controller, and in order to achieve real-time control, it is reduced.

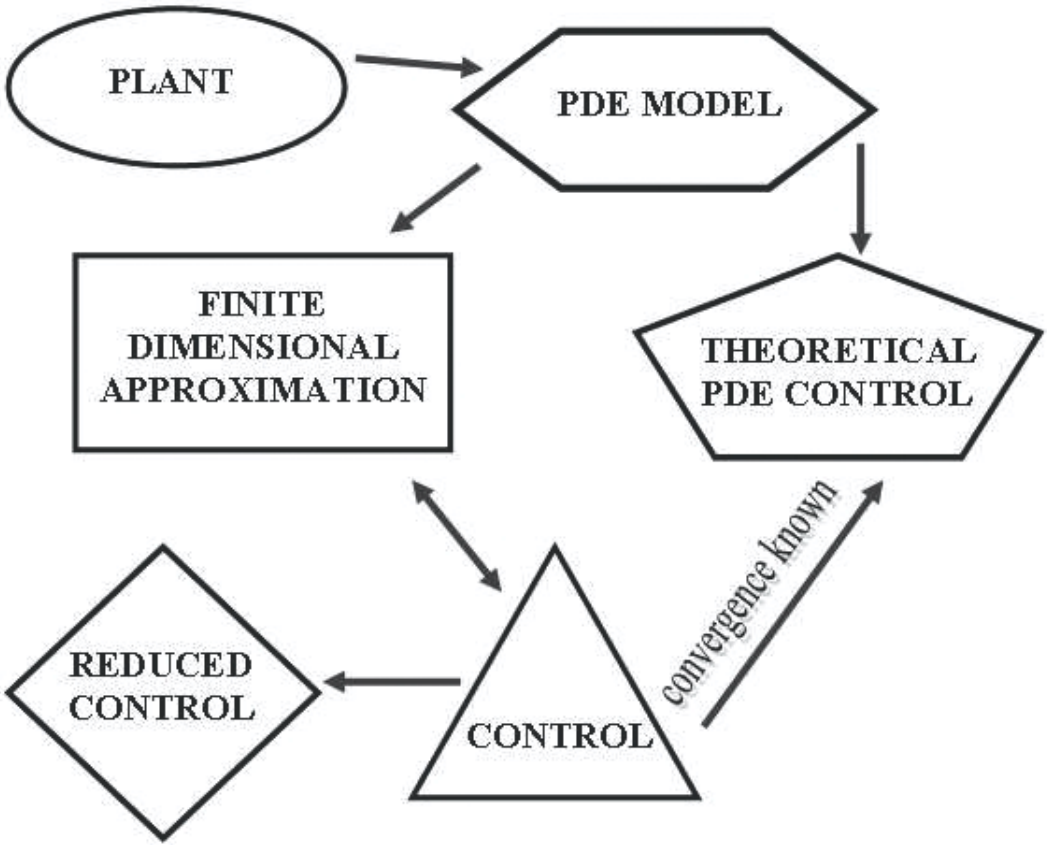

Figure 1.2: "Design-then-Reduce" Diagram

As an alternative to these POD approaches, we will compare two different balanced realization with truncation methods used to design low order controllers, one from each of the above described philosophies. One common balancing technique is balanced realization, which, when coupled with truncation, is a reduce-then-design method. It was established for finite dimensional systems in [37, 41] and for infinite dimensional systems in [14, 20, 21].

This balancing technique is inherently system-based; that is, to use this method there is no computation of a controller. Specifically, this balancing method makes no use of knowledge about the distributed parameter control for the PDE system. This idea gives rise to another balancing technique, LQG balanced realization, which is based on the distributed parameter controller. That is, LQG balanced truncation can be thought of as a design-then-reduce method. The fundamental idea behind the method is that the system is balanced around the solutions of the control and filter Riccati equations. LQG balanced realization was established for large-scale systems of ordinary differential equations in [25, 46, 47]. Recently, Curtain has extended these results to PDE systems [13].

In this thesis, we compare balanced truncation with LQG balanced truncation, by applying both methods to several PDE systems. In Chapter 2, we discuss semigroups, nuclearity, stability, and robustness measures. In Chapter 3, we present an overview of feedback control design and the two balancing techniques. In Chapter 4, we apply both balancing techniques with multiple control designs to the nonlinear cable-mass system discussed in [8, 29, 38]. In Chapters 5 and 6, we display comparable balancing results for the Klein-Gordon relativistic wave equation and the cantilevered Euler-Bernoulli beam equation, respectively. All numerical results include a comparison of performance and robustness properties of the closed loop systems. We conclude with observations in Chapter 7.

Chapter 2

Theoretical Background

Assume a PDE model for a physical system of interest, is given in abstract form as

$$\dot{x}(t) = Ax(t) + Bu(t), \qquad x(0) = x_0 \tag{2.1}$$

where $x(t)$ is the state of the system in Hilbert space X, and $u(t)$ is the control in Hilbert space U. The operator $A : X \to X$ contains the dynamics of the physical system being modelled while $B : U \to X$ describes how the control will be applied. Using the theory contained in [15, 33, 48, 49], PDE control systems can be formulated in this manner. Also note, the equation and initial condition

$$\dot{x}(t) = Ax(t), \qquad x(0) = x_0 \tag{2.2}$$

describe the uncontrolled dynamics of the system.

In addition to (2.1), we assume a state measurement, $y(t)$ in Hilbert space Y, of the form

$$y(t) \;\; = \;\; Cx(t). \tag{2.3}$$

The operator $C : X \to Y$ describes how we will measure, or observe, the state. We denote the state space system given by (2.1) and (2.3) as $\Sigma(A, B, C)$. The Laplace transform of $\Sigma(A, B, C)$ gives rise to the transfer function $G(s) = C(sI - A)^{-1}B$, also denoted by $G(s) \stackrel{s}{=} (A, B, C)$. We can also think of $G(s)$ as the input to output map of Σ, i.e $G(s) : U \to Y$. Although $G(s)$ is the unique transfer function for $\Sigma(A, B, C)$, there are many state space systems that would give rise to $G(s)$. This observation provides a rationale for balancing and will be discussed in Section 3.3.

2.1 Semigroups

We cite the following definitions regarding semigroups from [40].

Definition 2.1. *Let X be a Hilbert space. A family $T(t),\ 0 \leq t < \infty$, of bounded linear operators from X into X is a* ***semigroup*** *of bounded linear operators on X if*

1. *$T(0) = I$, where I is the identity operator on X*
2. *$T(t+s) = T(t)T(s)$ for every $t, s \geq 0$.*

A semigroup of bounded linear operators, $T(t)$ is ***uniformly continuous*** *if*

$$\lim_{t \downarrow 0} ||T(t) - I|| = 0. \tag{2.4}$$

A linear operator A defined by

$$D(A) = \left\{ x \in X : \lim_{t \downarrow 0} \frac{T(t)x - x}{t} \ \textit{exists} \right\} \tag{2.5}$$

and

$$Ax = \lim_{t \downarrow 0} \frac{T(t)x - x}{t} = \left. \frac{d^+ T(t)x}{dt} \right|_{t=0} \quad \textit{for } x \in D(A) \tag{2.6}$$

is the ***infinitesimal generator*** *of the semigroup $T(t)$, $D(A)$ is the domain of A.*

Definition 2.2. *A semigroup $T(t),\ 0 \leq t < \infty$, of bounded linear operators on X is a* ***strongly continuous*** *semigroup, or C_0-semigroup, of bounded linear operators if*

$$\lim_{t \downarrow 0} T(t)x = x \qquad \textit{for every } x \in X. \tag{2.7}$$

Definition 2.3. *Let $\Delta = \{z : \phi_1 < \arg z < \phi_2, \phi_1 < 0 < \phi_2\}$ and for $z \in \Delta$ let $T(z)$ be a bounded linear operator. The family $T(z),\ z \in \Delta$ is an* ***analytic semigroup*** *in Δ if*

1. *$z \to T(z)$ is analytic in Δ.*
2. *$T(0) = I$ and $\lim\limits_{\substack{z \to 0 \\ z \in \Delta}} T(z)x = x$ for every $x \in X$.*
3. *$T(z_1 + z_2) = T(z_1)T(z_2)$ for $z_1,\ z_2 \in \Delta$.*

As noted in [40], restricting an analytic semigroup to the real axis will result in a C_0-semigroup, which is what we would like to achieve in order to satisfy hypotheses of theorems to which we will later refer.

Theorem 2.4. *Let $T(t)$ be a C_0-semigroup. There exist constants $\omega \geq 0$ and $M \geq 1$ such that*

$$||T(t)|| \leq Me^{\omega t} \qquad \text{for } 0 \leq t < \infty \tag{2.8}$$

If $\omega < 0$ we say that $T(t)$ is an **exponentially stable** C_0-semigroup. If $\omega = 0$, $T(t)$ is said to be **uniformly bounded**, and moreover, if $M = 1$, $T(t)$ is called a C_0-semigroup of **contractions**.

Definition 2.5. *An operator A is **exponentially stable** if and only if A generates an exponentially stable C_0-semigroup.*

Definition 2.6. *The state linear system $\Sigma(A, B, C)$ is **exponentially stable** if A is exponentially stable.*

In this work, we assume that $\Sigma(A, B, C)$ is exponentially stable.

Definition 2.7. *$\Sigma(A, B, C)$ is **stabilizable** if there exists a linear operator $F : X \to U$ such that $A + BF$ is exponentially stable. For convenience, we refer to the pair (A, B) as being stabilizable.*

Definition 2.8. *$\Sigma(A, B, C)$ is **detectable** if there exists a linear operator $L : Y \to X$ such that $A + LC$ is exponentially stable. For convenience, we refer to the pair (A, C) as being detectable.*

Definition 2.9. *A linear operator A is **dissipative** if for every $x \in D(A)$ there is an $x^* \in X^*$ such that $Re\langle Ax, x^* \rangle \leq 0$.*

Theorem 2.10. *(Corollary 4.4 in [40]) Let A be a densely defined closed linear operator. If both A and A^* are dissipative, then A is the infinitesimal generator of a C_0-semigroup of contractions on X.*

2.2 Nuclearity of the Hankel Operator

Next we consider the nuclearity of the Hankel operator. Recall that in Section 3.3 we provided a bound on the truncation error between a plant's transfer and reduced transfer functions. In particular, the bound was in terms of an infinite sum of the Hankel singular values, and we noted that convergence of the sum was an issue of consideration for PDE systems. That is, we obviously want the truncation error associated with the transfer functions to be finite. This discussion leads to the following definition.

Definition 2.11. *A compact Hankel operator is* ***nuclear*** *if* $\sum_{k=1}^{\infty} \sigma_k < \infty$*, where* $\sigma_k's$ *are the Hankel singular values.*

Therefore, a compact, nuclear Hankel operator would guarantee a finite truncation error regarding the transfer and reduced transfer functions.

Definition 2.12. *We say* $\Sigma(A, B, C)$ *has bounded inputs and outputs if both* $B : U \to X$ *and* $C : X \to Y$ *are bounded linear operators.*

We assume in this work that $\Sigma(A, B, C)$ has bounded input and output operators. The following theorem from [43] provides a connection between the stability of a state linear system and the nuclearity of the Hankel operator.

Theorem 2.13. *(Theorem 3.2.1 in [43]) Let* A *be the infinitesimal generator of an exponentially stable* C_0*-semigroup on a separable Hilbert space,* X*. Suppose also that* $\Sigma(A, B, C)$ *has bounded inputs and outputs and finite dimensional input and output spaces. Then the Hankel operator,* $\Gamma_h = \mathcal{CB}$*, is nuclear.*

While this theorem provides a nice relationship between stability and nuclearity and offers a straightforward means to determine if the Hankel operator is nuclear, it may, upon first impression, seem restrictive due to the requirement that $\Sigma(A, B, C)$ has bounded input and output operators and corresponding finite dimensional spaces. However, this requirement is not particularly restrictive since most actuators and sensors can be modelled mathematically by bounded input and output operators, when actuator and sensor dynamics are taken into account. One type of actuation involves averaging, which leads to a bounded input. Another desirable way to apply a control might be through point actuation, often modelled with a delta function, which would give rise to an unbounded input. However, a point actuator at x_0 could also be modelled with an averaging measurement on $(x_0 - \epsilon, x_0 + \epsilon)$, thus giving rise to a bounded input. A similar discussion applies to both the C operator and the measurement of the state.

2.3 Lyapunov Stability

We will use Theorem 2.13 to show that the Hankel operator is nuclear for the applications to which we apply both balancing techniques. Therefore, it is also of interest to us that we be able to show A generates an exponentially stable C_0-semigroup. For the cable mass system and Euler-Bernoulli beam equation, this has already been shown in [8] and [5], respectively.

Since we want to make a Lyapunov argument to guarantee exponential stability for the Klein-Gordon equation, we take this opportunity to provide background definitions and theorems.

Definition 2.14. *We say $V(\Phi)$ is a Lyapunov function if $V(\Phi)$ is continuous, $V(\Phi) > 0$ for all $\Phi \neq 0$, and $\dot{V}(\Phi) < 0$ for all $\Phi \neq 0$.*

Theorem 2.15. *(Theorem 3.1 in [48]) If $V : \mathcal{X} \to I\!R$ be a continuous Lyapunov function on the open ball $\mathcal{S}_r(\Phi_e)$, for some $r > 0$, such that $V(\Phi) \geq V(\Phi_e) + f(||\Phi - \Phi_e||)$ for all $\Phi \in \mathcal{S}_r(\Phi_e)$ and some monotone function $f : ([0, r]) \subset I\!R \to I\!R$ with $f(0) = 0$, $f(\eta) > 0$ for all $\eta \in (0, r)$, then Φ_e is stable. If, in addition, $\dot{V}(\Phi) \leq -g(||\Phi - \Phi_e||)$ for all $\Phi \in \mathcal{S}_r(\Phi_e)$ and some monotone function $g : ([0, r]) \subset I\!R \to I\!R$ with $g(0) = 0$, $g(\eta) > 0$ for all $\eta \in (0, r)$, then Φ_e is asymptotically stable. Additionally, if there exist real numbers $c_2 \geq c_1 > 0$, $\mu > 0$, $k > 0$, such that $\dot{V}(\Phi) \leq -\mu[V(\Phi) - V(\Phi_e)]$ and $c_1||\Phi - \Phi_e||^k \leq V(\Phi) - V(\Phi_e) \leq c_2||\Phi - \Phi_e||^k$ for all $\Phi \in \mathcal{S}_r(\Phi_e)$, then Φ_e is exponentially stable with exponent $-\mu t/k$.*

2.4 Robustness

Our ultimate goal is to seek a robust low order controller that will stabilize the original plant, not just a PDE model of the plant or a high order finite dimensional approximation of it. In our numerical results, we will offer two measurements of robustness by which to compare our controllers for each physical system of interest. Since we will be comparing robustness of finite dimensional closed loop systems, the following discussion is phrased in a finite dimensional setting. One measurement is the stability margin, which measures the distance from the imaginary axis to the nearest eigenvalue for a given matrix. The second measurement is the complex stability radius as described in [24] and summarized here.

In computing the stability radius of a given matrix, A, we seek to find the distance from A to the nearest unstable matrix. Let $A \in \mathbb{C}^{n\times n}$ and define the matrix norm as

$$||A||_\infty = \max\{||Ax|| : x \in \mathbb{C}^n, ||x|| = 1\}. \tag{2.9}$$

We know that the smallest singular value of A defined as

$$s_n(A) = \min\left\{||A - S|| : S \in \mathbb{R}^{n\times n},\ 0 \in \sigma(S)\right\}, \tag{2.10}$$

where $A \in \mathbb{R}^{n\times n}$ and $\sigma(S)$ is the spectrum of S, gives the distance of A from singularity. This idea is generalized in the following theorem [24].

Theorem 2.16. *Let $\Gamma \subset \mathbb{C}$ be closed, $\partial\Gamma$ its boundary and $A \in \mathbb{C}^{n\times n}$ a matrix with $\sigma(A) \cap \Gamma = \emptyset$. Then*

$$\min_{\substack{X\in\mathbb{C}^{n\times n}\\ \sigma(X)\cap\Gamma\neq\emptyset}} ||A - X|| = \min_{\gamma\in\Gamma} s_n(\gamma I - A) = \min_{\gamma\in\partial\Gamma} s_n(\gamma I - A). \tag{2.11}$$

For our stability radius calculations, we have $\Gamma = i\mathbb{R}$ and this particular case yields the following corollary [24]:

Corollary 2.17. *If $A \in \mathbb{C}^{n\times n}$ is stable and $r_{\mathbb{C}}(A)$ is the complex stability radius, then*

$$r_{\mathbb{C}}(A) = \min_{\omega\in\mathbb{R}} s_n(i\omega I - A) = \min_{\omega\in\mathbb{R}} \min_{\substack{z\in\mathbb{C}^n \\ ||z||=1}} ||(i\omega I - A)z||. \tag{2.12}$$

To put some perspective on these two robustness measurements, we offer a simple 2×2 matrix example as a means of comparison.

Example 2.18. *Consider $A = \begin{pmatrix} -1 & 2000 \\ 0 & -2 \end{pmatrix}$ and $A_\Delta = \begin{pmatrix} -1 & 2000 \\ \frac{1}{1000} & -2 \end{pmatrix}$. We note the eigenvalues of A are $\lambda_1 = -1$ and $\lambda_2 = -2$. Thus the stability margin is 1.0. The stability radius was calculated to be $9.9\bar{9} \times 10^{-4}$. We now consider the perturbation $\Delta = \begin{pmatrix} 0 & 0 \\ \frac{1}{1000} & 0 \end{pmatrix}$ where $A+\Delta = A_\Delta$. Note $||\Delta||_\infty = .001$. Since the eigenvalues of A_Δ are $\lambda_1 = 0$ and $\lambda_2 = -3$, A_Δ is unstable. Thus, the stability margin and the stability radius are zero. As indicated by the stability radius of A, we see that A is "not far" from instability. However, the stability margin measurement would perhaps indicate quite the opposite. Since the stability margin is guaranteed to be greater than or equal to the stability radius [24], this simple example demonstrates one weakness of using the stability margin as a measure of robustness. But, perhaps more importantly, it emphasizes the need to consider multiple measures of robustness and put each in perspective.*

Chapter 3

Feedback Control Design

3.1 Full State Feedback Control Design (LQR)

The idea behind full state feedback control is that the entire state of the system is known at all values of time; then, at each value of time, the control input is based upon this complete knowledge of the system. A classical example of full state feedback control is the linear quadratic regulator design (LQR). LQR design finds an optimal control by minimizing the cost functional

$$J(u) \;=\; \int_0^\infty \{\langle Qx(t), x(t)\rangle_X + \langle Ru(t), u(t)\rangle_U\}dt \tag{3.1}$$

over all controls $u(t) \in U$, where $Q : X \to X$ is a weighting operator for the state and $R : U \to U$ is a weighting operator for the control. Particularly, we consider the steady-state LQR problem, meaning the optimization interval is infinite.

If (A, B) is stabilizable and (A, C) is detectable, there exists an optimal control, $u(t)$, it of the form

$$u(t) \;=\; -R^{-1}B^*\Pi x(t) \;=\; -Kx(t) \tag{3.2}$$

where Π is the unique, symmetric, positive definite solution to the control algebraic Riccati equation

$$A^*\Pi + \Pi A - \Pi BR^{-1}B^*\Pi + Q \;=\; 0 \tag{3.3}$$

and $K = R^{-1}B^*\Pi$ is the optimal feedback gain operator that yields a control in (3.2) guaranteed to stabilize (2.1). In this work, we take $R = cI$, where $c \in \mathbb{R}^+$ and I is the identity operator, and $Q = C^*C$. After determining K, the closed loop PDE system can be formulated as

$$\dot{x}(t) = (A - BK)x(t), \qquad x(0) = x_0. \tag{3.4}$$

However, there is a problem with implementing full state feedback control. It is typically impractical and often impossible. For these reasons, an alternative approach to full state feedback control is needed.

3.2 State Estimate Feedback Control Design

State estimate feedback control offers a viable option in place of full state feedback control. It is based upon a compensator, or observer, which provides an estimate of the state. The estimate of the state is based on measurements, which are taken according to (2.3), and is then used in the control law in place of the state in (3.2). In this section, we introduce three different state estimate feedback control designs: LQG, MinMax, and central. We apply all three designs in our numerical simulations.

3.2.1 Linear Quadratic Gaussian Controller (LQG)

Just as LQR is a classical example of full state feedback control, linear quadratic Gaussian (LQG) compensator design is a classical example of state estimate feedback control. Both types of control design are discussed in [6, 16, 31]. The LQG problem is to find a dynamical system that optimally estimates the state of the system $x(t)$ given the measurements $y(t)$. The solution provides a state estimate, $x_c(t)$, and control, $u(t)$, that are given by the equations

$$\begin{aligned} \dot{x}_c(t) &= A_c x_c(t) + F y(t), \qquad x_c(0) = x_{c_0} \\ u(t) &= -K x_c(t). \end{aligned} \tag{3.5}$$

Design of a controller entails determining A_c, F and K that produce a stable closed loop system

$$\begin{bmatrix} \dot{x} \\ \dot{x}_c \end{bmatrix} = \begin{bmatrix} A & -BK \\ FC & A_c \end{bmatrix} \begin{bmatrix} x \\ x_c \end{bmatrix}, \qquad \begin{bmatrix} x(0) \\ x_c(0) \end{bmatrix} = \begin{bmatrix} x_0 \\ x_{c_0} \end{bmatrix}. \tag{3.6}$$

Under conditions of stabilizability of (A, B) and detectability of (A, C) (see for example, [6, 15, 19]), the operators A_c, F and K can be obtained by the solution of (3.3) and the filter algebraic Riccati equation

$$AP + PA^* - PC^*CP + M = 0, \tag{3.7}$$

where $M = BB^*$ in this work. Once the solutions of the control Riccati equation, Π, and the filter Riccati equation, P, are obtained, then

$$\begin{aligned} K &= R^{-1}B^*\Pi \\ F &= PC^* \\ A_c &= A - BK - FC. \end{aligned} \tag{3.8}$$

Note that the feedback operator K is the same as previously described for full state feedback control.

For certain PDEs, the control law can be written in integral form. For example, if the control space U is finite dimensional, then it follows from the Riesz Representation Theorem. That is,

$$u(t) = -Kx_c(t) = -\langle k_i(s), x_c(t)\rangle, \tag{3.9}$$

for spatial variable s and where $k_i \in X$ for $i = 1, 2, \ldots, m$ (see for example [28]). The kernel of the integral, $k(s)$, is called a functional gain and is important for several reasons. First, gains can be computed off-line and stored, so that in computation of the control, the gain is multiplied by the state estimate and numerically integrated. In addition, research has been done involving reduced order controllers and sensor design based on information in the functional gains in [2, 3, 18, 27, 29]. It was noted in [1, 2, 3] that a reduce-then-design approach based on POD reduction of the model followed by control design can yield finite dimensional approximations of the functional gains that do not converge. We also examine gains from the two balancing methods.

3.2.2 MinMax Controller

In this work, we also apply MinMax control design to the reduced order models. The MinMax control design is considered to be more robust than the LQG design and is discussed in detail in [42]. In terms of implementation, the only difference between the computation of LQG and MinMax controllers is the Riccati equations that are solved and how the control design operators are then defined. We must solve

$$A^*\Pi + \Pi A - \Pi[BR^{-1}B^* - \theta^2 M]\Pi + Q = 0 \tag{3.10}$$

$$\tag{3.11}$$

$$AP + PA^* - P[C^*C - \theta^2 Q]P + M = 0. \tag{3.12}$$

For sufficiently small θ, we are guaranteed minimal solutions Π and P such that

$$[I - \theta^2 P\Pi] > 0, \tag{3.13}$$

i.e., positive definite, and the closed loop system in (3.6) is stable. We then define the control design operators to be

$$\begin{aligned} K &= R^{-1}B^*\Pi \\ F &= [I-\theta^2 P\Pi]^{-1}PC^* \\ A_c &= A - BK - FC + \theta^2 M\Pi. \end{aligned} \tag{3.14}$$

Note that $\theta = 0$ results in the LQG controller.

3.2.3 Central Controller

We now turn our attention to the central control design, which we also use for the low order controllers since it is guaranteed to stabilize the system for which it is designed with a guaranteed *robustness margin*. Another justification for using this controller will be discussed in Section 3.3.2.

Though the central controller gives rise to concise to state space formulas (that we will use to implement the controller numerically), to begin to understand its origins, we must consider the frequency domain. Much of the following discussion is summarized from [36, 44]. Suppose a PDE transfer function, $G(s)$, has a left coprime factorization

$$G(s) = M(s)^{-1}N(s), \tag{3.15}$$

where $M(s)$ and $N(s)$ are stable transfer functions. We define transfer functions for a set of systems that are "close" to the PDE, $G(s)$, as

$$G_\Delta(s) = (M(s) + \Delta_M(s))^{-1}(N(s) + \Delta_N(s)), \tag{3.16}$$

where the perturbations $\Delta_M(s)$ and $\Delta_N(s)$ are stable transfer functions representing unstructured uncertainty in $G(s)$. By "unstructured" we mean we have no information about how the uncertainty affects a given process, only an upper bound on its magnitude. We seek to stabilize the plants in the set

$$G_\Delta(s) = \{(M(s) + \Delta_M(s))^{-1}(N(s) + \Delta_N(s)) : ||[\Delta_N(s) \;\; \Delta_M(s)]||_\infty < \epsilon\} \tag{3.17}$$

where ϵ is the *robustness margin*. The norm in use is defined as $||G||_\infty = \sup_{w\in\mathbb{R}} \bar{\sigma}[G(iw)]$, where $\bar{\sigma}$ is the maximum singular value. The notation $[\Delta_N(s) \;\; \Delta_M(s)]$ means the combined, or stacked, perturbations, as in a partitioned matrix, and we could rewrite this by defining a total perturbation as $\Delta_C(s) = [\Delta_N(s) \;\; \Delta_M(s)]$. As [44] notes, bounding the combined uncertainty is not the same as bounding the individual uncertainties, whose bound will be larger by a factor of $\sqrt{2}$.

Maximizing the robustness margin allows the H_∞ norm of the coprime factor perturbations to be as large as possible while maintaining stability of the closed loop system given in (3.22). McFarlane and Glover in [36] note that the robust stabilization problem of finding a feedback controller which stabilizes all plants in (3.17) for as large a robustness margin as possible can be solved using H_∞ optimization methods introduced by Zames in [51]. From a computational perspective, this is a weakness since solutions to H_∞ optimization problems are generally iterative in nature in the sense that one must search through a range of values for the optimal parameter value since it is not provided explicitly in a formula. However, McFarlane and Glover show that this iterative process can be avoided if the coprime factors in (3.15) are *normalized*. That is, a normalized left coprime factorization of $G(s)$ means the pair $(N(s), M(s))$ must also satisfy Bezout's identity

$$N(s)N(s)^* + M(s)M(s)^* = I \qquad \text{for all } s \in i\mathbb{R}. \tag{3.18}$$

To summarize, finding a feedback controller which will stabilize all the plants in (3.17) for as large a robustness margin as possible is the *normalized coprime factor robust stabilization problem*, and the solution gives rise to the *central controller*.

A method for obtaining the central controller is given by McFarlane and Glover in [22]. There it was determined in that the lowest value of γ, $\gamma_{\min}$, and the maximum robustness margin, $\epsilon_{\max}$, are given by

$$\frac{1}{\gamma_{\min}} = \epsilon_{\max} = \frac{1}{\sqrt{1+\rho(\Pi P)}}, \tag{3.19}$$

where ρ is the spectral radius, or maximum eigenvalue, and Π and P are solutions to (3.3) and (3.7), respectively. This value provides an upper bound for the size of perturbations that can still be stabilized by the central controller.

The central controller provides a state estimate, $x_c(t)$, and control, $u(t)$, that are given by the equations

$$\begin{aligned} \dot{x}_c(t) &= A_c x_c(t) + F y(t), \qquad x_c(0) = x_{c_0} \\ u(t) &= K x_c(t), \end{aligned} \tag{3.20}$$

where A_c, F, and K are to be determined as follows. As with designing the LQG controller, under conditions of stabilizability of (A, B) and detectability of (A, C), the operators A_c, F, and K can be obtained by the solution of the two algebraic Riccati equations in (3.3) and (3.7). Once the solutions of the control Riccati equation, Π, and the filter Riccati equation,

P, are obtained, then define

$$\begin{aligned} K &= B^*\Pi, \\ L &= (1-\gamma^2)I + \Pi P, \\ F &= \gamma^2 (L^*)^{-1} P C^*, \\ A_c &= A - BR^{-1}B\Pi + \gamma^2 (L^*)^{-1} P C^* C. \end{aligned} \tag{3.21}$$

The operators $A_c,\ F$ and K defined in this way produce a stable closed loop system

$$\begin{bmatrix} \dot{x} \\ \dot{x}_c \end{bmatrix} = \begin{bmatrix} A & BK \\ FC & A_c \end{bmatrix} \begin{bmatrix} x \\ x_c \end{bmatrix}, \qquad \begin{bmatrix} x(0) \\ x_c(0) \end{bmatrix} = \begin{bmatrix} x_0 \\ x_{c_0} \end{bmatrix} \tag{3.22}$$

and satisfies the conditions in (3.17) and (3.19).

3.2.4 Reduced Order Compensators

In order to compute the PDE controller, an approximation scheme for which convergence is known is applied to (2.1) and (2.3)[19]. In the case of a finite element scheme with basis of dimension N (where $N \to \infty$ yields the PDE system), the approximating system is given by

$$\begin{aligned} \dot{x}^N(t) &= A^N x^N(t) + B^N u^N(t), \qquad x^N(0) = x_0^N \\ y^N(t) &= C^N x^N(t). \end{aligned} \tag{3.23}$$

We use the notation $\Sigma(A^N, B^N, C^N)$ to denote the approximating system in (3.23). A finite dimensional compensator for the approximating system can then be obtained by solving

$$\begin{aligned} \dot{x}_c^N(t) &= A_c^N x_c^N(t) + F^N y(t), \qquad x_c^N(0) = x_{c_0}^N \\ u^N(t) &= -K^N x_c^N(t), \end{aligned} \tag{3.24}$$

where the control design operators $A_c,\ F$ and K are defined after solving the two Riccati equations, either (3.3) and 3.7) for the LQG controller or (3.10) and (3.12) for the MinMax controller. For the central controller, the minus sign does not appear in the equation for $u^N(t)$. (Note that one can sometimes have difficulty computing the symmetric, positive definite, numerical solutions to the Riccati equations due to numerical instabilities. To ensure that Π and P are positive definite, for all of our numerical results in Chapters 4, 5, and 6, we add $10^{-5} * I$ to Π and P, where I is the identity matrix. This acts to shift

the eigenvalues.) Then combining equations (3.23) and (3.24) yields the finite dimensional approximation to the LQG or MinMax closed loop system given by

$$\begin{bmatrix} \dot{x}^N \\ \dot{x}_c^N \end{bmatrix} = \begin{bmatrix} A^N & -B^N K^N \\ F^N C^N & A_c^N \end{bmatrix} \begin{bmatrix} x^N \\ x_c^N \end{bmatrix}, \qquad \begin{bmatrix} x^N(0) \\ x_c^N(0) \end{bmatrix} = \begin{bmatrix} x_0^N \\ x_{c_0}^N \end{bmatrix}. \tag{3.25}$$

Eliminating the negative sign on the $B^N K^N$ term yields the approximation to the central closed loop system. We assume that N is large enough so that the behavior of the approximating system has converged to the behavior of the PDE model. We refer to this large-scale finite dimensional approximation as the *full order closed loop system*.

Note that an implementation problem exists at this point, in that a full order compensator will not offer real time control for most physical problems. For this reason, reduced order compensators need to be considered. As discussed in the introduction, one way to obtain a low order compensator is to perform model reduction followed by control design. We can think of the reduced order model as

$$\begin{aligned} \dot{x}^q(t) &= A^q x^q(t) + B^q u^q(t), \qquad x^q(0) = x_0^q \\ y^q(t) &= C^q x^q(t), \end{aligned} \tag{3.26}$$

where $q << N$. By solving (3.3) and (3.7) with A^q, B^q, and C^q, we obtain the low order compensator and control law

$$\begin{aligned} \dot{x}_c^q(t) &= A_c^q x_c^q(t) + F^q y(t), \qquad x_c^q(0) = x_{c0}^q \\ u^q(t) &= -K^q x_c^q(t), \end{aligned} \tag{3.27}$$

for the LQG and MinMax controllers. To simulate the performance of the low order compensator, we apply it to $\Sigma(A^N, B^N, C^N)$; that is, we simulate the *reduced order closed loop system*

$$\begin{bmatrix} \dot{x}^N(t) \\ \dot{x}_c^q(t) \end{bmatrix} = \begin{bmatrix} A^N & -B^N K^q \\ F^q C^N & A_c^q \end{bmatrix} \begin{bmatrix} x^N(t) \\ x_c^q(t) \end{bmatrix}, \qquad \begin{bmatrix} x^N(0) \\ x_c^q(0) \end{bmatrix} = \begin{bmatrix} x_0^N \\ x_{c0}^q \end{bmatrix}. \tag{3.28}$$

There are many ways of forming the reduced order model in (3.26), including POD, balanced truncation, and coarse approximation. To form the low order system in (3.26) we will use balanced truncation and LQG balanced truncation. We discuss these truncation methods in the following section.

3.3 Balancing

3.3.1 System Balancing

Balanced realization and truncation is a common procedure that can be found in standard references on control, e.g., [15] for PDE systems. It is based on the premise that a low order approximation to $\Sigma(A, B, C)$ could be obtained by eliminating any states that are difficult to control and to observe. Then, the reduced order system, denoted by $\Sigma(A^q, B^q, C^q)$ where $q << N$, is used as described above to obtain the approximate solutions Π^q, P^q to the algebraic Riccati equations, either (3.3) and (3.7) for the LQG or central controller or (3.10) and (3.12) for the MinMax controller, and the corresponding $K^q,\ F^q,$ and A_c^q.

We need to establish some definitions in order to proceed with the balancing discussion. Since we have assumed $\Sigma(A, B, C)$ is an exponentially stable state linear system, we can define the *extended controllability map* as

$$\mathcal{B} \ = \ \int_0^\infty e^{As} B \ ds \tag{3.29}$$

and the *extended controllability Gramian* as

$$L_B \ = \mathcal{B}\mathcal{B}^* \ = \ \int_0^\infty e^{As} B B^* e^{A^* s} ds. \tag{3.30}$$

The *extended observability map* is

$$\mathcal{C} \ = \ \int_0^\infty C e^{As} \ ds \tag{3.31}$$

and the *extended observability Gramian* is

$$L_C \ = \mathcal{C}^*\mathcal{C} \ = \ \int_0^\infty e^{A^* s} C^* C e^{As} ds. \tag{3.32}$$

Based on our assumption that B and C are bounded linear operators, we draw attention to a special operator. The Hankel operator, $\Gamma_h = \mathcal{C}\mathcal{B}$, is compact and Hilbert Schmidt on $L_2(0, \infty)$, i.e., $\sum_{k=1}^{\infty} \sigma_k^2 < \infty$ and σ_k's are the Hankel singular values.

Definition 3.1. *$\Sigma(A, B, C)$ is **approximately controllable** on $[0, \tau]$, for some finite $\tau > 0$, if given an arbitrary $\varepsilon > 0$ it is possible to steer from the origin to within distance ε from all points in the state space at time τ, i.e., if $\overline{ran\ (\mathcal{B}^\tau)} = X$, where $\mathcal{B}^\tau$ is the controllability map on $[0, \tau]$. For convenience, we will refer to the pair (A, B) as being controllable.*

Definition 3.2. $\Sigma(A, B, C)$ *is* ***approximately observable*** *on* $[0, \tau]$*, for some finite* $\tau > 0$*, if knowledge of the output in* $L_2([0, \tau]; Y)$ *determines the initial state uniquely, i.e., ker* $\mathcal{C}^\tau = \{0\}$*, where* $\mathcal{C}^\tau$ *is the observability map on* $[0, \tau]$*. For convenience, we will refer to the pair* (A, C) *as being observable.*

Necessary and sufficient conditions for controllability and observability are provided in [15]. In this work, we suppose the pair (A, B) is controllable and the pair (A, C) is observable.

The Gramians provide measures of controllability and observability [15, 41] in certain directions of the state space. The Gramians are not invariant under coordinate transformation, i.e., they are realization dependent. That is, one can choose two systems $\Sigma(A_1, B_1, C_1)$ and $\Sigma(A_2, B_2, C_2)$ that both give rise to the transfer function $G(s)$, but have different Gramians. Thus, if a realization was sought which led to few controllable states (therefore many states to truncate), that realization may have many observable states (therefore few states to truncate) and vice versa. This apparent dilemma is addressed by the *balanced realization*, in which states that are difficult to control coincide with states that are difficult to observe [37]. In particular, it is shown in [37] that there exists a coordinate system in which the Gramians are equal and diagonal in the finite dimensional setting. This result is extended to the infinite dimensional setting in [14]. We note that balanced realization is inherently system based, as opposed to controller based, since it only involves information from the Gramians which are computed using only $A,\ B,\ C$.

The following theorem, see for example [14, 20, 21], gives conditions for existence of the Gramians.

Theorem 3.3. *If* $\Sigma(A, B, C)$ *is exponentially stable, then the controllability and observability Gramians,* $L_B,\ L_C$*, exist and are the unique positive definite solutions to the Lyapunov equations*

$$AL_B + L_B A^* = -BB^*, \tag{3.33}$$

$$A^* L_C + L_C A = -C^* C. \tag{3.34}$$

If L_B, L_C exist, then there exists a similarity transformation S that gives rise to the balanced state space system, denoted as $\hat{\Sigma}(\hat{A}, \hat{B}, \hat{C})$, which we obtain in the following fashion.

Define a transformation

$$z \ = \ Sx \tag{3.35}$$

where S is a bounded, nonsingular operator. Then consider the system

$$\begin{aligned} \dot{z}(t) &= Az(t) + Bu(t) \\ y(t) &= Cz(t). \end{aligned} \tag{3.36}$$

Now, replace z and $\dot{z}$ in (3.36) by the transformation in (3.35) as appropriate to get

$$\begin{aligned} S\dot{x}(t) &= ASx(t) + Bu(t) \\ y(t) &= CSx(t). \end{aligned} \tag{3.37}$$

Or to write the system a little differently,

$$\begin{aligned} \dot{x}(t) &= S^{-1}ASx(t) + S^{-1}Bu(t) \\ y(t) &= CSx(t). \end{aligned} \tag{3.38}$$

Note that this is just another realization of the system given by (2.1, 2.3). In this particular realization, $\Sigma(A, B, C)$ is transformed into $\hat{\Sigma}(\hat{A}, \hat{B}, \hat{C}) = (S^{-1}AS, S^{-1}B, CS)$, and the transformed Gramians are $\hat{L}_B = SL_BS^*$ and $\hat{L}_C = (S^{-1})^*L_CS^{-1}$. Additionally,

$$\hat{L}_B = \hat{L}_C = diag(\sigma_1, \sigma_1, \ldots, \sigma_n, \ldots), \qquad \sigma_1 \geq \sigma_2 \geq, \cdots, \geq \sigma_n \geq \cdots \geq 0$$

where $\sigma_i = \sqrt{\lambda_i(L_BL_C)}$ are the Hankel singular values and are realization invariant [14, 37].

The ordering of the Hankel singular values gives information on the states that are insignificant with regard to both controllability and observability of the system. In particular, we write

$$\hat{A} = \begin{bmatrix} A_{11} & A_{12} \\ A_{21} & A_{22} \end{bmatrix} \qquad \hat{B} = \begin{bmatrix} B_1 \\ B_2 \end{bmatrix} \qquad \hat{C} = \begin{bmatrix} C_1 & C_2 \end{bmatrix}$$

where $\hat{A},\ \hat{B},\ \hat{C}$ are partitioned so that the states corresponding to the q most "significant" Hankel singular values are given by the truncated system $\Sigma(A_{11}, B_1, C_1)$. Note that we can think of $A_{12},\ A_{21},\ A_{22},\ B_2,$ and C_2 as being infinite dimensional. The corresponding reduced transfer function is $G_q(s) = C_1(sI - A_{11})^{-1}B_1$, and the truncation error can be represented as

$$||G(s) - G_q(s)||_\infty \leq 2 \sum_{i=q+1}^{\infty} \sigma_i.$$

Note that for infinite dimensional (PDE) systems, convergence of this expression is an issue that must be considered (see [13]). We will address this topic further in Chapter 2. We can use the following algorithm to numerically compute the balancing transformation S in finite dimensions.

Algorithm 1.

- *Compute L_B and L_C from $A^N,\ B^N,$ and C^N.*
- *L_B is symmetric positive definite, so the Cholesky decomposition yields $L_B = R^*R$.*

- *R^*L_CR is a way of writing L_BL_C which is symmetric positive definite.*
- *R^*L_CR can be diagonalized by a unitary matrix U such that $R^*L_CR = U\Sigma^2U^*$ where Σ^2 is a diagonal matrix containing the square of the Hankel singular values.*
- *Define $S = \Sigma^{\frac{1}{2}}U^*R$. It follows that $(S^{-1})^*L_CS^{-1} = \Sigma = SL_BS^*$.*

3.3.2 LQG Balancing

Recall that in Section 3.2.1, the Riccati operators Π and P were identified as the solutions of the control and filter algebraic Riccati equations found respectively in (3.3) and (3.7). Another set of invariants for $\Sigma(A, B, C)$ is the eigenvalues of ΠP [25, 46, 47], which are called the ***LQG characteristic values***. Instead of balancing around the Gramians as previously described, which could be considered as a type of model balancing, a control type of balancing can be used. That is, the balancing can be based on the Riccati operators. This process allows for the computation of a controller before any physical information is discarded. The balancing process is the same as that previously described. LQG balancing is discussed for finite dimensional systems in [25, 46, 47], and infinite dimensional systems are addressed in [13]. Since the focus of this research is the design of low order controllers for infinite dimensional systems, we provide the recent infinite dimensional results from [13] here.

Theorem 3.4. *(Corollary 3.3 in [13]) Let $\Sigma(A, B, C)$ be an exponentially stabilizable and detectable state linear system on the Hilbert space X. There exist unique, self-adjoint operators, Π and P, on X that are solutions to (3.3) and (3.7), respectively. Further, the eigenvalues of ΠP are positive, and they are realization invariant.*

Theorem 3.5. *(Theorem 3.4 in [13]) Let $\Sigma(A, B, C)$ be exponentially stabilizable and detectable with bounded, finite-rank input and output operators. The transfer function, $G(s)$, possesses an LQG balanced realization on the state space ℓ_2. The balanced Riccati equations, (3.3) and (3.7) based on $\hat{\Sigma}(\hat{A}, \hat{B}, \hat{C})$, both have the solution*

$$\Lambda = diag\frac{\sigma_i}{\sqrt{1-\sigma_i^2}} = diag(\mu_i), \tag{3.39}$$

where σ_i are the Hankel singular values and μ_i are the LQG characteristic values.

Theorem 3.6. *(Theorem 3.5 in [13]) The transfer functions $G_q(s)$ of the LQG balanced truncations $\Sigma(A_{11}, B_1, C_1)$ converge in the gap topology as $q \to \infty$ to $G(s)$.*

The weakness of LQG balanced truncation pointed out in [50] is that the controller reduction method will not always delete the unobservable, uncontrollable states from the LQG optimal controller, whenever they exist. Since the LQG characteristic values are not based on

controllability and observability information, the scheme will not guarantee a minimal realization of the LQG optimal controller. By minimal we mean (A, B) controllable and (A, C) observable, or another way to think about it is eliminating the unobservable, uncontrollable part of the optimal controller. We note that the balanced truncation method proposed by Moore is guaranteed to achieve the minimal realization only with a slight modification, given in [50].

The primary benefits of LQG balancing over regular balancing are $\Sigma(A, B, C)$ need not be stable, only stabilizable and detectable, and the low order model is designed around the controller which is designed using distributed parameter theory. The advantage of the latter is that the control design is based on all physical information available as opposed to eliminating the physics before control design. Additionally, if we couple LQG balancing with central control design under the assumptions described in [13], which will be satisfied for our numerical examples, we are guaranteed that the low order central controller obtained through LQG balanced truncation will stabilize the PDE system. The theorem is provided here.

Theorem 3.7. *(Theorem 5.1 in [13]) Suppose that the exponentially stabilizable and detectable state linear system $\Sigma(A, B, C)$ with finite-rank and bounded input and output operators has transfer function $G(s)$ and denote the solutions to the control and filter Riccati equations (3.3) and (3.7) by Π and P, respectively. Let $\Sigma(A^N, B^N, C^N)$ be a sequence of finite dimensional linear systems which satisfies the following assumptions:*

1. *X^N is a sequence of finite dimensional subspaces of X and Q^N is the orthogonal projection of X onto X^N such that $Q^N x \to x$ as $N \to \infty$ for all $x \in X$. Also, $B^N = Q^N B$ and $C^N = C|_{X^N}$.*

2. *$A^N : X^N \to X^N$ is a linear operator, and for each $x \in X$ there holds*

   (a) $e^{A^N t} Q^N x \to S(t)x$

   (b) $(e^{A^N t})^* Q^N x \to S(t)^* x$

   uniformly in t on bounded intervals as $N \to \infty$.

3. *(A^N, B^N) is uniformly exponentially stabilizable, i.e., there exists a uniformly bounded sequence of bounded linear operators $F^N : X^N \to \mathbb{C}^m$ such that $||e^{(A^N - B^N F^N)t} \Pi^N x||_X \leq M_1 e^{-\alpha t} ||x||_X$, for some positive constants $M_1 \geq 1$ and α.*

4. *(A^N, C^N) is uniformly exponentially detectable, i.e., there exists a uniformly bounded sequence of bounded linear operators $L^N : \mathbb{C}^k \to X^N$ such that $||e^{(A^N - C^N L^N)t} \Pi^N x||_X \leq M_2 e^{-\beta t} ||x||_X$, for some positive constants $M_2 \geq 1$ and β.*

Let Π^N and P^N be the unique stabilizing solutions to the LQG Riccati equations (3.3) and (3.7), respectively, corresponding to $\Sigma(A^N, B^N, C^N)$ with transfer function G^N. Then, given a positive $\epsilon < \sqrt{1-\sigma_1^2}$, we can always find two integers $N >> q$ such that the central controller of order q, obtained through LQG balanced truncation, stabilizes $G(s)$ with a robustness margin with respect to left coprime factor perturbations of $\epsilon - \sqrt{1-\sigma_1^2}$.

3.3.3 Effects of Balancing on Control Design

As described in Chapter 1, LQG balanced truncation is a design-then-reduce controller reduction method, and Figure 1.2 summarizes the control design process. After developing a finite dimensional approximation to the PDE, we design an LQG control for this high order approximating system, meaning we need to compute solutions to the Riccati equations in (3.3) and (3.7). Then, in order to obtain a low order controller, we balance around the Riccati operators and determine the number of states to eliminate, thereby yielding $\hat{\Sigma}(\hat{A}^q, \hat{B}^q, \hat{C}^q)$, the system on which we base a low order control design, where q represents a low order finite dimensional approximation to the PDE. We desire to design low order LQG, MinMax, and central controllers, meaning we must compute solutions to the appropriate Riccati equations based on $\hat{\Sigma}(\hat{A}^q, \hat{B}^q, \hat{C}^q)$. Since the LQG and central control designs are both based on knowing solutions to the same Riccatis used for LQG balancing, we must recompute solutions to (3.3) and (3.7), except now using low order, balanced system matrices. To save computational effort, it is possible to compute the solutions to (3.3) and (3.7), based on $\Sigma(A, B, C)$, multiply them appropriately by the LQG balancing similarity transformation, and then truncate the appropriate states of the balanced Π and P, as opposed to recomputing the Riccati solutions with low order balanced A, B, and C matrices. Here we demonstrate the appropriate way to multiply the Riccati solutions by the LQG balancing similarity transformation, S.

Suppose Π is the unique, symmetric, positive definite solution to the control Riccati equation

$$A^*\Pi + \Pi A - \Pi B R^{-1} B^* \Pi + C^* C = 0. \tag{3.40}$$

Note that balancing transforms $\Sigma(A, B, C)$ into $\hat{\Sigma}(S^{-1}AS, S^{-1}B, CS) = \hat{\Sigma}(\hat{A}, \hat{B}, \hat{C})$. We now replace A, B, and C with their balanced representations and note that Π_2 provides the unique, symmetric, positive definite solution to

$$(S^{-1}AS)^*\Pi_2 + \Pi_2(S^{-1}AS) - \Pi_2(S^{-1}B)R^{-1}(S^{-1}B)^*\Pi_2 + (CS)^*(CS) = 0, \tag{3.41}$$

which, after some algebraic manipulation, can be written as

$$A^*\hat{\Pi} + \hat{\Pi}A - \hat{\Pi}BR^{-1}B^*\hat{\Pi} + C^*C = 0, \tag{3.42}$$

where $\hat{\Pi} = (S^{-1})^*\Pi_2 S^{-1}$. That is, Π and $\hat{\Pi}$ both satisfy (3.40). Note also that $\hat{\Pi}$ is symmetric since

$$(\hat{\Pi})^* = ((S^{-1})^*\Pi_2 S^{-1})^* = (S^{-1})^*\Pi_2 S^{-1} = \hat{\Pi} \tag{3.43}$$

since Π_2 is the unique, symmetric, positive definite solution to (3.41). Therefore $\hat{\Pi} = \Pi$ and $\Pi_2 = S^*\Pi S$, thereby providing a direct way of computing Π_2 without solving (3.41).

A similar argument follows regarding the filter Riccati equation. Here we consider

$$AP + PA^* - PC^*CP + BB^* = 0, \tag{3.44}$$

where P is the unique, symmetric, positive definite solution. Then the corresponding balanced equation is

$$(S^{-1}AS)P_2 + P_2(S^{-1}AS)^* - P_2(CS)^*(CS)P_2 + (S^{-1}B)(S^{-1}B)^* = 0, \tag{3.45}$$

which can be manipulated to look like

$$A\hat{P} + \hat{P}A^* - \hat{P}C^*C\hat{P} + BB^* = 0, \tag{3.46}$$

where $\hat{P} = SP_2S^*$. Thus, both P and $\hat{P}$ satisfy (3.44). We note that $\hat{P}$ is symmetric since

$$\hat{P}^* = (SP_2S^*)^* = SP_2S^* = \hat{P}, \tag{3.47}$$

since P_2 is the unique, symmetric, positive definite solution to (3.45). Then $\hat{P} = P$ and $P_2 = S^{-1}P(S^{-1})^*$. Therefore, when computing the LQG and central controllers for the balanced system $\hat{\Sigma}(\hat{A}, \hat{B}, \hat{C})$, it is possible to multiply the solutions of the Riccati equations corresponding to $\Sigma(A, B, C)$ by the similarity transformation S in an appropriate manner, as demonstrated above, instead of recomputing the solutions to the Riccati equations.

We will now show how this is also the case when computing the solutions of (3.10), (3.12) in order to design a MinMax controller for $\hat{\Sigma}(\hat{A}, \hat{B}, \hat{C})$. Suppose Π is the unique, symmetric, positive definite solution to the control Riccati equation

$$A^*\Pi + \Pi A - \Pi[BR^{-1}B^* - \theta^2 BB^*]\Pi + C^*C = 0, \tag{3.48}$$

which can be slightly rewritten as

$$A^*\Pi + \Pi A - \Pi BR^{-1}B^*\Pi + \theta^2\Pi BB^*\Pi + C^*C = 0. \tag{3.49}$$

We now replace A, B, and C with their balanced representations and note that Π_2 is the unique, symmetric, positive definite solution to

$$\begin{aligned}(S^{-1}AS)^*\Pi_2 + \Pi_2(S^{-1}AS) - \Pi_2(S^{-1}B)R^{-1}(S^{-1}B)^*\Pi_2 \\ +\theta^2\Pi_2 S^{-1}B(S^{-1}B)^*\Pi_2 + (CS)^*(CS) = 0,\end{aligned} \tag{3.50}$$

which can be viewed as

$$A^*\hat{\Pi} + \hat{\Pi}A - \hat{\Pi}BR^{-1}B^*\hat{\Pi} + \theta^2\hat{\Pi}BB^*\hat{\Pi} + C^*C = 0, \tag{3.51}$$

where $\hat{\Pi} = (S^{-1})^*\Pi_2 S^{-1}$. Both Π and $\hat{\Pi}$ satisfy (3.48). Based on the above argument in (3.43), we know $\hat{\Pi}$ is symmetric and, in fact, $\Pi = \hat{\Pi}$.

We can make a similar argument for the filter Riccati equation

$$AP + PA^* - PC^*CP + \theta^2 PC^*CP + BB^* = 0, \tag{3.52}$$

which, after replacing A, B, and C by their balanced representations, becomes

$$\begin{aligned}(S^{-1}AS)P_2 + P_2(S^{-1}AS)^* - P_2(CS)^*(CS)P_2 \\ +\theta^2 P_2(CS)^*CSP_2 + (S^{-1}B)(S^{-1}B)^* = 0.\end{aligned} \tag{3.53}$$

After manipulation, we can write (3.53) as

$$A\hat{P} + \hat{P}A^* - \hat{P}C^*C\hat{P} + \theta^2\hat{P}C^*C\hat{P} + BB^* = 0, \tag{3.54}$$

where $\hat{P} = SP_2S^*$. From (3.47) we know $\hat{P}$ is symmetric and $P = \hat{P}$. Therefore, $P_2 = S^{-1}P(S^{-1})^*$.

We now consider how balancing affects control design, in particular, the LQG, MinMax, and central controllers. Balanced realization acts as a change of basis, so it should not inherently change the control design operators. Since this is not necessarily obvious, especially for the MinMax and central controllers, we examine the effects of balancing on control design in detail. We first consider the LQG controller. We take the control design operators given by (3.8) and replace A, B, C, Π, and P with their balanced representations to obtain the balanced control design operators

$$\begin{aligned}\hat{K} &= R^{-1}B^*\Pi S \\ \hat{F} &= S^{-1}PC^* \\ \hat{A}_c &= S^{-1}(A - BK - FC)S.\end{aligned} \tag{3.55}$$

Then for the balanced LQG controller, the corresponding closed loop PDE system is given by

$$\begin{aligned}\begin{bmatrix} \dot{x} \\ \dot{x}_c \end{bmatrix} &= \begin{bmatrix} S^{-1}AS & -S^{-1}BKS \\ S^{-1}FCS & S^{-1}A_cS \end{bmatrix}\begin{bmatrix} x \\ x_c \end{bmatrix} \\ \begin{bmatrix} x(0) \\ x_c(0) \end{bmatrix} &= \begin{bmatrix} x_0 \\ x_{c0} \end{bmatrix},\end{aligned} \tag{3.56}$$

which can be rewritten as

$$\begin{aligned}\begin{bmatrix} \dot{x} \\ \dot{x}_c \end{bmatrix} &= \begin{bmatrix} S^{-1} & 0 \\ 0 & S^{-1} \end{bmatrix} \begin{bmatrix} A & -BK \\ FC & A_c \end{bmatrix} \begin{bmatrix} S & 0 \\ 0 & S \end{bmatrix} \begin{bmatrix} x \\ x_c \end{bmatrix} \\ \begin{bmatrix} x(0) \\ x_c(0) \end{bmatrix} &= \begin{bmatrix} x_0 \\ x_{c_0} \end{bmatrix}.\end{aligned} \tag{3.57}$$

Considering only the right hand side of this expression, it is important to note how S^{-1} and S can be pulled out on the left and right, respectively, thereby leaving us with (3.6) if we multiply by S and S^{-1} on the left and right, respectively. When simulating (3.57), we can pre-multiply the initial condition vector by $\begin{bmatrix} S^{-1} & 0 \\ 0 & S^{-1} \end{bmatrix}$ to cancel $\begin{bmatrix} S & 0 \\ 0 & S \end{bmatrix}$ factored out on the right and pre-multiply the solution vector by $\begin{bmatrix} S & 0 \\ 0 & S \end{bmatrix}$ to cancel $\begin{bmatrix} S^{-1} & 0 \\ 0 & S^{-1} \end{bmatrix}$ factored out on the left. This demonstrates that balancing will not inherently alter the closed loop compensator system.

We now analyze the MinMax controller in a similar fashion. Using the control design operators from (3.14), we replace A, B, C, Π, and P with their balanced representations to obtain

$$\begin{aligned}\hat{K} &= R^{-1}B^*\Pi S \\ \hat{F} &= [I - \theta^2 S^{-1}P\Pi S]^{-1}S^{-1}PC^* \\ \hat{A}_c &= S^{-1}(A - BK)S - [I - \theta^2 S^{-1}P\Pi S]^{-1}S^{-1}PC^*CS + \theta^2 S^{-1}BB^*\Pi S.\end{aligned} \tag{3.58}$$

Upon first inspection, it might appear that since the similarity transformation, S, is contained in the inverse term of $\hat{F}$, the process of balancing en route to model reduction actually changes the control design operator. However, after manipulation, we will see that balancing does not change the control design operators. That is, balancing is indeed only a change of basis. To see this, let us consider the following algebraic manipulation of $\hat{F}$:

$$\begin{aligned}\hat{F} &= [S(I - \theta^2 S^{-1}P\Pi S)]^{-1}PC^* \\ &= [S - \theta^2 P\Pi S]^{-1}PC^* \\ &= [(I - \theta^2 P\Pi)S]^{-1}PC^* \\ &= S^{-1}[I - \theta^2 P\Pi]^{-1}PC^*.\end{aligned} \tag{3.59}$$

This alternate representation of $\hat{F}$ transforms $\hat{A}_c$ in the following way:

$$\begin{aligned}\hat{A}_c &= S^{-1}(A-BK)S - S^{-1}[I-\theta^2 P\Pi]^{-1}PC^*CS + \theta^2 S^{-1}BB^*\Pi S \\ &= S^{-1}[A-BK-[I-\theta^2 P\Pi]^{-1}PC^*C + \theta^2 BB^*\Pi]S.\end{aligned} \tag{3.60}$$

Then the closed loop PDE system for the balanced MinMax controller is given by

$$\begin{aligned}\begin{bmatrix} \dot{x} \\ \dot{x}_c \end{bmatrix} &= \begin{bmatrix} S^{-1}AS & -S^{-1}BKS \\ S^{-1}FCS & S^{-1}A_cS \end{bmatrix}\begin{bmatrix} x \\ x_c \end{bmatrix} \\ \begin{bmatrix} x(0) \\ x_c(0) \end{bmatrix} &= \begin{bmatrix} x_0 \\ x_{c_0} \end{bmatrix},\end{aligned} \tag{3.61}$$

which can be rewritten as

$$\begin{aligned}\begin{bmatrix} \dot{x} \\ \dot{x}_c \end{bmatrix} &= \begin{bmatrix} S^{-1} & 0 \\ 0 & S^{-1} \end{bmatrix}\begin{bmatrix} A & -BK \\ FC & A_c \end{bmatrix}\begin{bmatrix} S & 0 \\ 0 & S \end{bmatrix}\begin{bmatrix} x \\ x_c \end{bmatrix} \\ \begin{bmatrix} x(0) \\ x_c(0) \end{bmatrix} &= \begin{bmatrix} x_0 \\ x_{c_0} \end{bmatrix}.\end{aligned} \tag{3.62}$$

Following the same argument provided for the LQG controller, we have demonstrated that balancing does not alter the MinMax controller.

Finally, we turn our attention to the central controller. We take the control design operators given by (3.21) and replace A, B, C, Π, and P with their balanced representations to obtain the balanced control design operators

$$\begin{aligned}\hat{K} &= B^*\Pi S \\ \hat{F} &= \gamma^2[(1-\gamma^2)I + S^{-1}P\Pi S]^{-1}S^{-1}PC^* \\ \hat{A}_c &= S^{-1}(A-BR^{-1}B^*\Pi)S + \gamma^2[(1-\gamma^2)I + S^{-1}P\Pi S]^{-1}S^{-1}PC^*CS.\end{aligned} \tag{3.63}$$

Upon first inspection, it might appear that since the similarity transformation, S, is contained in the inverse term of $\hat{F}$, the process of balancing en route to model reduction actually changes the control design operator. However, after manipulation, we will see that balancing does not change the control design operators. That is, balancing is indeed only a change of basis.

To see this, let us consider the following algebraic manipulation of $\hat{F}$:

$$\begin{aligned}\hat{F} &= \gamma^2[S((1-\gamma^2)I + S^{-1}P\Pi S)]^{-1}PC^* \\ &= \gamma^2[(1-\gamma^2)S + P\Pi S]^{-1}PC^* \\ &= \gamma^2[((1-\gamma^2)I + P\Pi)S]^{-1}PC^* \\ &= \gamma^2 S^{-1}[(1-\gamma^2)I + P\Pi]^{-1}PC^*.\end{aligned} \tag{3.64}$$

This alternate representation of $\hat{F}$ transforms $\hat{A}_c$ in the following way:

$$\begin{aligned}\hat{A}_c &= S^{-1}(A - BR^{-1}B^*\Pi)S + \gamma^2 S^{-1}[(1-\gamma^2)I + P\Pi]^{-1}PC^*CS \\ &= S^{-1}[(A - BR^{-1}B^*\Pi) + \gamma^2[(1-\gamma^2)I + P\Pi]^{-1}PC^*C]S.\end{aligned} \tag{3.65}$$

Then the closed loop PDE system for the balanced central controller is given by

$$\begin{aligned}\begin{bmatrix} \dot{x} \\ \dot{x}_c \end{bmatrix} &= \begin{bmatrix} S^{-1}AS & S^{-1}BKS \\ S^{-1}FCS & S^{-1}A_cS \end{bmatrix} \begin{bmatrix} x \\ x_c \end{bmatrix} \\ \begin{bmatrix} x(0) \\ x_c(0) \end{bmatrix} &= \begin{bmatrix} x_0 \\ x_{c_0} \end{bmatrix},\end{aligned} \tag{3.66}$$

which can be rewritten as

$$\begin{aligned}\begin{bmatrix} \dot{x} \\ \dot{x}_c \end{bmatrix} &= \begin{bmatrix} S^{-1} & 0 \\ 0 & S^{-1} \end{bmatrix} \begin{bmatrix} A & BK \\ FC & A_c \end{bmatrix} \begin{bmatrix} S & 0 \\ 0 & S \end{bmatrix} \begin{bmatrix} x \\ x_c \end{bmatrix} \\ \begin{bmatrix} x(0) \\ x_c(0) \end{bmatrix} &= \begin{bmatrix} x_0 \\ x_{c_0} \end{bmatrix}.\end{aligned} \tag{3.67}$$

By the above argument this demonstrates that balancing acts only as a change of basis and does not inherently change the central controller in any way.

3.3.4 The Effect of Truncation on the Guaranteed Maximum Robustness Margin

As described in Section 3.2.3, the central controller has an associated guaranteed maximum robustness margin. This measurement is based on the maximum eigenvalue of ΠP, the

solutions to (3.3) and (3.7). Since the LQG characteristic values, $\mu_i = \sqrt{\Pi P}$, which are also based on eigenvalues of ΠP, are realization invariant, the maximum LQG characteristic value under full order balanced realization or LQG balanced realization are the same. Since LQG balanced realization leads to the decreasing ordering of the LQG characteristic values along the diagonal of the balanced Π and P operators, even when states are truncated in order to achieve a low order controller, the maximum LQG characteristic value will be the same. That is, the maximum robustness margin guaranteed by the central controller is not affected when states are truncated. However, this is not the case when we consider truncating a balanced realization. That is, the guaranteed maximum robustness margin for a truncated balanced realization will be different than the guaranteed maximum robustness margin for a full order balanced realization.

Chapter 4

Nonlinear Cable Mass System

To study the effects of regular and LQG balancing, the cable-mass system (CM) described in [8, 38] is used as an example. This model can be viewed as an elastic cable fixed at one end and attached to a mass at the other end. The mass is suspended by a spring, which contains nonlinear stiffening terms and is being forced by a sinusoidal disturbance.

In particular, a wave equation with Kelvin-Voigt damping models the elastic cable for $0 < s < \ell$, and a Duffing's type equation models the oscillator for $s = \ell$. The equations governing this system are as follows:

$$\rho \frac{\partial^2}{\partial t^2} w(t,s) - \frac{\partial}{\partial s}\left[\tau \frac{\partial}{\partial s} w(t,s) + \gamma \frac{\partial^2}{\partial t \partial s} w(t,s)\right] = 0, \tag{4.1}$$

for $0 < s < \ell,\ t > 0$, and

$$m \frac{\partial^2}{\partial t^2} w(t,\ell) + \tau \frac{\partial}{\partial s} w(t,\ell) + \gamma \frac{\partial^2}{\partial t \partial s} w(t,\ell) + \alpha_1 w(t,\ell) + \alpha_3 [w(t,\ell)]^3 = \eta(t) + u(t), \tag{4.2}$$

with boundary condition

$$w(t,0) = 0, \tag{4.3}$$

where $w(t,s)$ represents the displacement of the cable at time t and position s, $w(t,\ell)$ gives the position of the mass at time t, ρ and m are the densities of the cable and mass respectively, τ is tension in the cable, and γ is the coefficient of the damping terms. The spring's stiffening terms have coefficients of α_1 and α_3, with α_3 being associated with the nonlinear effects in the spring. A disturbance enters the system through $\eta(t)$, while the control enters the system through $u(t)$. This view of the cable mass system can be seen in Figure 4.1. We assume the control acts exclusively on the mass, and the only available measured information is the

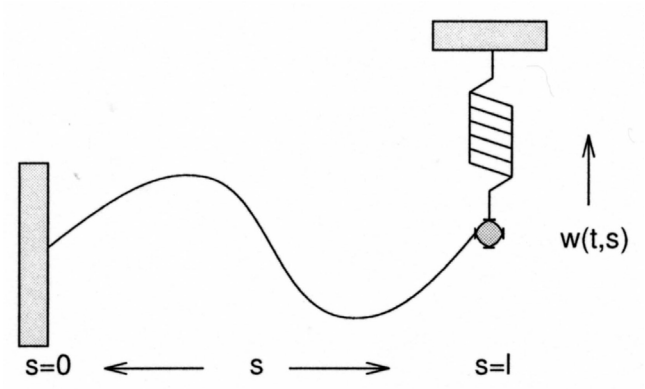

Figure 4.1: Cable-mass system.

position and velocity of the mass. These two observations take the form

$$\begin{aligned} y_1(t) &= w(t,\ell), \\ y_2(t) &= \frac{\partial}{\partial t} w(t,\ell). \end{aligned} \tag{4.4}$$

Much of the following discussion is detailed in [8], but we include it here for completeness. We use PDE framework to formulate (4.1) and (4.2) as a first order system. We now define the operators, the state space, and our choice of an inner product on the state space.

In order to write the cable mass problem as an abstract differential equation, similar to (2.1), we make the following definitions, taken from [15]. Let X be an arbitrary Banach space and f a function with $f : \mathbb{R} \to X$.

Definition 4.1. *We say f is **differentiable** if f is Frechet differentiable, that is if there exists a $w \in X$ such that*

$$\lim_{h \to 0} \frac{||f(t+h) - f(t) - wh||_X}{|h|} = 0. \tag{4.5}$$

Then define $f'(t) = w$.

Definition 4.2. *The function $f' : \mathbb{R} \to X$ is defined by $f' : t \to f'(t)$ for each t. Higher order derivatives $f^{(k)}$ are defined similarly.*

These ideas provide the basis for the following definitions. Note that we take the same approach in Chapters 5 and 6, for the Klein-Gordon and Euler-Bernoulli beam equations, respectively. From this point forward, it is understood that rewriting these PDEs as abstract

differential equations relies upon the idea of Frechet derivatives. Let $\omega(t,s) = d(s)$ be the position of the cable at s, $\omega(t,\ell) = d(\ell) = d_\ell$ be the position of the mass, $\omega_t(t,s) = v(s) = \dot{d}(s)$ be the velocity of the cable at s, and $\omega_t(t,\ell) = v(\ell) = v_\ell$ be the velocity of the mass. Now (4.1, 4.2) can be written as a first order system of the form

$$\begin{aligned} \dot{x}(t) &= Ax(t) + \mathcal{N}(x(t)) + Bu(t) + D\eta(t), \qquad x(0) = x_0 \\ y(t) &= Cx(t), \end{aligned} \tag{4.6}$$

such that at time t, the state $x(t) = [\omega(t,\cdot),\ \omega(t,\ell),\ \dot{\omega}(t,\cdot),\ \dot{\omega}(t,\ell)]^T \in X = H_L^1 \times \mathbb{R} \times L_2 \times \mathbb{R}$, the control $u(t) \in U = \mathbb{R}$, and the state measurement $y(t) = [y_1(t), y_2(t)]^T \in Y = \mathbb{R}^2$. We take the inner product on X to be

$$\begin{aligned} \langle [d(\cdot), d_\ell, v(\cdot), v_\ell]^T, [\hat{d}(\cdot), \hat{d}_\ell, \hat{v}(\cdot), \hat{v}_\ell]^T \rangle = \tau \int_0^\ell \frac{\partial}{\partial s} d(s) \frac{\partial}{\partial s} \hat{d}(s)\ ds + \alpha_1 d_\ell \hat{d}_\ell \\ + \rho \int_0^\ell v(s)\hat{v}(s)\ ds + m v_\ell \hat{v}_\ell. \end{aligned} \tag{4.7}$$

Denoting the "evaluation operator" by δ_ℓ, defined on $H^1(0,\ell)$ by $\delta_\ell(\phi(s)) = \phi(\ell)$, we can define the linear operator A on the domain $D(A) \subseteq X$ by

$$\begin{aligned} D(A) = \Bigg\{ & x = [d, d_\ell, v, v_\ell]^T \in X : d, v \in H_L^1, \\ & \left[\frac{\tau}{\rho} \frac{d}{ds} d + \frac{\gamma}{\rho} \frac{d}{ds} v \right] \in H^1, d(\ell) = d_\ell, v(\ell) = v_\ell \Bigg\}, \end{aligned} \tag{4.8}$$

and

$$Ax = \left[v, v_\ell, \frac{d}{ds} \left[\frac{\tau}{\rho} \frac{d}{ds} d + \frac{\gamma}{\rho} \frac{d}{ds} v \right], -\delta_\ell \left[\frac{\tau}{m} \frac{d}{ds} d + \frac{\gamma}{m} \frac{d}{ds} v \right] - \frac{\alpha_1}{m} d_\ell \right]^T. \tag{4.9}$$

We define the control input, disturbance input, and output, or state measurement, operators, respectively, by

$$B = D = \left[0, 0, 0, \frac{1}{m} \right]^T \text{ and } C = \begin{bmatrix} 0 & 1 & 0 & 0 \\ 0 & 0 & 0 & 1 \end{bmatrix}. \tag{4.10}$$

The nonlinear operator $\mathcal{N}$ is defined on X as

$$\mathcal{N}(s) = \mathcal{N}\left([d(\cdot), d_\ell, v(\cdot), v_\ell]^T \right) = \left[0, 0, 0, -\frac{\alpha_3}{m} [d_\ell]^3 \right]^T = [0, 0, 0, \mathcal{N}_0(d_\ell)]^T, \tag{4.11}$$

where $\mathcal{N}_0 : \mathbb{R} \to \mathbb{R}$ is continuous. It follows from the proofs in [8, 12] that A, as given by (4.9) and established in this framework, generates an exponentially stable analytic semigroup. This is stronger than an exponentially stable C_0-semigroup.

We now consider the weak form of CM in order to develop a Galerkin finite element approximation of the problem. We want to find an $\omega(s) \in V = \{\varphi = [\varphi_1(\cdot), \varphi_2]^T \in E : \varphi_1(\ell) = \varphi_2\} \subset E = H_L^1(0,\ell) \times \mathbb{R}$ such that for all $\varphi \in V$

$$\begin{aligned} &\int_0^\ell \rho\ddot{\omega}(t,s)\varphi_1(s)\ ds - \int_0^\ell \tau\omega''(t,s)\varphi_1(s)\ ds - \int_0^\ell \gamma\dot{\omega}''(t,s)\varphi_1(s)\ ds \\ &+m\ddot{\omega}(t,\ell)\varphi_2 - \tau\omega'(t,\ell)\varphi_2 - \gamma\dot{\omega}'(t,\ell)\varphi_2 + \alpha_1\omega(t,\ell)\varphi_2 + \alpha_3\left[\omega(t,\ell)\right]^3\varphi_2 \\ &= \eta(t)\varphi_2 + u(t)b(s)\varphi_2. \end{aligned} \tag{4.12}$$

After integrating by parts, we have

$$\begin{aligned} &\int_0^\ell \rho\ddot{\omega}(t,s)\varphi_1(s)\ ds + \int_0^\ell \tau\omega'(t,s)\varphi_1'(s)\ ds + \int_0^\ell \gamma\dot{\omega}'(t,s)\varphi_1'(s)\ ds \\ &+m\ddot{\omega}(t,\ell)\varphi_2 - \tau\omega'(t,\ell)\varphi_2 - \gamma\dot{\omega}'(t,\ell)\varphi_2 + \tau\omega'(t,\ell)\varphi_2 + \gamma\dot{\omega}'(t,\ell)\varphi_2 \\ &+\alpha_1\omega(t,\ell)\varphi_2 + \alpha_3\left[\omega(t,\ell)\right]^3\varphi_2 = \eta(t)\varphi_2 + u(t)b(s)\varphi_2, \end{aligned} \tag{4.13}$$

since $\varphi_1(\ell) = \varphi_2$. We now choose a basis $\{e_i\}_{i=1}^N$ for the approximating space $V^N \subseteq V$, where N corresponds to the number of gridpoints. In particular, the state is approximated by a linear combination of linear B-splines, satisfying $b_i(0) = 0$, of the form

$$e_i = \begin{bmatrix} b_i(s) \\ b_i(\ell) \end{bmatrix} \text{ for } i = 1, \ldots, N. \tag{4.14}$$

The N^{th} linear spline is the only one which is nonzero at $s = \ell$. Thus, the second entry of the basis vectors is zero for $i = 1, \ldots, N-1$ and one for $i = N$. We approximate the state as

$$\begin{bmatrix} \omega(t,s) \\ \omega(t,\ell) \end{bmatrix} \approx \begin{bmatrix} \omega^N(t,s) \\ \omega^N(t,\ell) \end{bmatrix} = \sum_{i=1}^N c_i(t)e_i(s) = \begin{bmatrix} \sum_{i=1}^N c_i(t)b_i(s) \\ c_N(t) \end{bmatrix}. \tag{4.15}$$

Then (4.13) becomes

$$\begin{aligned} &\int_0^\ell \rho\ddot{\omega}^N(t,s)\varphi_1(s)\ ds + \int_0^\ell \tau\omega'^N(t,s)\varphi_1'(s)\ ds + \int_0^\ell \gamma\dot{\omega}'^N(t,s)\varphi_1'(s)\ ds \\ &+m\ddot{\omega}^N(t,\ell)\varphi_2 + \alpha_1\omega^N(t,\ell)\varphi_2 + \alpha_3\left[\omega^N(t,\ell)\right]^3\varphi_2 \\ &= \left[\eta(t) + u(t)b(s)\right]\varphi_2, \end{aligned} \tag{4.16}$$

or equivalently,

$$\int_0^\ell \rho \sum_{i=1}^N \ddot{c}_i(t) b_i(s) \varphi_1(s)\, ds + \int_0^\ell \tau \sum_{i=1}^N c_i(t) b_i'(s) \varphi_1'(s)\, ds$$

$$+ \int_0^\ell \gamma \sum_{i=1}^N \dot{c}_i(t) b_i'(s) \varphi_1'(s)\, ds + m\ddot{c}_N(t) b_i(\ell)\varphi_2 + \alpha_1 c_N(t) b_i(\ell)\varphi_2 \tag{4.17}$$

$$+\alpha_3 \left[c_N(t) b_i(\ell)\right]^3 \varphi_2 = \left[\eta(t) + u(t) b(s)\right] \varphi_2.$$

We let $\varphi_1(s)$ range over $b_j(s)$ for $j = 1, \ldots, N$ and φ_2 range over $b_j(\ell)$ for $j = 1, \ldots, N$, thus yielding

$$\int_0^\ell \rho \sum_{i=1}^N \ddot{c}_i(t) b_i(s) b_j(s)\, ds + \int_0^\ell \tau \sum_{i=1}^N c_i(t) b_i'(s) b_j'(s)\, ds$$

$$+ \int_0^\ell \gamma \sum_{i=1}^N \dot{c}_i(t) b_i'(s) b_j'(s)\, ds + m\ddot{c}_N(t) b_i(\ell) b_j(\ell) + \alpha_1 c_N(t) b_i(\ell) b_j(\ell) \tag{4.18}$$

$$+\alpha_3 \left[c_N(t) b_i(\ell)\right]^3 b_j(\ell) = \left[\eta(t) + u(t) b(s)\right] b_j(\ell).$$

We can rewrite (4.18) as a matrix equation

$$\begin{gathered} M_0 \ddot{c}(t) + D_0 \dot{c}(t) + K_0 c(t) + F_0(c(t)) = B_0 u(t) + G_0 \eta(t), \\ c(0) = c_0, \qquad \dot{c}(0) = c_1, \end{gathered} \tag{4.19}$$

where $c(t) = [c_1(t), \ldots, c_N(t)]^T$, M_0 is the mass matrix, D_0 is the damping matrix, K_0 is the stiffness matrix, $F_0(c(t))$ contains the nonlinear terms, B_0 is the input matrix, G_0 is the disturbance matrix, all defined by the following:

$$\begin{aligned} [M_0]_{i,j} &= \int_0^\ell \rho b_i(s) b_j(s)\, ds + m b_i(\ell) b_j(\ell), \qquad i,j = 1, \ldots, N \\ [D_0]_{i,j} &= \int_0^\ell \gamma b_i'(s) b_j'(s)\, ds, \qquad i,j = 1, \ldots, N \\ [K_0]_{i,j} &= \int_0^\ell \tau b_i'(s) b_j'(s)\, ds + \alpha_1 b_i(\ell) b_j(\ell) \qquad i,j = 1, \ldots, N \\ F_0(c(t)) &= \alpha_3 \left[\omega_N\right]^3 \\ B_0 = G_0 &= \left[b_1(\ell), \ldots, b_N(\ell)\right]^T. \end{aligned} \tag{4.20}$$

Convert (4.19) into a first order system by defining $x_1(t) = c(t)$ and $x_2(t) = \dot{x}_1(t) = \dot{c}(t)$, thereby yielding

$$\begin{bmatrix} \dot{x}_1(t) \\ \dot{x}_2(t) \end{bmatrix} = \begin{bmatrix} 0 & I \\ -M_0^{-1}K_0 & -M_0^{-1}D_0 \end{bmatrix} \begin{bmatrix} x_1(t) \\ x_2(t) \end{bmatrix}$$

$$+ \begin{bmatrix} 0 \\ M_0^{-1}B_0 \end{bmatrix} u(t) + \begin{bmatrix} 0 \\ M_0^{-1}G_0 \end{bmatrix} \eta(t) - \begin{bmatrix} 0 \\ M_0^{-1}F_0(\omega(t)) \end{bmatrix}, \tag{4.21}$$

$$x(0) = x_0,$$

where $x = [x_1(t), x_2(t)]^T = \left[x_1(t), \frac{d}{dt}x_1(t)\right]^T$, with output equation

$$y(t) = Cx(t) \in \mathbb{R}^2, \tag{4.22}$$

where

$$C = \begin{bmatrix} 0_{1\times N-1} & 1 & 0_{1\times N-1} & 0 \\ 0_{1\times N-1} & 0 & 0_{1\times N-1} & 1 \end{bmatrix}. \tag{4.23}$$

This framework now provides the basis for implementing control design techniques discussed in Chapter 3.

We now turn our attention to numerical results. We take the values of our system parameters the same as is found in [8], and they are given in the following table: Additionally,

ρ	τ	γ	m	ℓ	α_1	α_3
1.0	1.0	.005	1.5	2	.01	3

Table 4.1: System Parameters

we choose $\eta(t)$, the system disturbance, to be $\cos(2.233181t)$. Note that we assume the sensor disturbance to be zero. This disturbance choice was motivated by discussion in [8]. In particular, the frequency for the disturbance is the sum of 0.480208 and 1.752973, the lowest two frequencies of the uncontrolled system. By choosing this sum, we seek to achieve "combination resonance," as described in [39], and excite the natural chaotic structure of Duffing's equation. Similar numerical results can be found in [11].

4.1 Numerical Results with $R = 1$

For all numerical results in this section we take $N = 80$. Gain convergence and convergence of our Galerkin finite element scheme is achieved at $N = 40$. Additionally, we take the

MinMax parameter, θ, to be as large as possible such that the conditions described in Section 3.2.2 are satisfied. Specifically, we are able to take $\theta = .45$. The results we will discuss are singular values, uncontrolled simulations, functional gains, controlled simulations, and finally, controller robustness.

4.1.1 Uncontrolled Results

Figure 4.2 shows the Hankel singular values on the left and the LQG characteristic values on the right. Table 4.2 indicates the number of states holding 95% and 99% of the information in the singular values. We provide this information since those who typically use POD for low order controller design often refer to values of this nature in order to determine the order of the controller.

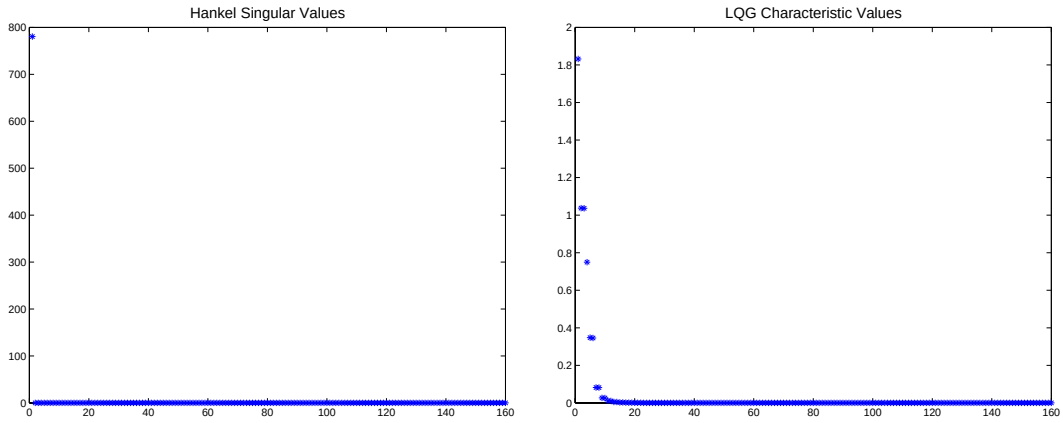

Figure 4.2: Hankel Singular Values (left), LQG Characteristic Values (right)

	Values needed for	
	95% significance	99% significance
Hankel singular values	1	1
LQG characteristic values	6	10

Table 4.2: Values needed to retain 95% and 99% information.

Even though 6 states are required to maintain 95% of the information, when using MinMax or central control design, our numerical results will show that we can obtain an effective low order controller with only one state. The low order controller performance seems to

be more dependent on the type of control design used as opposed to the number of states retained in the low order state estimate. This is not to say that the low order controllers are outperforming the full order controllers. Rather, our observation has been that increasing the order of the reduced controller tends to not enhance performance.

To obtain a solution to the system, we choose initial conditions of the form

$$\left[x(0,s), \frac{\partial}{\partial t}x(0,s)\right] = [s,-2], \qquad \left[x_c(0,s), \frac{\partial}{\partial t}x_c(0,s)\right] = [.5s,0]. \tag{4.24}$$

The uncontrolled position and velocity states, $\omega(t,s)$ and $\omega_t(t,s)$ respectively, as well as the mass and midcable phase portraits, are found in Figure 4.3. Quite obviously, there is a great deal of oscillation in the states and non-periodic behavior in the phase portraits. After we apply a control, the ideal scenario would be that the position and velocity states tend to zero and the mass and midcable phase portraits would tend to $[0,0]^T$ since $[0,0]^T$ is an exponentially stable equilibrium for the cable mass system. Note that $[0,0]^T$ is an exponentially stable equilibrium regardless of the disturbance entering our system. Recall that the exponential stability of $[0,0]^T$ is based on the A operator defined by (4.8) and (4.9).

4.1.2 Controlled Results

Before examining the controlled simulation plots, we want to look at the functional gains plots, as discussed in Section 3.2.1, in order to visually verify that we have gain convergence. Figures 4.4, 4.5, and 4.6 show the full order and reduced order functional gains for the LQG, MinMax, and central controllers, respectively. Since there is only one actuator in the system, see (4.10), there will only be one position and one velocity gain for each controller type. As we can see from these plots, it appears that we have functional gain convergence for all three controllers with both balanced truncation methods. For all three sets of plots, the color legend is as follows: $N = 10$ cyan, $N = 20$ blue, $N = 40$ green, and $N = 80$ red.

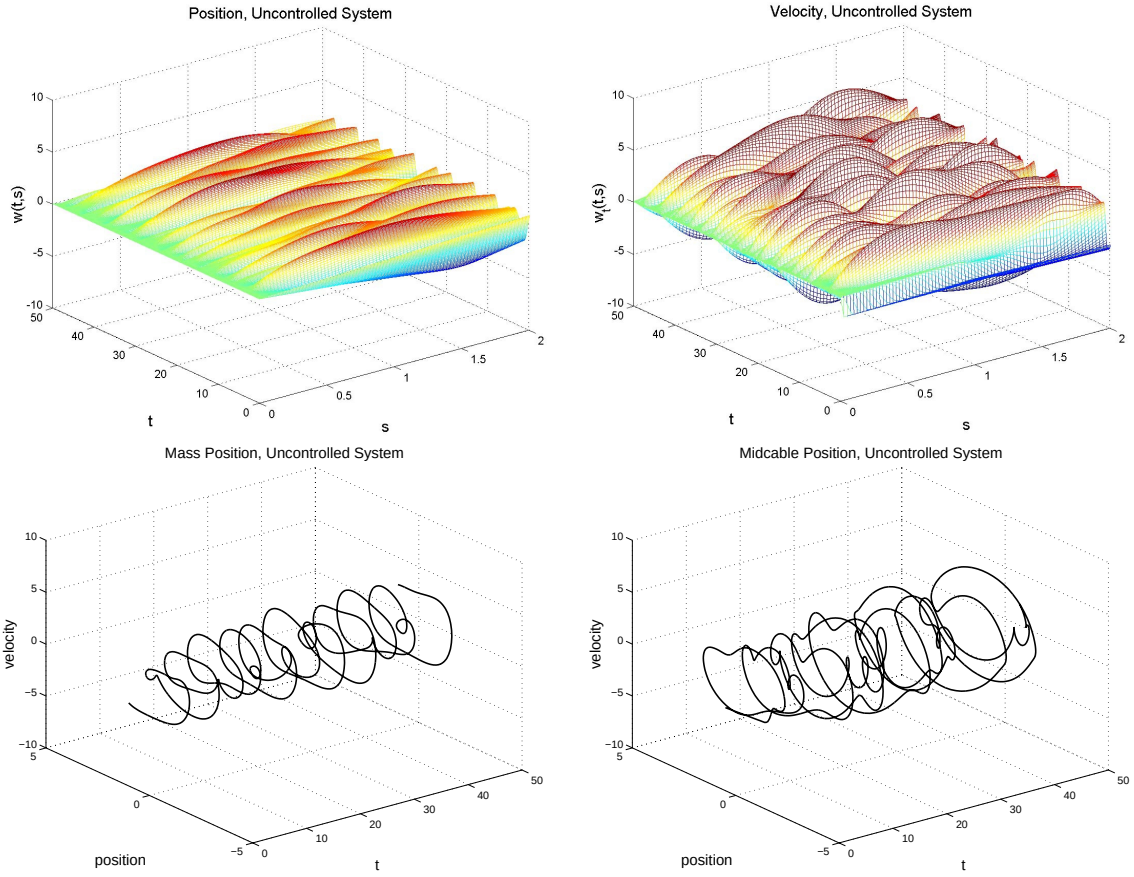

Figure 4.3: Uncontrolled: Position State (top left), Velocity State (top right), Mass Phase Portrait (bottom left), and Midcable Phase Portrait (bottom right)

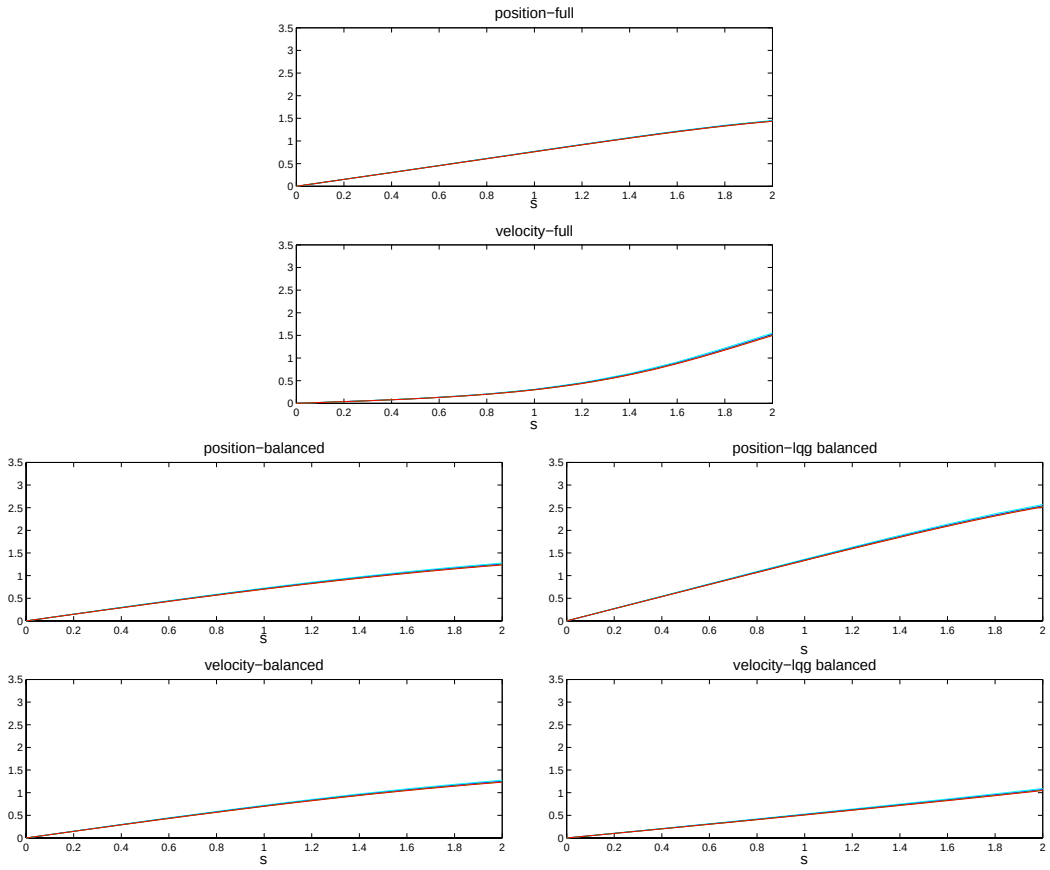

Figure 4.4: LQG Controller: Full Order Functional Gains (top), Reduced Order Balanced Gains (bottom left), Reduced Order LQG Balanced Gains (bottom right)

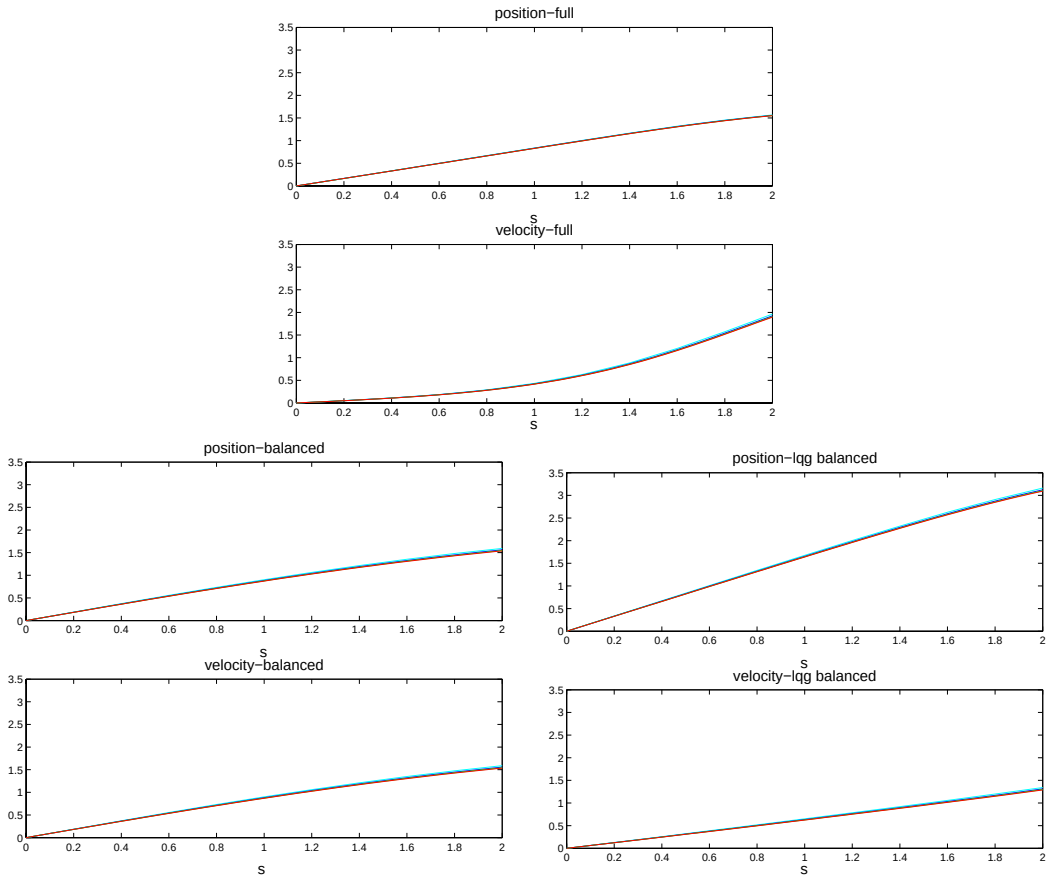

Figure 4.5: MinMax Controller: Full Order Functional Gains (top), Reduced Order Balanced Gains (bottom left), Reduced Order LQG Balanced Gains (bottom right)

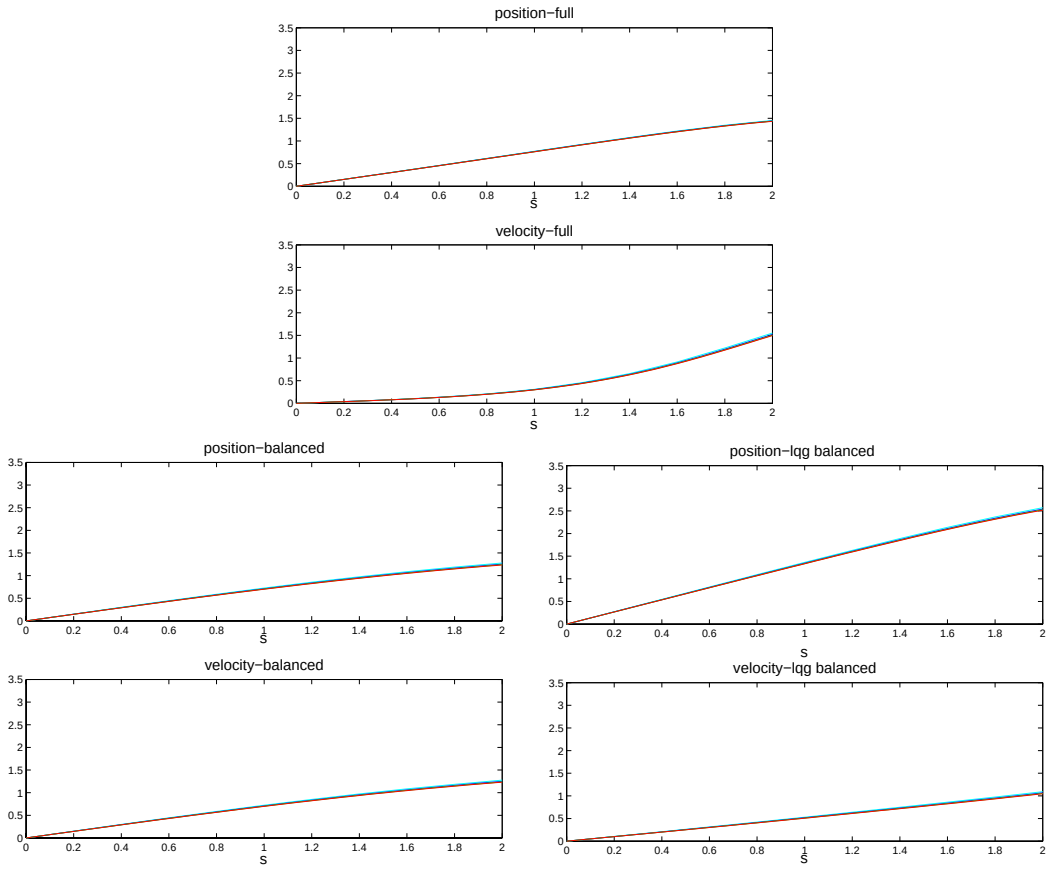

Figure 4.6: Central Controller: Full Order Functional Gains (top), Reduced Order Balanced Gains (bottom left), Reduced Order LQG Balanced Gains (bottom right)

We now look at simulations where the control is provided by a full order compensator. The application of the LQG, MinMax, and central controllers are contained in Figures 4.7, 4.8, and 4.9, respectively.

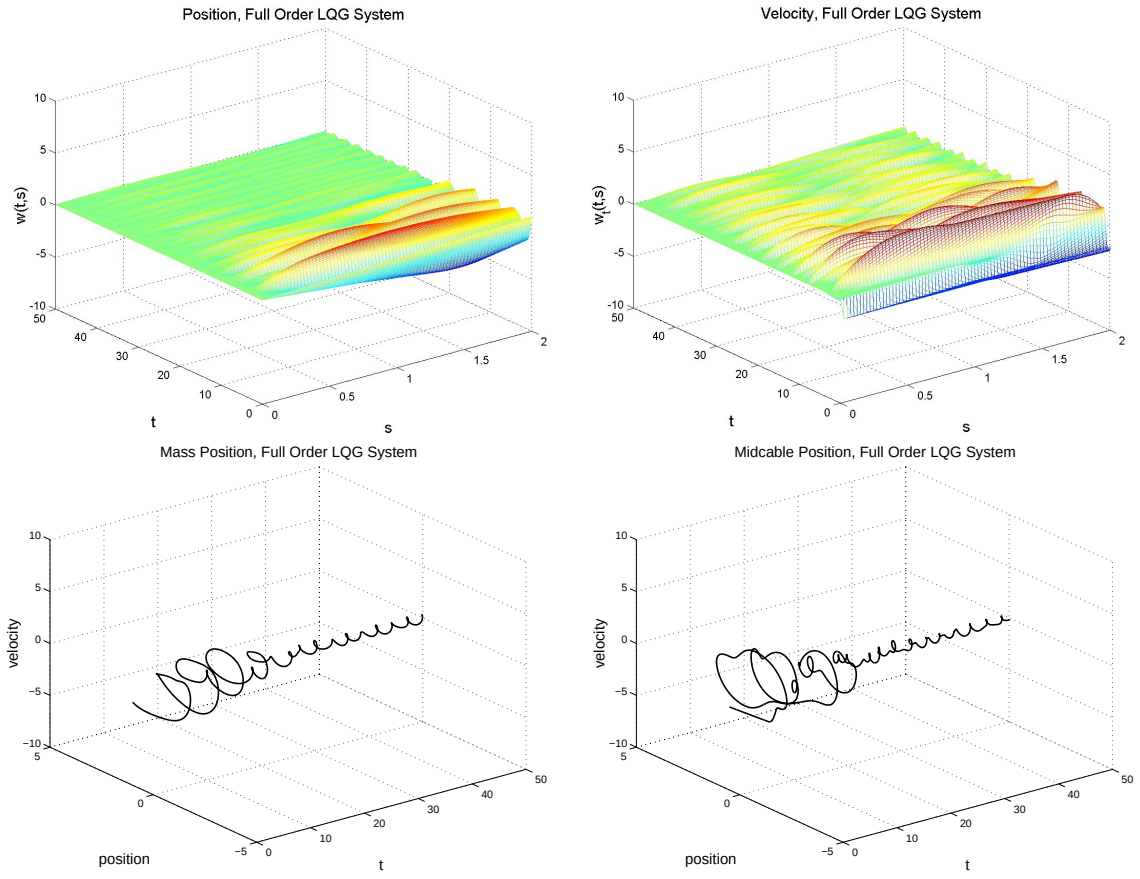

Figure 4.7: LQG Controller: Full Order Position State (top left), Full Order Velocity State (top right), Full Order Mass Phase Portrait (bottom left), and Full Order Midcable Phase Portrait (bottom right)

We first note that all three controllers do a nice job at driving the position and velocity states toward zero, even though none of them are able to regulate the phase portraits to $[0, 0]^T$. However, this is not surprising given that we chose a disturbance, $\eta(t)$, that would particularly excite the inherent chaotic structure of Duffing's equation. This observation is consistent with the results in [8], where LQG and MinMax controllers are applied to this system.

Although all three controllers regulate the system adequately, there are visible differences in their performances. For example, the MinMax controller results in lower amplitudes of the

position and velocity states, as compared with the LQG and central controllers. Additionally, the MinMax controller forces the phase portraits to be closer to $[0, 0]^T$, both sooner and with more periodic behavior, than either of the other controllers over the entire time interval. The full order MinMax controller outperforms both the LQG and central controllers. Based on amplitude of the states and phase portrait information, we must also note that the central controller does better than the LQG controller.

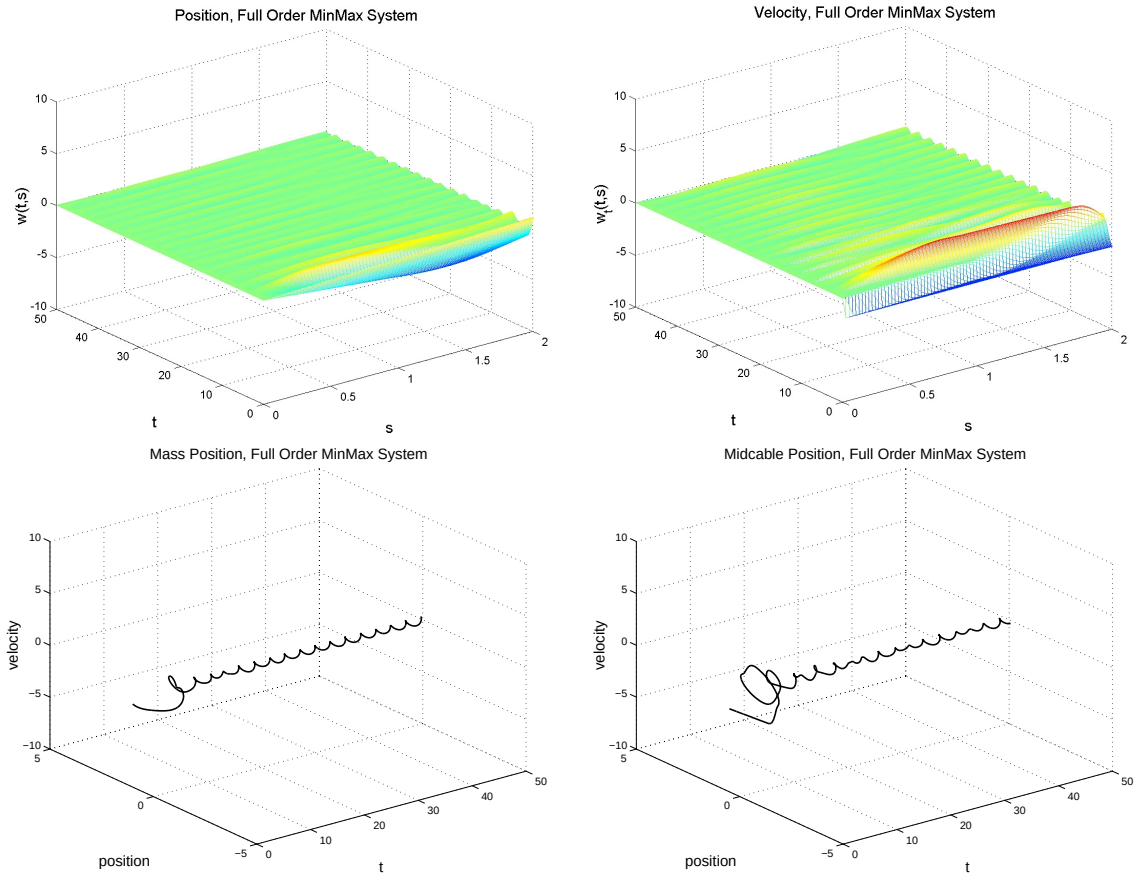

Figure 4.8: MinMax Controller: Full Order Position State (top left), Full Order Velocity State (top right), Full Order Mass Phase Portrait (bottom left), and Full Order Midcable Phase Portrait (bottom right)

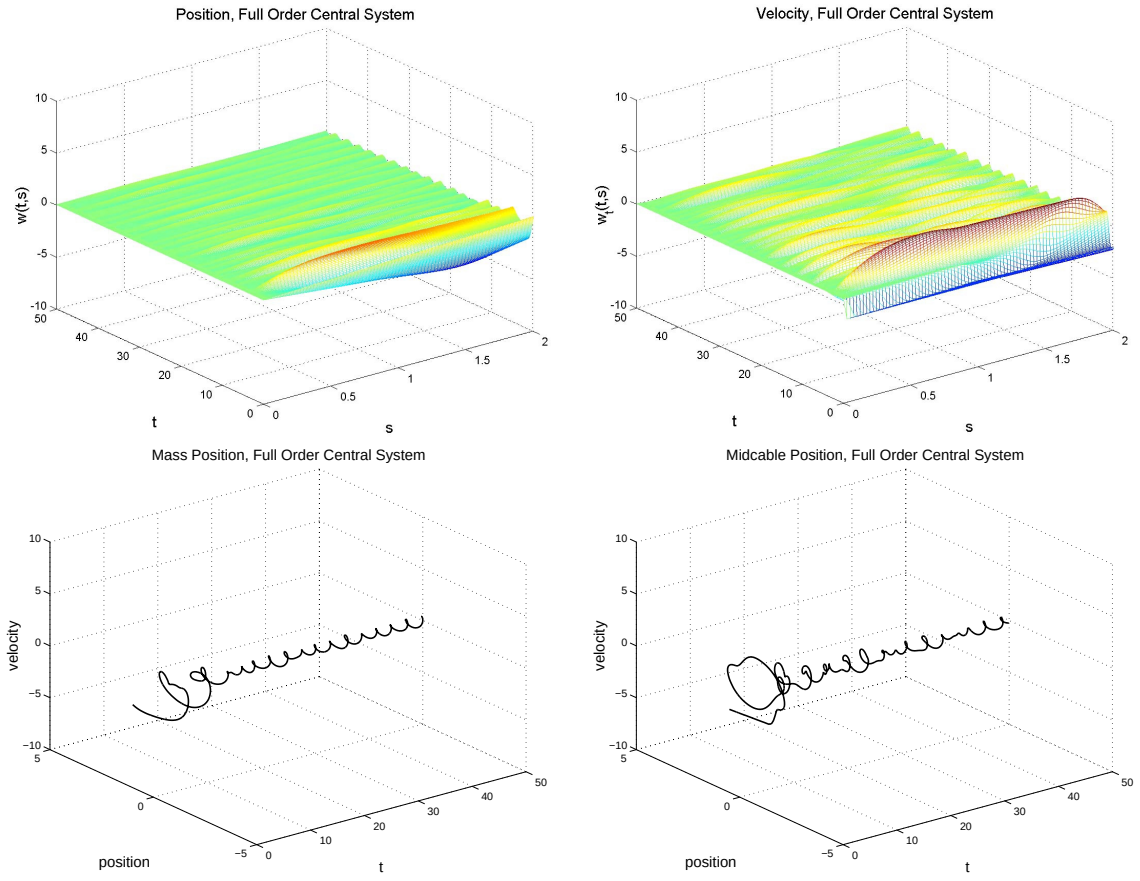

Figure 4.9: Central Controller: Full Order Position State (top left), Full Order Velocity State (top right), Full Order Mass Phase Portrait (bottom left), and Full Order Midcable Phase Portrait (bottom right)

However, system performance is not the only issue of concern. In a practical application, the control input, $u(t) = -Kx_c$ for the LQG or MinMax controller and $u(t) = Kx_c$ for the central controller, does not have an unlimited power supply. For example, if the full order MinMax compensator system is outperforming the LQG and central controller compensator systems because it requires much more control effort than the LQG and central controllers, then this is a drawback, of which we must be made aware. For this reason, we plot the three controllers to examine the control effort required by each. The plots are contained in Figure 4.10, which indicates that the MinMax controller requires more control effort than the LQG or central controllers. However, the effort required by the three controllers is on the same order of magnitude, so there is not a significant difference between them regarding this issue.

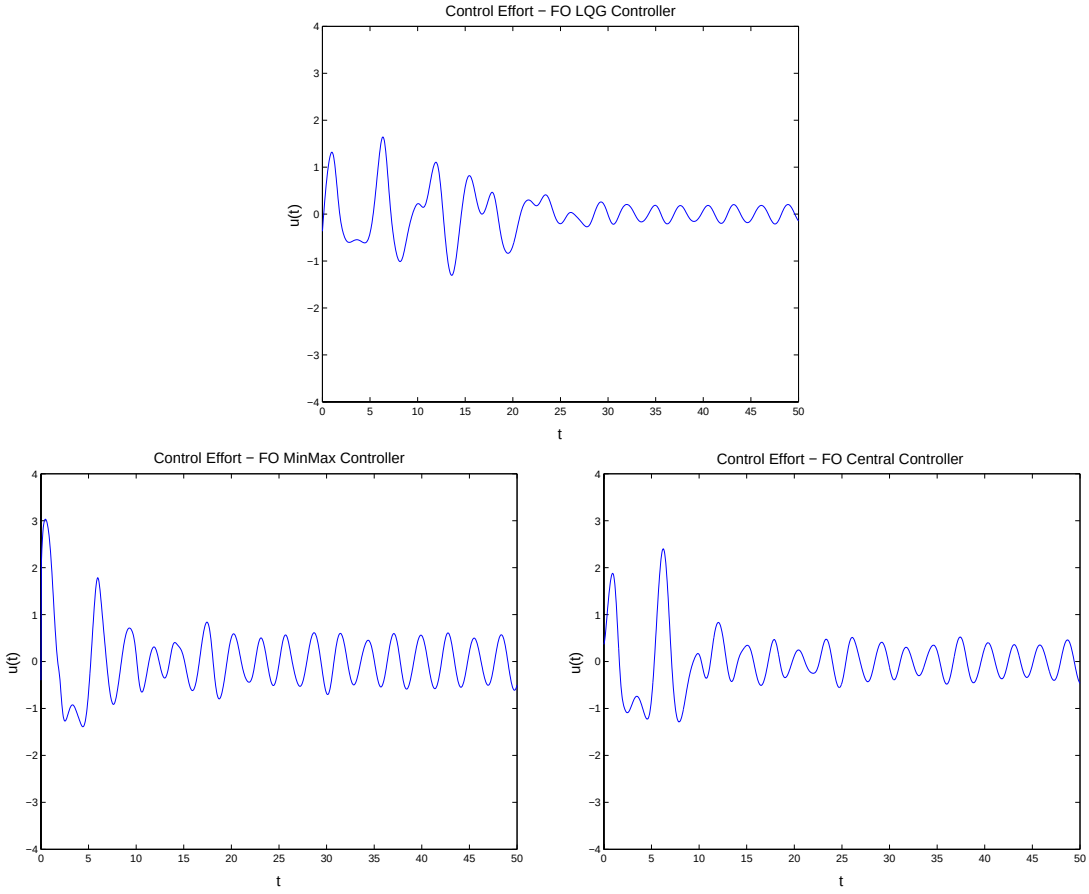

Figure 4.10: Control Effort: Full Order LQG (top), Full Order MinMax (bottom left), Full Order Central (bottom right)

As we have already discussed, in order to achieve real time control, we typically need to

turn to reduced order controllers. Thus, we now focus our attention on low order controllers designed using balanced truncation and LQG balanced truncation. In particular, we design first order controllers, i.e., $q = 1$ in (3.28). Our approach will be to compare low order LQG controllers obtained through these two reduction methods, low order MinMax controllers, and then low order central controllers. We will then compare the performance of each control design in this low order setting.

First Order Controllers

Figures 4.11 and 4.12 provide the behavior of the system when low order LQG controllers obtained through balanced truncation and LQG balanced truncation, respectively, are applied.

As is evident from the figures, the balanced LQG controller outperforms the LQG balanced LQG controller. To be clear, the phase, "LQG balanced LQG controller" refers to a low order LQG controller obtained through LQG balanced truncation. Although not as well as any of the full order controllers, the balanced LQG controller forces the states toward zero and the phase portraits toward $[0, 0]^T$. However, the performance of the LQG balanced LQG controller is terrible. In fact, the system does not even look stable, but, as we will see in Section 4.1.3, examining the eigenvalues indicate that the system is stable. The amplitude of the states is larger than even the uncontrolled states, and the mass and midcable positions appear to be moving *away* from the equilibrium as opposed to toward it. This is certainly not a favorable result, but we should not be too discouraged, or even surprised. As discussed in Chapter 3, a reduced order system can be thought of as a perturbed system of the original one. Also, from [17] we know that the LQG controller is not robust, so it should not be surprising when it does not perform well when used as a low order control design.

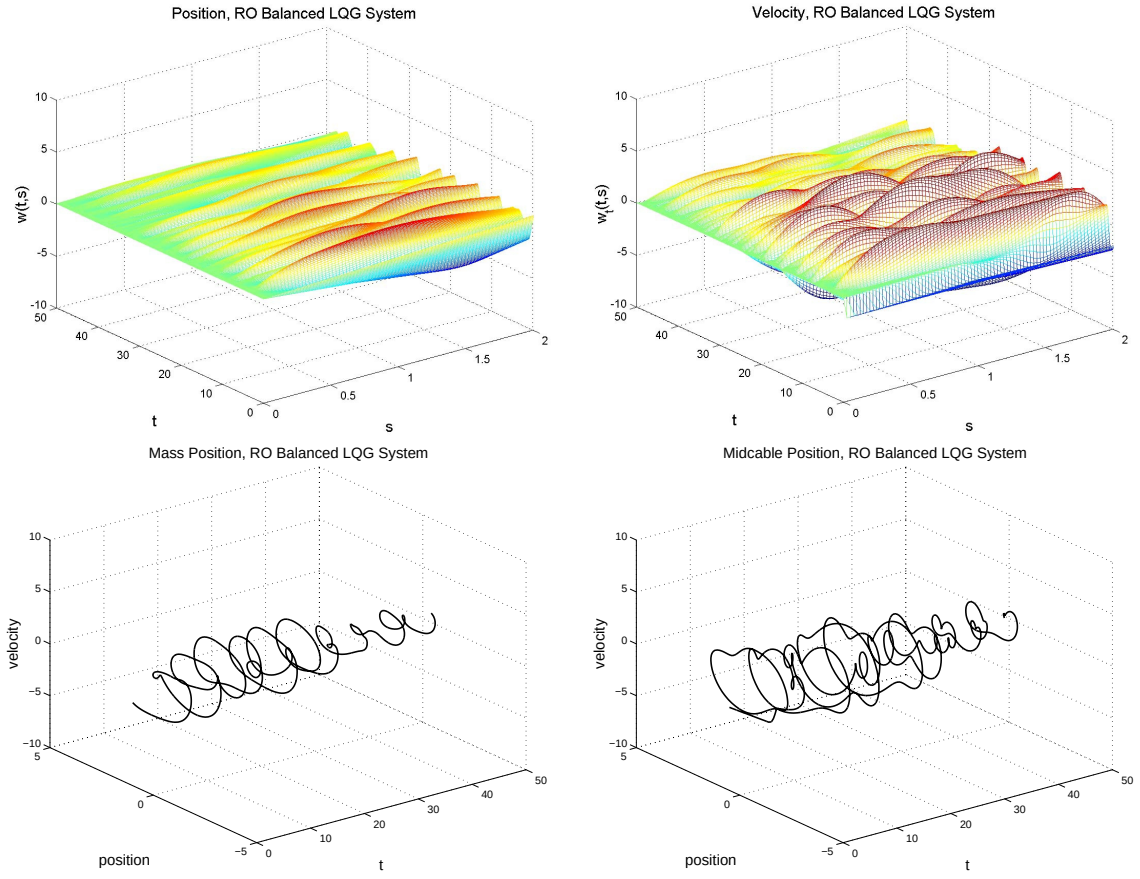

Figure 4.11: Balanced LQG Controller: Reduced Order Position State (top left), Reduced Order Velocity State (top right), Reduced Order Mass Phase Portrait (bottom left), and Reduced Order Midcable Phase Portrait (bottom right)

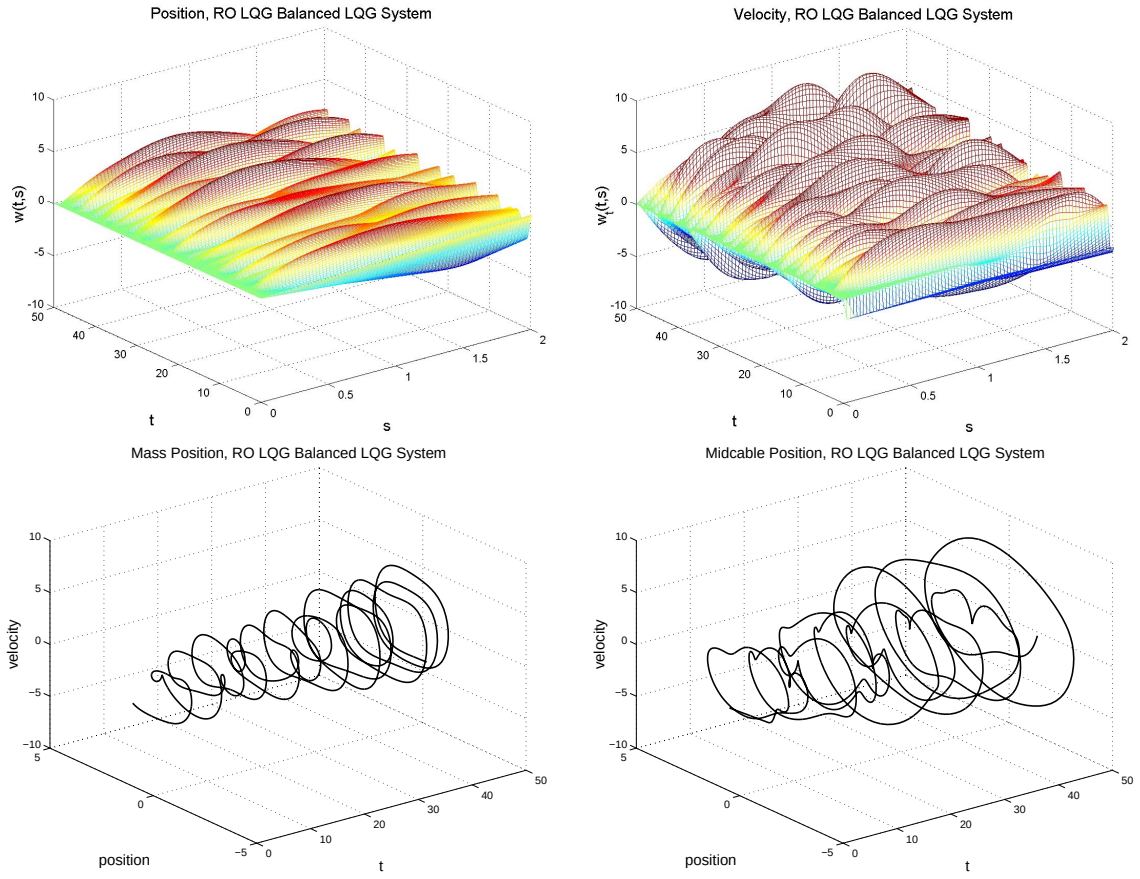

Figure 4.12: LQG Balanced LQG Controller: Reduced Order Position State (top left), Reduced Order Velocity State (top right), Reduced Order Mass Phase Portrait (bottom left), and Reduced Order Midcable Phase Portrait (bottom right)

We now consider the first order MinMax controllers, where the systems with these controllers are found in Figures 4.13 and 4.14. Both controllers perform superbly, each regulating just as well as the full order MinMax controller found in Figure 4.8. In particular, there is virtually no visible difference between the two controller results to the naked eye.

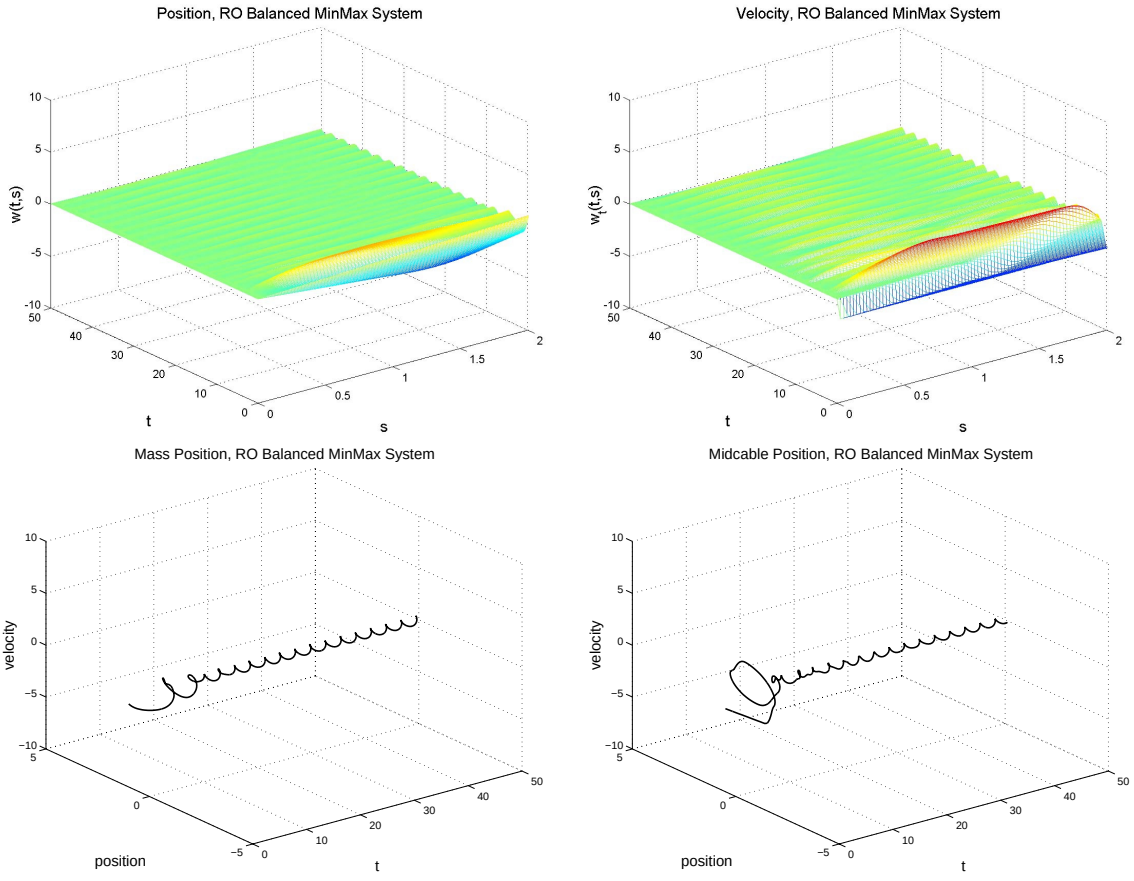

Figure 4.13: Balanced MinMax Controller: Reduced Order Position State (top left), Reduced Order Velocity State (top right), Reduced Order Mass Phase Portrait (bottom left), and Reduced Order Midcable Phase Portrait (bottom right)

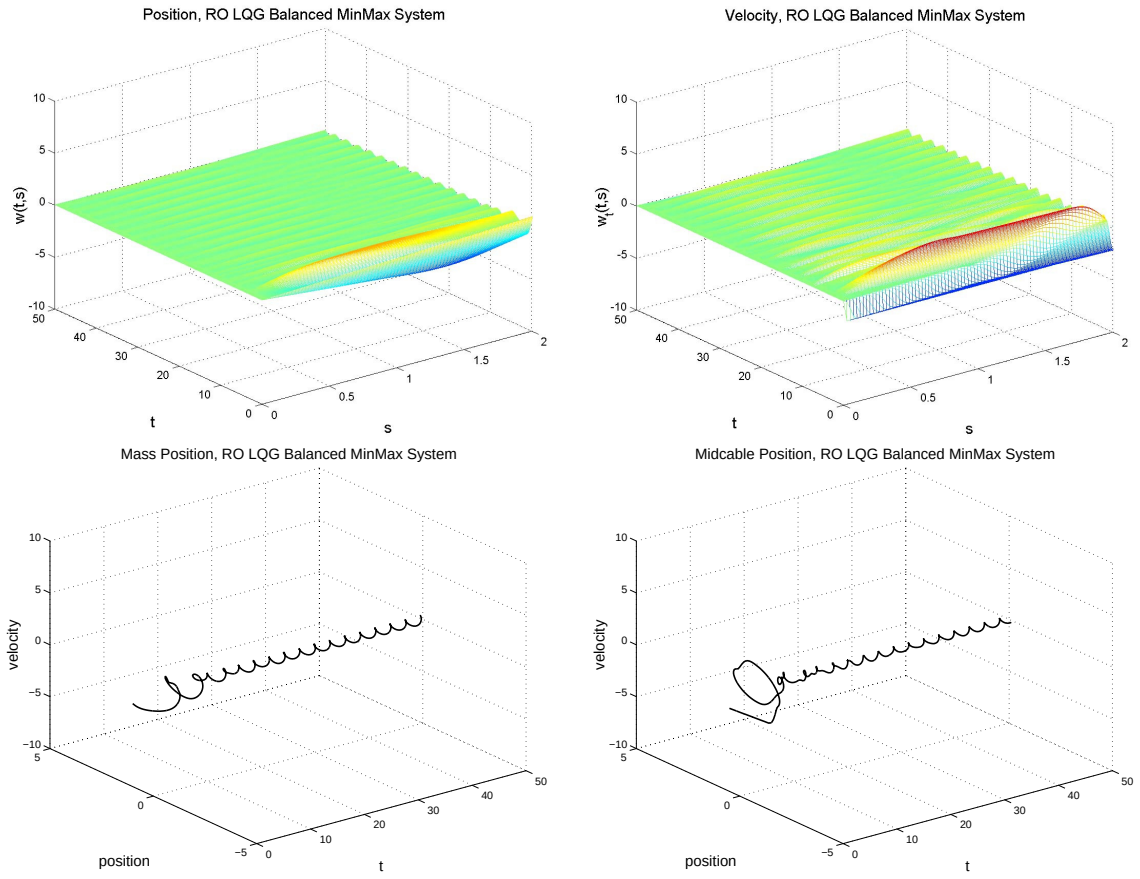

Figure 4.14: LQG Balanced MinMax Controller: Reduced Order Position State (top left), Reduced Order Velocity State (top right), Reduced Order Mass Phase Portrait (bottom left), and Reduced Order Midcable Phase Portrait (bottom right)

Next we consider our third control design. Figures 4.15 and 4.16 show the systems with central controllers obtained through balanced truncation and LQG balanced truncation, respectively. As with the MinMax controllers just previously discussed, there is little to distinguish the performance of these two low order central controllers. Each regulates adequately, but they do not perform as well as the full order central controller, displayed in Figure 4.9. It should be noted that they do outperform the full order LQG controller, found in Figure 4.7.

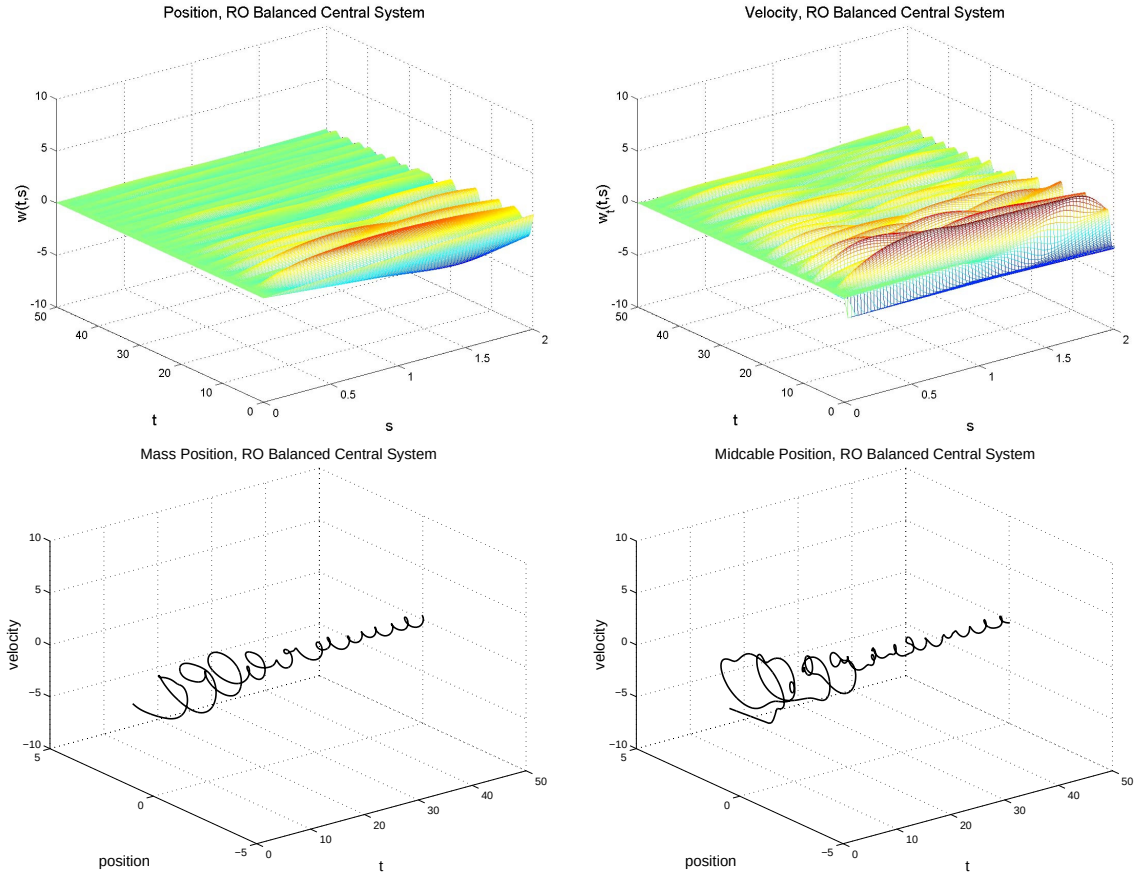

Figure 4.15: Balanced Central Controller: Reduced Order Position State (top left), Reduced Order Velocity State (top right), Reduced Order Mass Phase Portrait (bottom left), and Reduced Order Midcable Phase Portrait (bottom right)

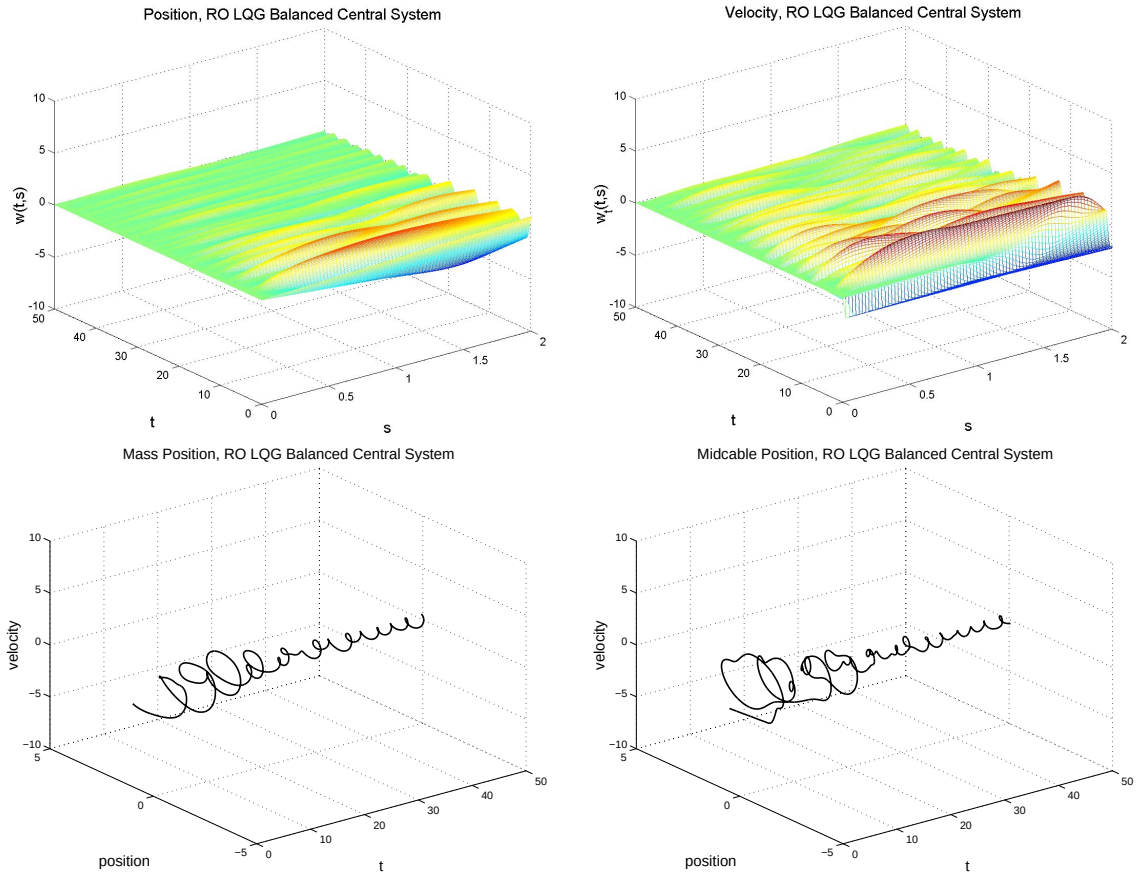

Figure 4.16: LQG Balanced Central Controller: Reduced Order Position State (top left), Reduced Order Velocity State (top right), Reduced Order Mass Phase Portrait (bottom left), and Reduced Order Midcable Phase Portrait (bottom right)

As with the full order controllers, we are still concerned about the control effort required by the low order controllers. Figures 4.17, 4.18, and 4.19 display the low order LQG, MinMax, and central controllers. We readily note that the balanced controllers require significantly more control effort than the LQG balanced controllers. The vertical axis scale on the plots makes it appear that the LQG balanced controllers are identically zero. This is not actually the case, but there are orders of magnitude difference between the balanced and LQG balanced controllers.

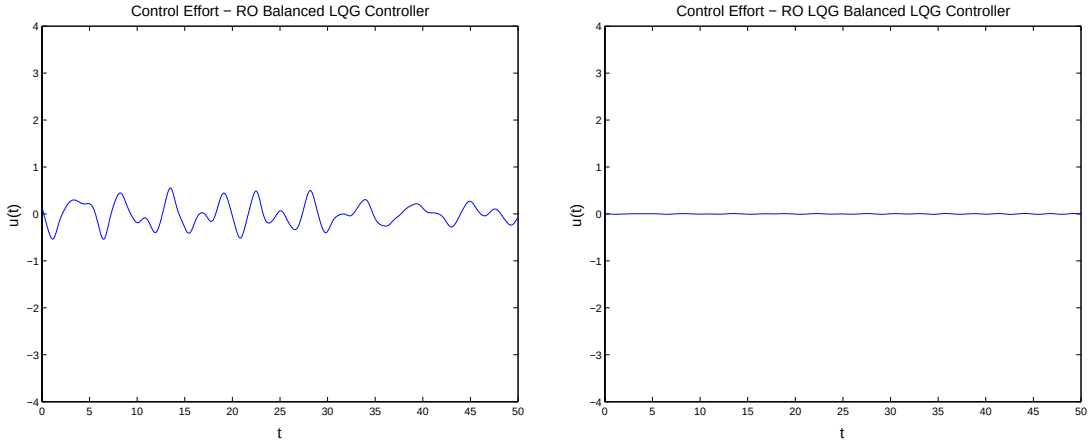

Figure 4.17: Control Effort: Reduced Order Balanced LQG (left) and Reduced Order LQG Balanced LQG (right)

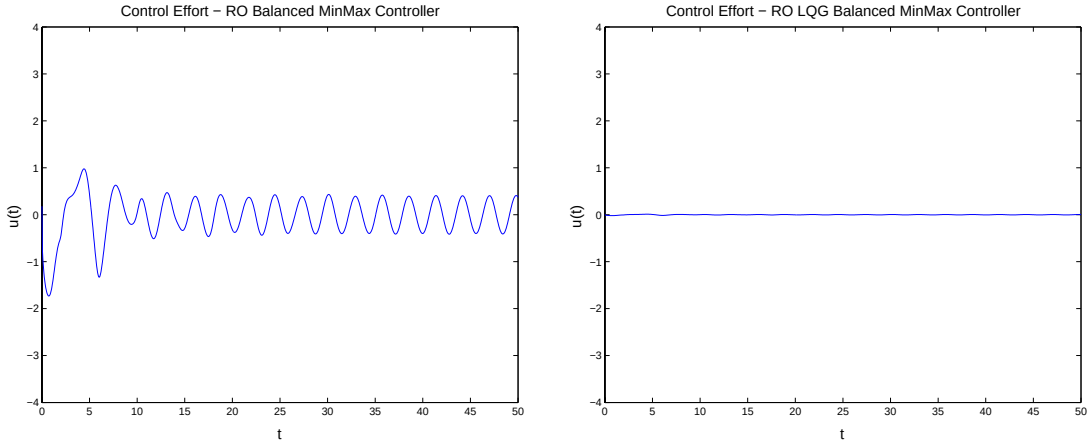

Figure 4.18: Control Effort: Reduced Order Balanced MinMax (left) and Reduced Order LQG Balanced MinMax (right)

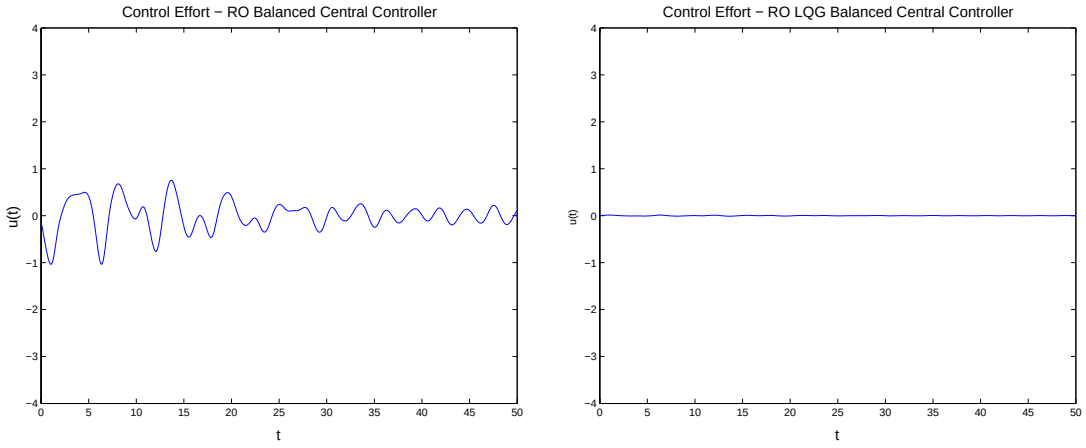

Figure 4.19: Control Effort: Reduced Order Balanced Central (left) and Reduced Order LQG Balanced Central (right)

When we examine the reduced order compensator systems, the MinMax controller outperforms the central controller, which in turn outperforms the LQG controller. There is a great deal of difference in the control effort required by the balanced controllers as compared with the effort required by the LQG balanced controllers. However, there is little difference in the control effort required among the balanced controllers and among the LQG balanced controllers. Additionally, not surprisingly, the low order controllers require less control effort than the full order controllers.

Controllers of Other Orders

Although the MinMax and central first order controllers perform acceptably, we recognize the possibility that by taking a controller of slightly higher order we may significantly enhance controller performance. Therefore, we now explore the possibility of using a second, third, fourth, or fifth order controller.

If we use a second order controller, there is no visible difference in the performances of any of the low order controllers. Using a third order controller results in the balanced LQG, MinMax, and central controllers being unstable, with no clear performance enhancement of the LQG balanced controllers. It may seem surprising that including additional states, or information about the system, would result in some of the low order controllers not being able to stabilize the system. However, this is a consistent observation among our numerical results. One explanation for this behavior might be that with the additional states in the controller we are including unimportant information, and thus the controller is less effective.

It is not until we use a fourth order controller that we see improved performance over the first order controllers. The fourth order controller simulations are now presented. We also note here that a fifth order controller results in the balanced LQG, MinMax, and central controllers being unstable.

Figures 4.20 and 4.21 provide the behavior when the LQG controllers obtained through balanced truncation and LQG balanced truncation are applied, respectively. Comparing the first and fourth order LQG controlled systems, in Figures 4.11 and 4.12 and Figures 4.20 and 4.21, respectively, we see there is a significant improvement of the fourth order LQG controllers over the first order ones. Clearly, if one wanted to implement either of the balanced LQG controllers for this problem, it would be wise to use the fourth order instead of the first order one.

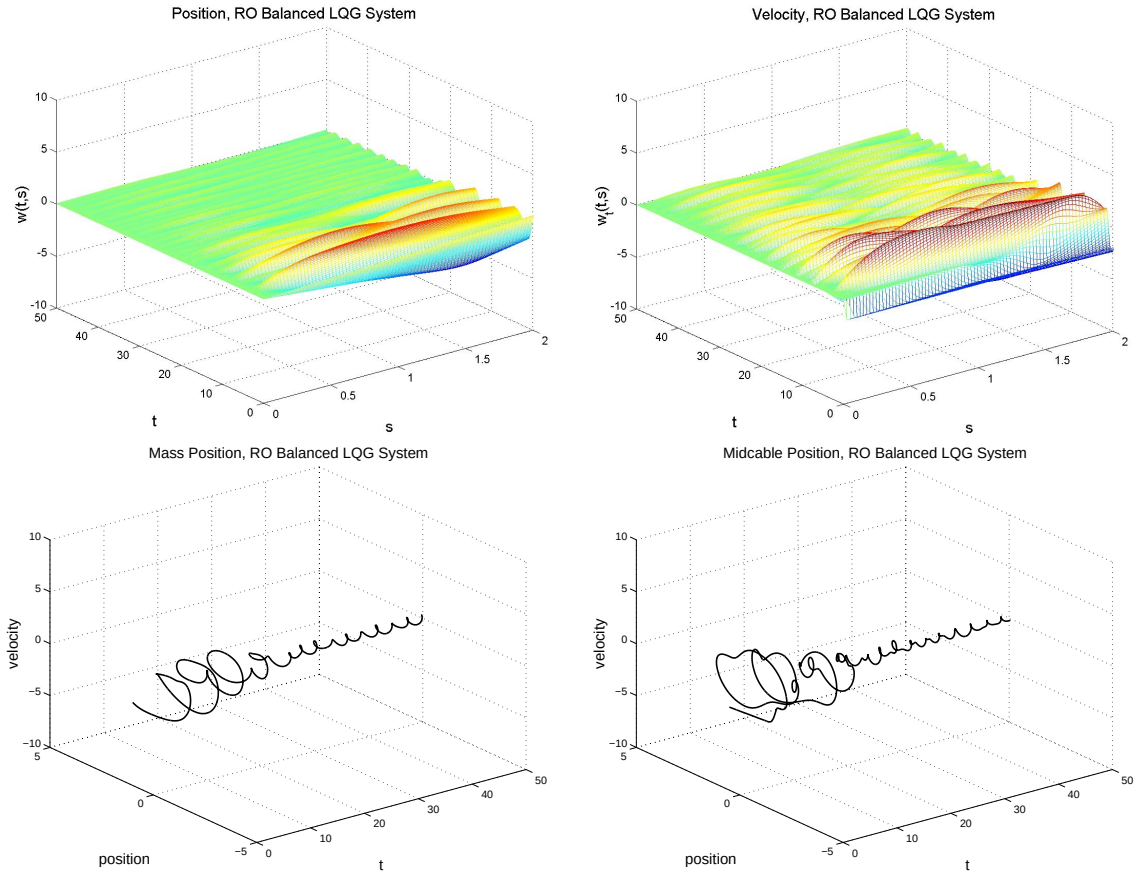

Figure 4.20: Balanced LQG Controller: Reduced Order Position State (top left), Reduced Order Velocity State (top right), Reduced Order Mass Phase Portrait (bottom left), and Reduced Order Midcable Phase Portrait (bottom right)

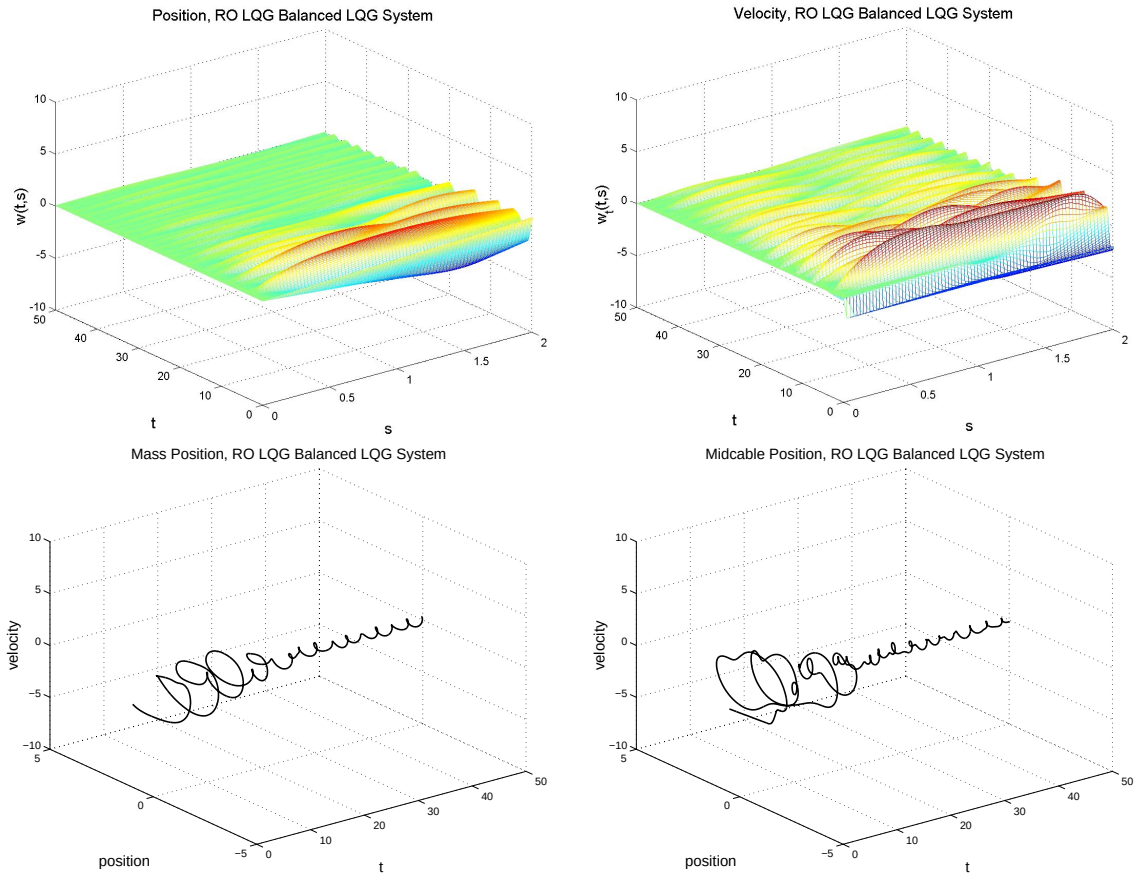

Figure 4.21: LQG Balanced LQG Controller: Reduced Order Position State (top left), Reduced Order Velocity State (top right), Reduced Order Mass Phase Portrait (bottom left), and Reduced Order Midcable Phase Portrait (bottom right)

Alternatively, if we compare the first order MinMax controlled systems in Figures 4.13 and 4.14 and the fourth order MinMax controlled systems in Figures 4.22 and 4.23, we see virtually no difference. That is, one need not bother to include the additional three states since the first order controller regulates just as well.

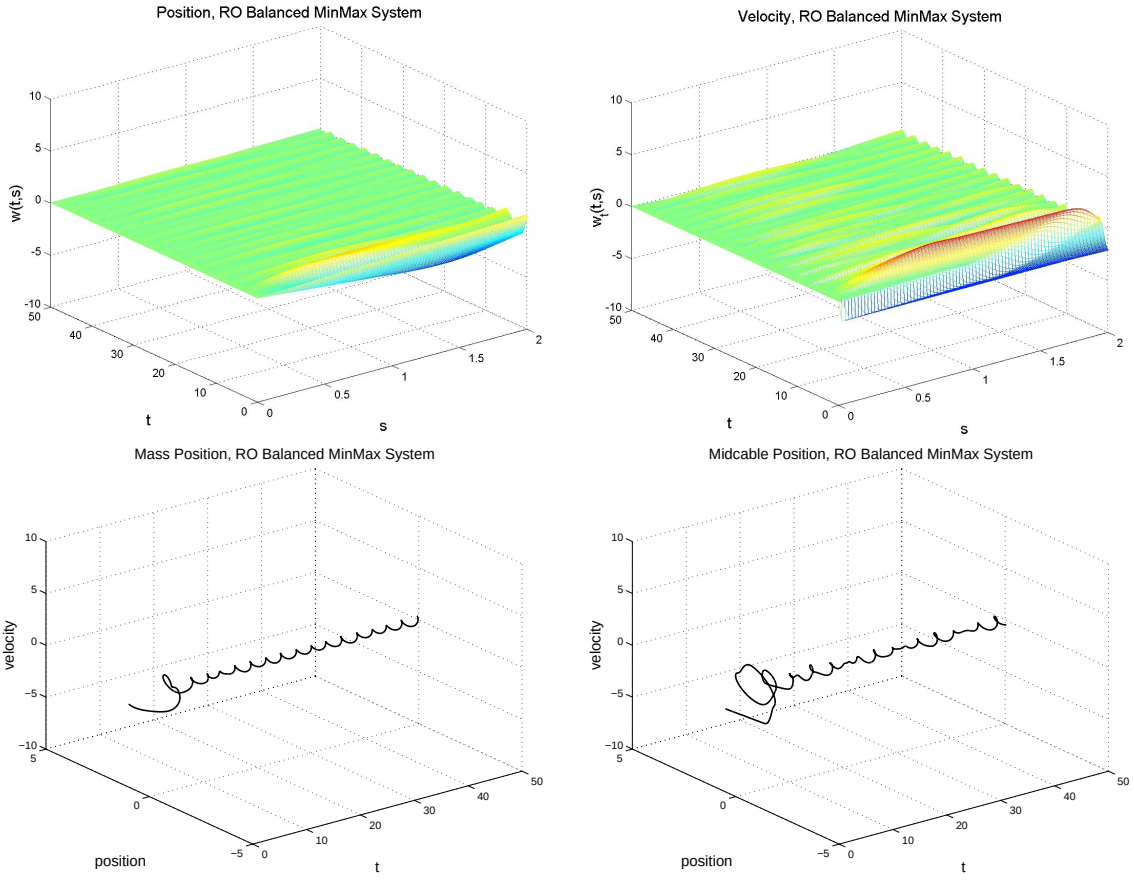

Figure 4.22: Balanced MinMax Controller: Reduced Order Position State (top left), Reduced Order Velocity State (top right), Reduced Order Mass Phase Portrait (bottom left), and Reduced Order Midcable Phase Portrait (bottom right)

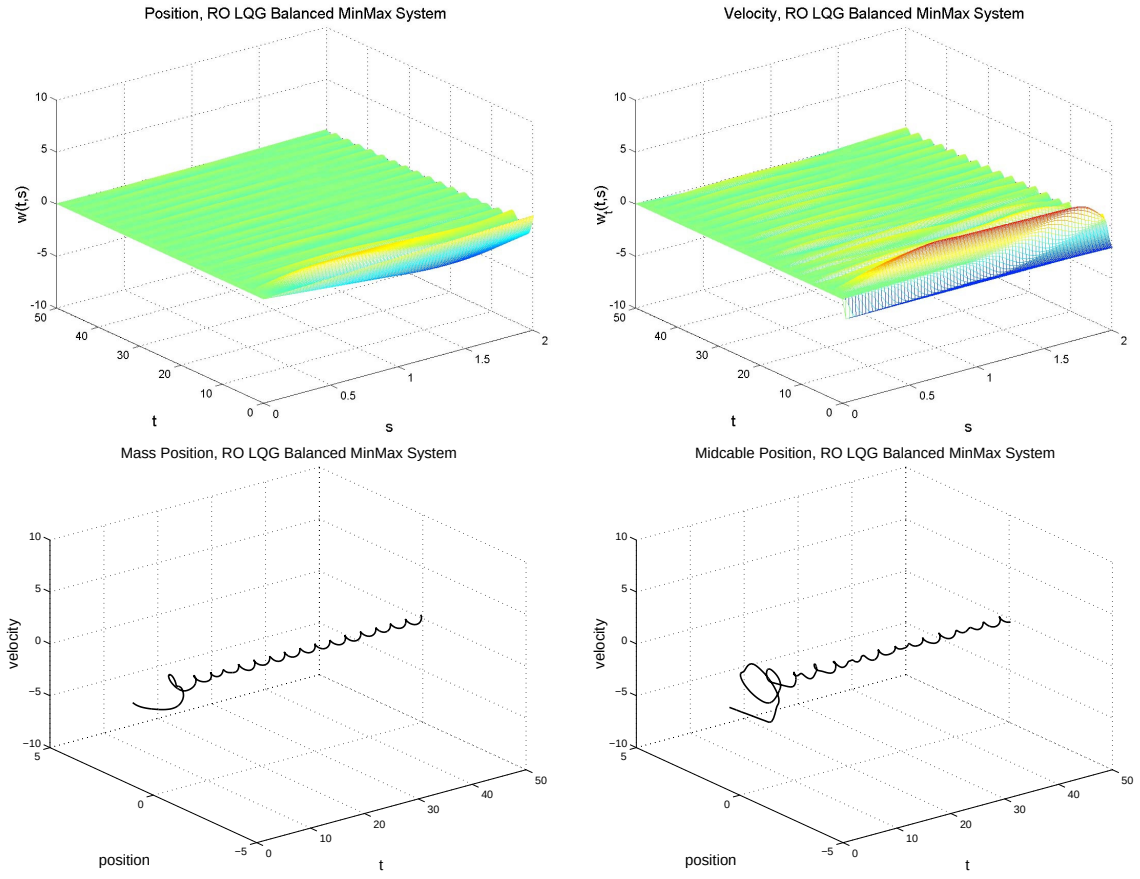

Figure 4.23: LQG Balanced MinMax Controller: Reduced Order Position State (top left), Reduced Order Velocity State (top right), Reduced Order Mass Phase Portrait (bottom left), and Reduced Order Midcable Phase Portrait (bottom right)

In a similar fashion, we compare the first order central controlled systems in Figures 4.15 and 4.16 with the fourth order central controlled systems in Figures 4.24 and 4.25. We find that both fourth order controllers offer improved performance over both of the first order controllers. The enhancement is not as significant as what we observed in the LQG controllers, so one must decide if there is enough improvement to counter the additional cost of three extra states in the controller.

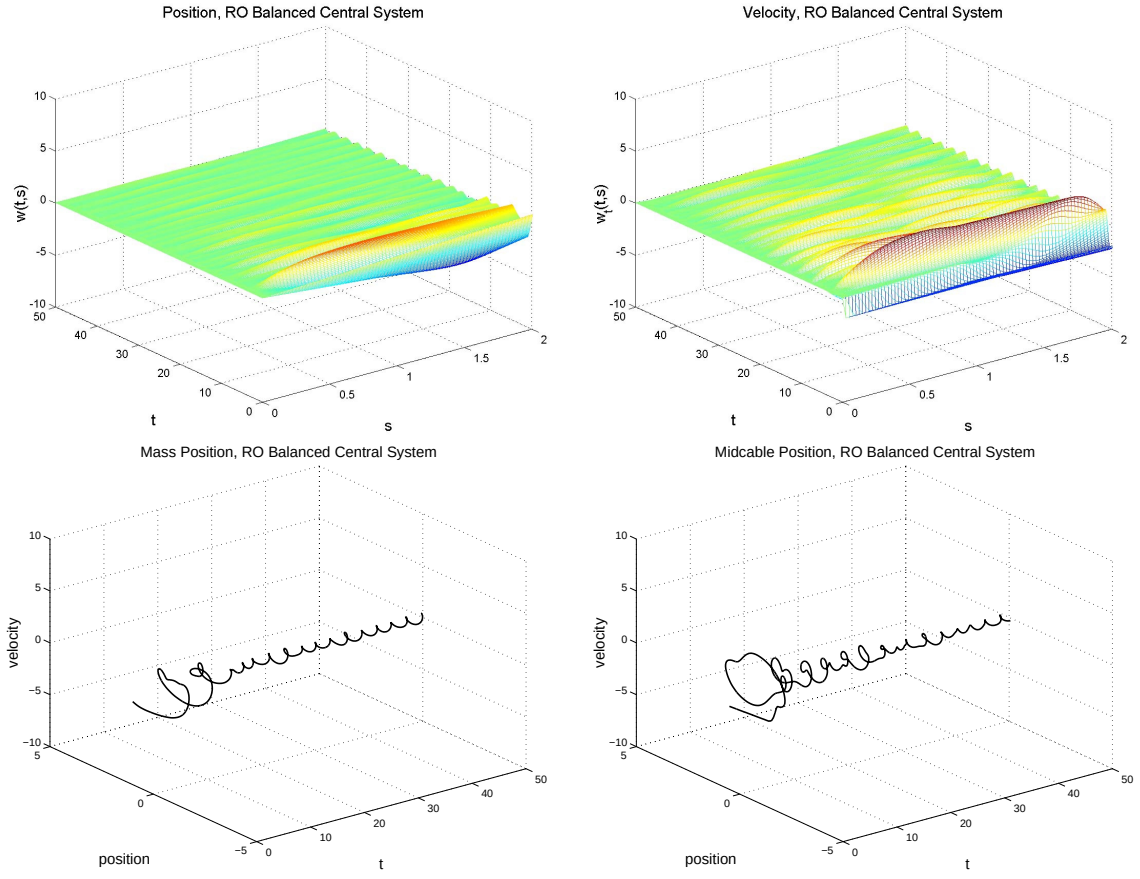

Figure 4.24: Balanced Central Controller: Reduced Order Position State (top left), Reduced Order Velocity State (top right), Reduced Order Mass Phase Portrait (bottom left), and Reduced Order Midcable Phase Portrait (bottom right)

To summarize, whether we design a first order controller or a fourth order controller, the MinMax outperforms the central which outperforms the LQG controllers for this problem. There seems to be very little difference between the controllers designed through balanced truncation and the ones designed through LQG balanced truncation.

As discussed in Chapters 1, 2, and 3 we recognize that performance is not the only issue of

consideration. In order to design robust controllers, we must look at how susceptible each of these low order controllers is to perturbation.

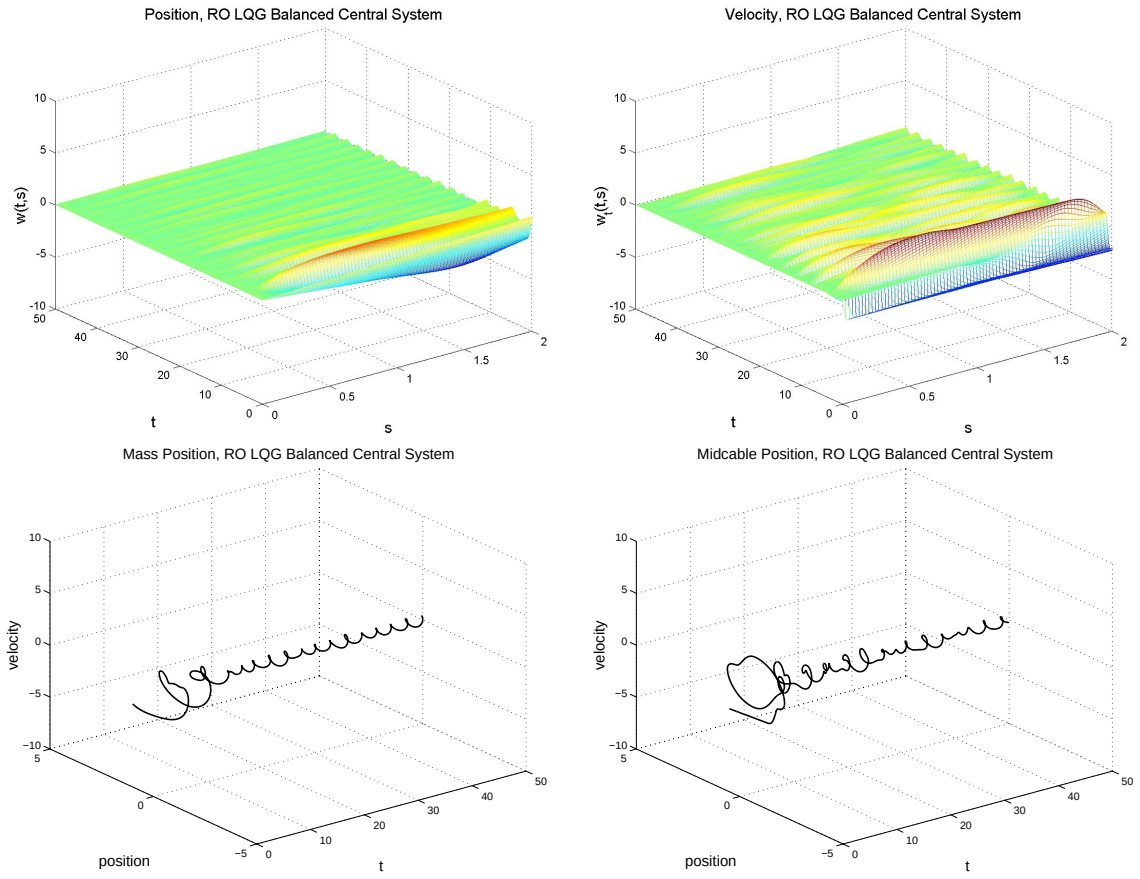

Figure 4.25: LQG Balanced Central Controller: Reduced Order Position State (top left), Reduced Order Velocity State (top right), Reduced Order Mass Phase Portrait (bottom left), and Reduced Order Midcable Phase Portrait (bottom right)

4.1.3 Robustness of Low Order Controllers

First Order Controllers

As discussed in Chapter 2, we will offer two measures of robustness, the stability margin and the stability radius. To first gain some insight into the stability margin, we will look at the eigenvalues of all relevant systems in Figure 4.26, focusing, in particular, on the eigenvalues nearest the imaginary axis.

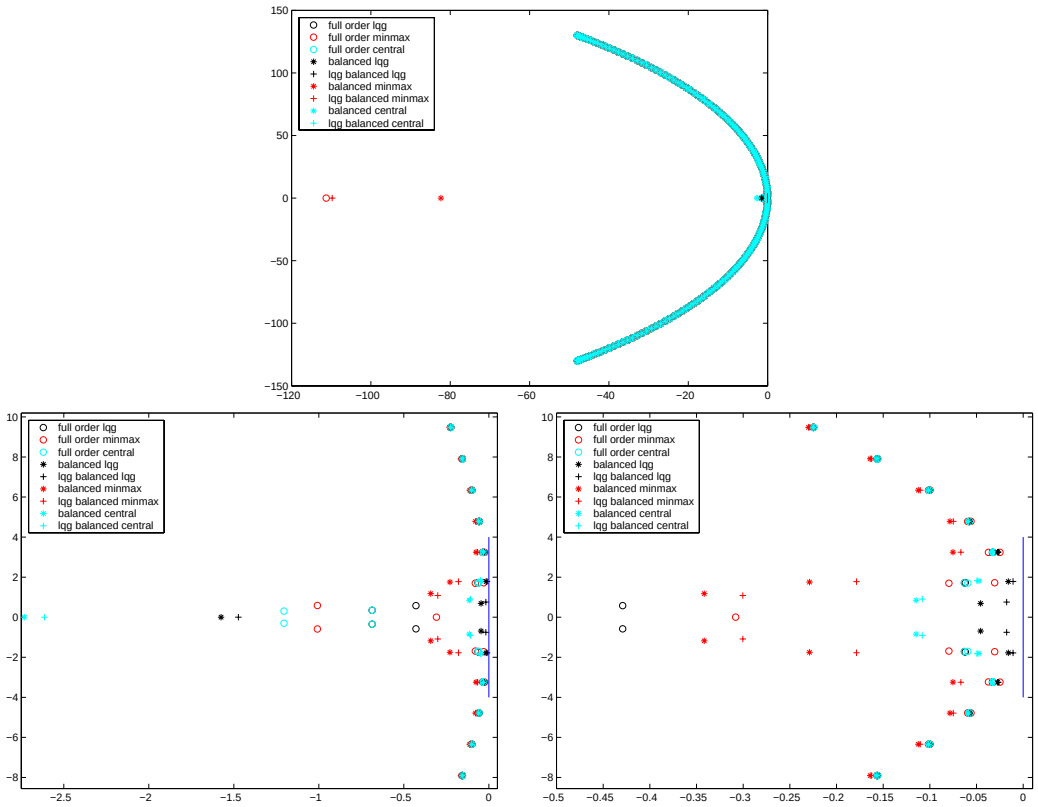

Figure 4.26: Eigenvalues (top), Zoomed In Views (bottom)

As we can see, especially from the zoomed in views of the eigenvalues, there is a shift to the left of eigenvalues for the low order MinMax systems, as compared with the full order MinMax system. That is, we should expect larger stability margins for the low order MinMax systems than the full order one. Additionally, we see a shift to the right for the low order LQG eigenvalues, as compared with the full order LQG system. The eigenvalues for the full and reduced order central controllers are comparable, and therefore, we expect similar stability margin values. These comments are quantified in Table 4.3, where we actually

compute the stability margins. We observe that an increased stability margin for the low order MinMax controllers will result in a faster decay of the solution and, in some sense, enhanced performance. On the other hand, the decreased stability margins for the low order LQG controllers will result in a slower decay of solution and decreased performance.

Matrix	Stability Margin	Stability Radius	Guaranteed Robustness Margin
Full order LQG	0.03213	0.03312	n/a
Full order MinMax	0.02499	0.03330	n/a
Full order central	0.03219	0.03661	0.47916
Balanced LQG	0.01591	0.00478	n/a
LQG balanced LQG	0.01090	0.34019	n/a
Balanced MinMax	0.07528	0.00826	n/a
LQG balanced MinMax	0.06678	0.45574	n/a
Balanced central	0.03318	0.00629	0.46888
LQG balanced central	0.03308	0.39502	0.47916

Table 4.3: Stability Margins and Radii for Full and Reduced Order Compensators.

We note that the stability margins for all systems of consideration are on the same order of magnitude. As we described in Example 2.18, one should not rely solely on the stability margin as a robustness measure. Thus, we compute the stability radii, which can also be found in Table 4.3. When we look at the stability radii, it is quite a different story from that for stability margins. The three full order controlled systems are on the same order of magnitude and, in fact, within 3.5×10^{-3} of each other. The interesting part of the picture concerns the low order controllers. The stability radii of all three LQG balanced controllers are an order of magnitude greater then the radii of the full order controllers. Additionally, the stability radii of all three balanced controllers are an order of magnitude less than those of the full order controllers, thereby yielding two orders of magnitude difference between the stability radii of the two different types of low order systems. The robustness margins guaranteed by the central controller, and thus not applicable to the LQG or MinMax controllers, tell us that each central controller will stabilize perturbations of approximately the same size.

Although parameter studies do not provide a numerical measure of robustness, they should offer some insight into the robustness of the controllers. Using the LQG controller as an example, we explain how we develop the parameter studies. We design balanced and LQG balanced first order LQG controllers based on a low order system with $N = 10$. We then apply these low order LQG controllers to a high order system with $N = 80$. These systems are denoted with diamond shapes in Figures 4.27, 4.28, and 4.29 where we display the LQG, MinMax, and central parameter studies, respectively. Additionally, we apply the above

described first order LQG controllers to high order systems where we vary the values of the mass and damping parameters. This provides us with information about the ability of our first order controllers to stabilize nearby systems. Following the pattern in [45], if the low order controller stabilizes the high order system, then there is a dot on the graph for the corresponding mass and damping pair. If the low order controller does not stabilize the high order system, there is a square on the plot for the related mass and damping. Note that when we take $N = 10$, the largest we may take the MinMax parameter to be is $\theta = .44$.

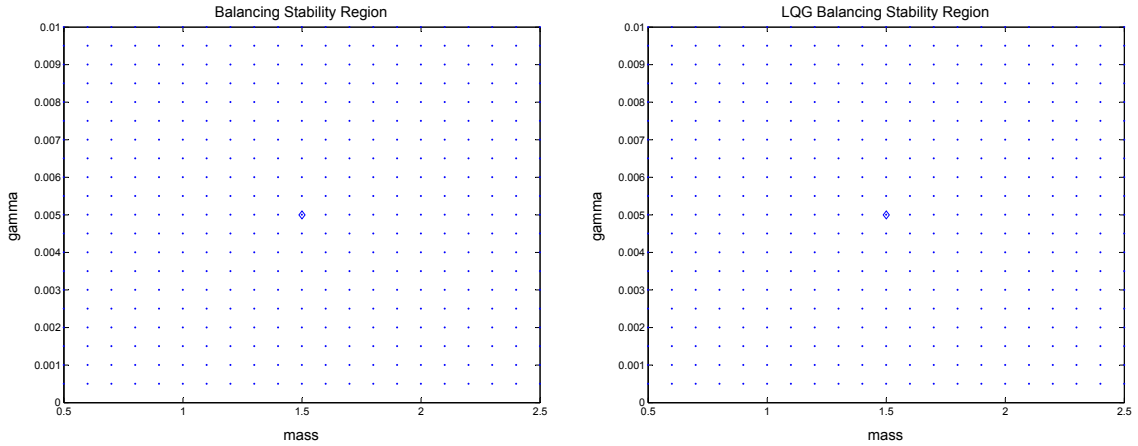

Figure 4.27: Parameter Studies: Reduced Order Balanced LQG Controller (left), Reduced Order LQG Balanced LQG Controller (right)

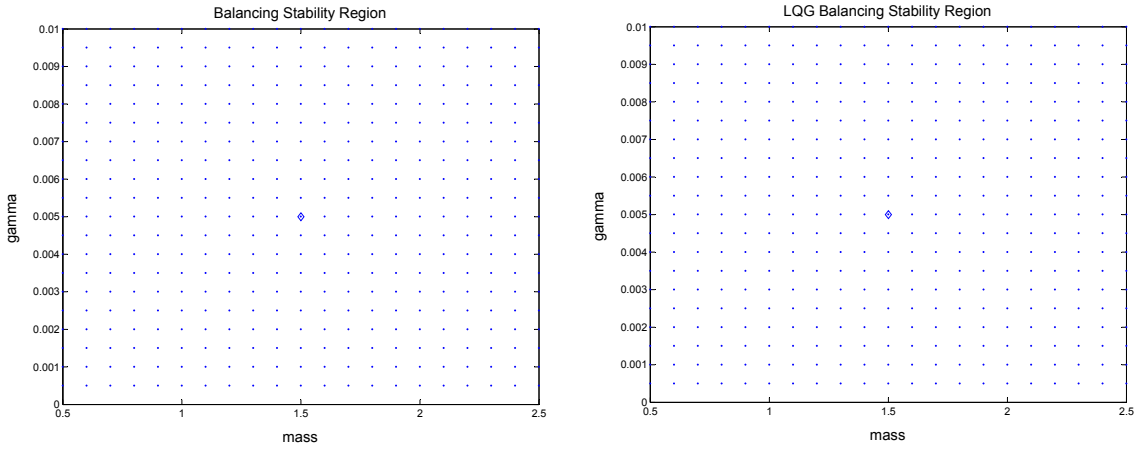

Figure 4.28: Parameter Studies: Reduced Order Balanced MinMax Controller (left), Reduced Order LQG Balanced MinMax Controller (right)

As can be seen from these three figures, all low order controllers designed stabilize not only the high order systems with the same mass and damping parameters, but also the high order systems with nearby mass and damping combination choices. The range of damping values chosen for the parameter studies is based on the idea that enough damping must be included so that the system is stable in order to do compute a low order controller through balanced truncation.

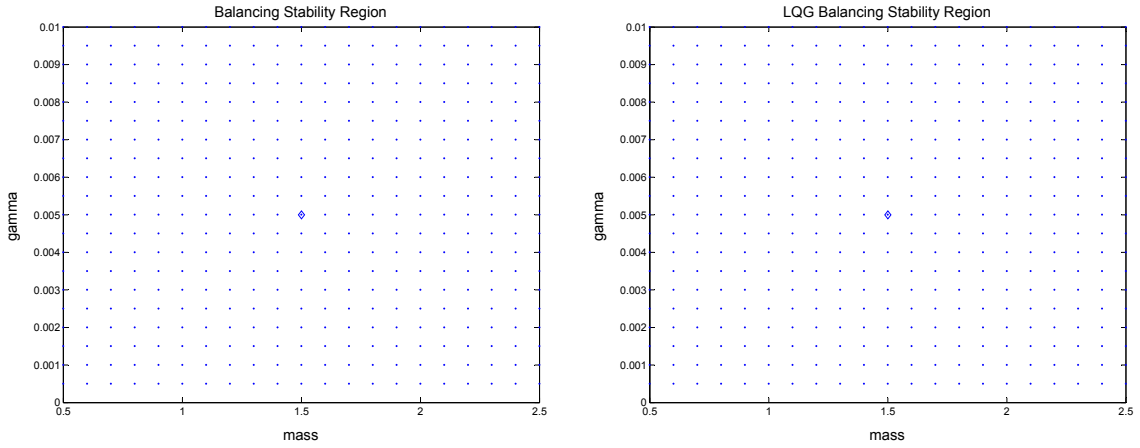

Figure 4.29: Parameter Studies: Reduced Order Balanced Central Controller (left), Reduced Order LQG Balanced Central Controller (right)

Fourth Order Controllers

Similar to our treatment of the first order controllers in the previous section, we now look at robustness issues regarding fourth order controllers. We first look at the eigenvalues of all relevant systems in Figure 4.30.

As we can see from the zoomed in views of the eigenvalues, there are no noticeable shifts in the eigenvalues for the low order controller systems. This observation is quantified in Table 4.4, where we compute the stability margins. We note that there is little difference in any of the stability margins, with all of the values falling within 1.4×10^{-2} of each other. Just as with the first order controllers, the stability radii of all three LQG balanced controllers are an order of magnitude greater than the radii of the full order controllers. Again, radii of all three balanced controllers are an order of magnitude less than those of the full order controllers, thus creating two orders of magnitude difference between the balanced and LQG balanced controllers. We also note that even though the radii for the LQG balanced controllers are on the same order of magnitude for both the first and fourth order controllers, the radii are still

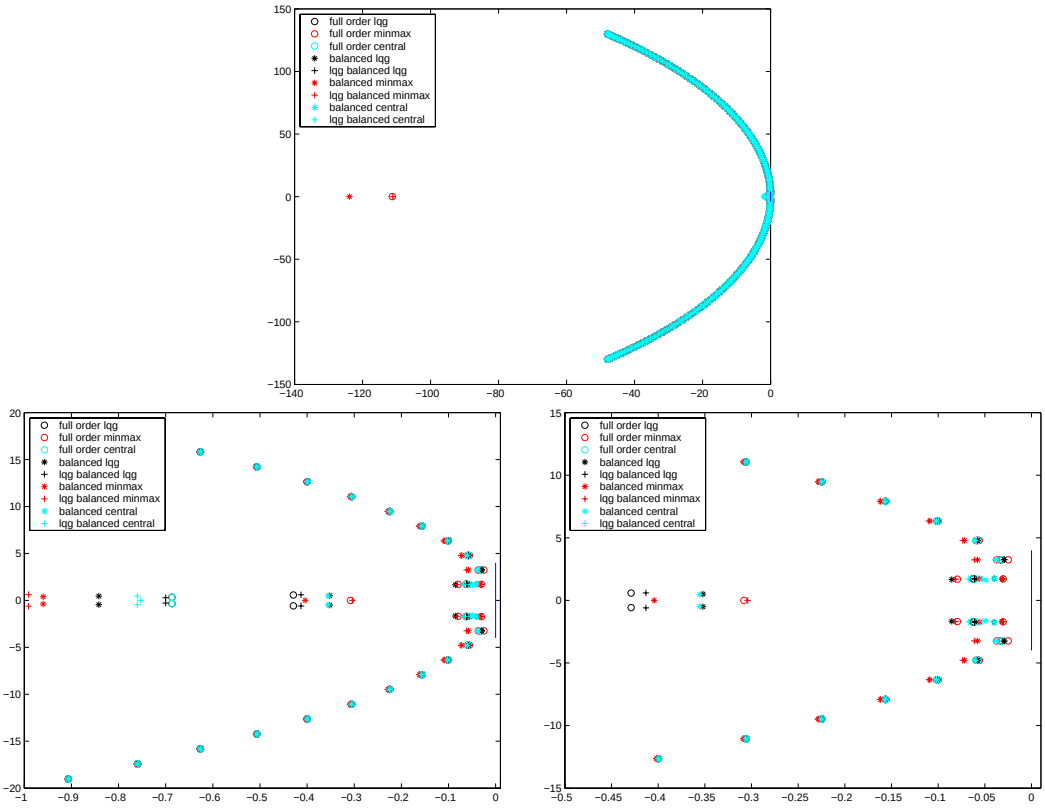

Figure 4.30: Eigenvalues (top), Zoomed In Views (bottom)

greater for the first order LQG balanced controllers. The guaranteed robustness margins indicate that each central controller should stabilize perturbations of almost identical size.

Matrix	Stability Margin	Stability Radius	Guaranteed Robustness Margin
Full order LQG	0.03213	0.03312	n/a
Full order MinMax	0.02499	0.03330	n/a
Full order central	0.03219	0.03661	0.47916
Balanced LQG	0.02935	0.00241	n/a
LQG balanced LQG	0.02912	0.15816	n/a
Balanced MinMax	0.03161	0.00243	n/a
LQG balanced MinMax	0.03061	0.17844	n/a
Balanced central	0.03831	0.00288	0.47139
LQG balanced central	0.03880	0.17948	0.47916

Table 4.4: Stability Margins and Radii for Full and Reduced Order Compensators.

4.2 Numerical Results with $R = .001$

In this section, we change the value of the control weighting so that $R = .001 * I$ to offer more control authority. We let $\theta = .75$, which is as large as possible. It turns out that all three full order controlled systems perform worse with this modified control weighting. We do note, however, that the MinMax performance does not decline as significantly as the LQG and central controllers. Due to this poor performance, we only display the full order simulation plots. Figures 4.31, 4.32, and 4.33 display the full order LQG, MinMax, and central controlled simulation plots, respectively.

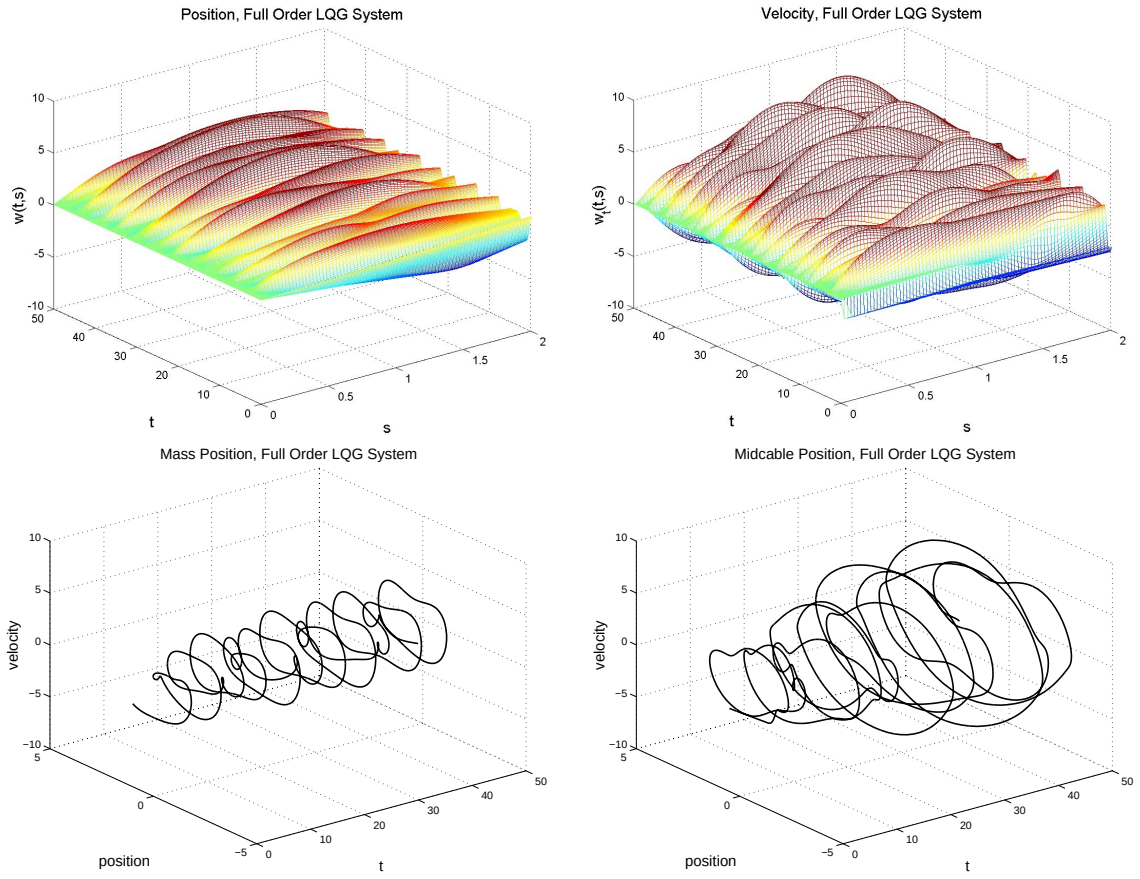

Figure 4.31: LQG Controller: Full Order Position State (top left), Full Order Velocity State (top right), Full Order Mass Phase Portrait (bottom left), and Full Order Midcable Phase Portrait (bottom right)

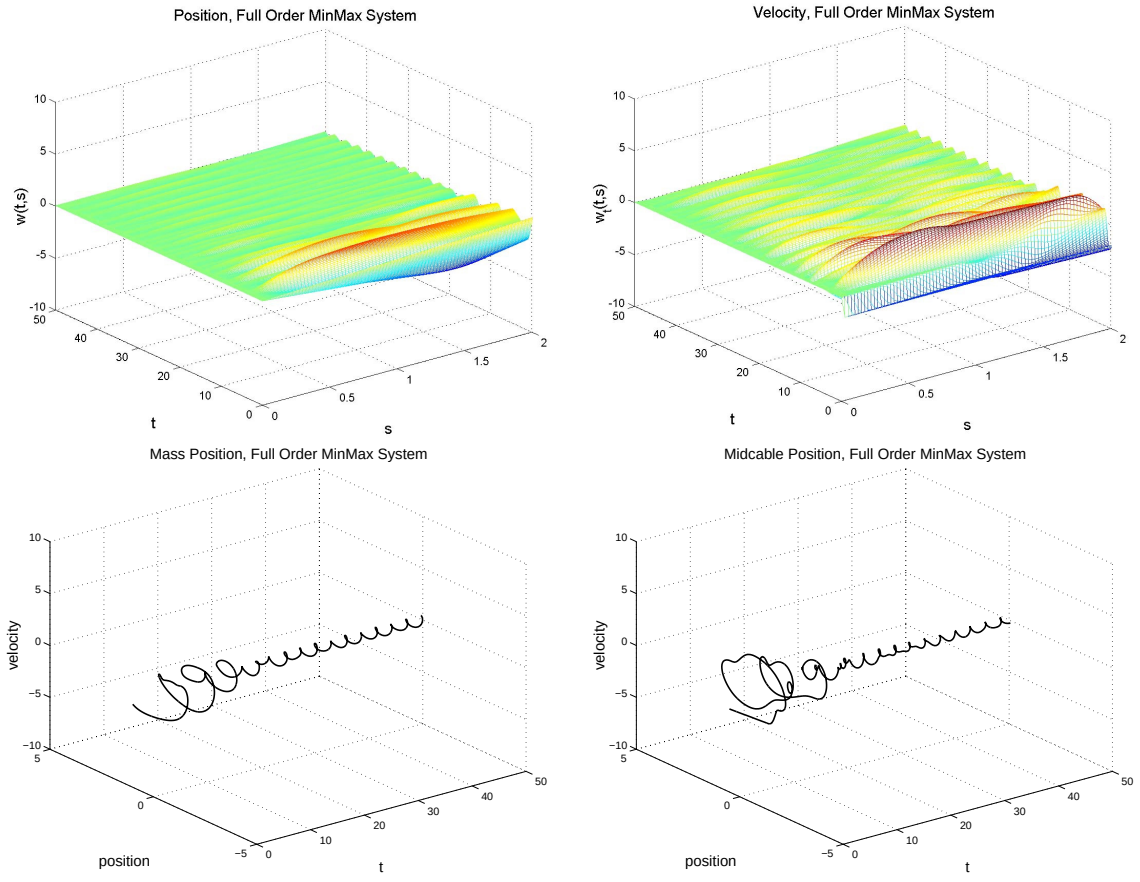

Figure 4.32: MinMax Controller: Full Order Position State (top left), Full Order Velocity State (top right), Full Order Mass Phase Portrait (bottom left), and Full Order Midcable Phase Portrait (bottom right)

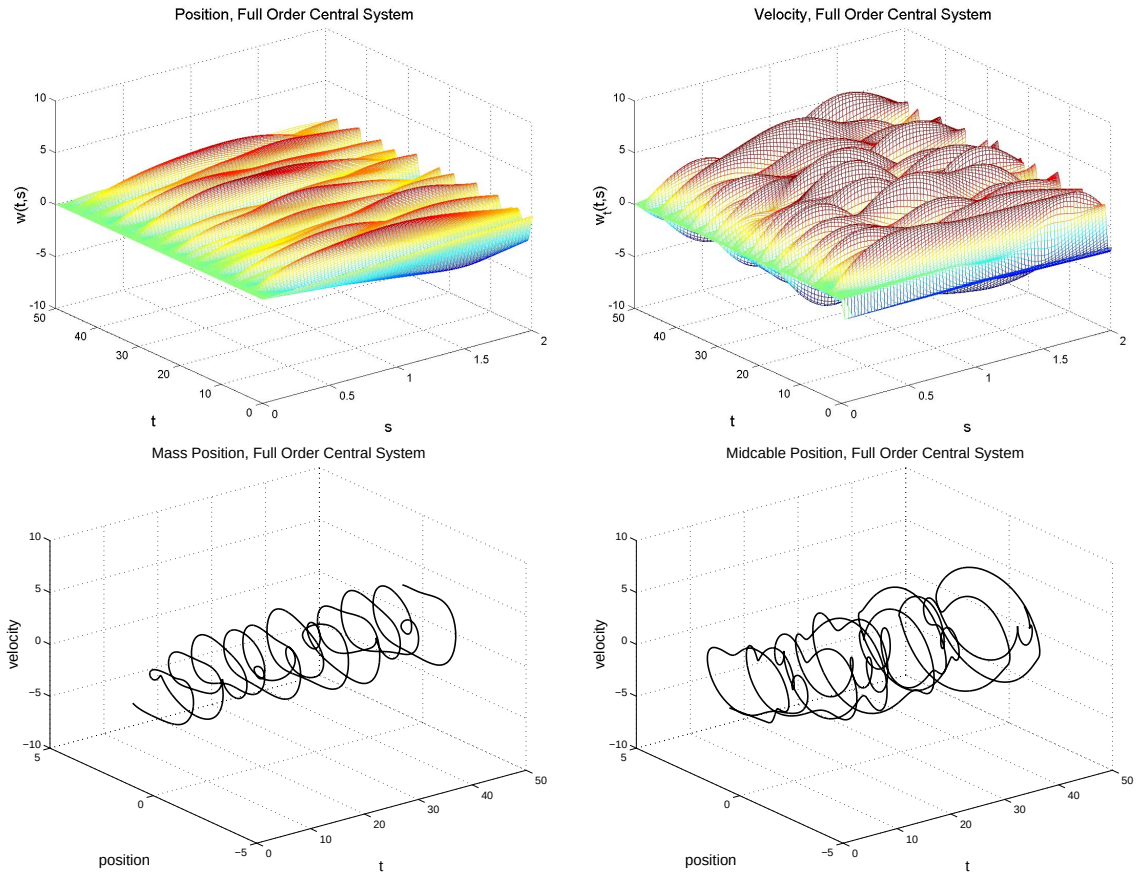

Figure 4.33: Central Controller: Full Order Position State (top left), Full Order Velocity State (top right), Full Order Mass Phase Portrait (bottom left), and Full Order Midcable Phase Portrait (bottom right)

Figure 4.34 gives the control effort of the full order LQG, MinMax, and central controllers. The LQG and MinMax controllers require more effort than when the control weight was taken to be the identity, i.e., $R = 1$, while the central controller is using much less effort than it did with the previous control weight. This is not surprising given the definitions of the gain operators for the three controllers. We remind the reader that for the LQG and MinMax control designs, the gain operator is given by $K = R^{-1}B^*\Pi$, while $K = B^*\Pi$ for the central control design. Thus for the central controller, the control weight change only affects the solution of the control Riccati equation in (3.3), while this change also affects the gain operator directly for the LQG and MinMax controllers. Thus, it is not surprising there is a large difference in the control efforts of the LQG and MinMax controllers as compared with the central controller when $R = .001$.

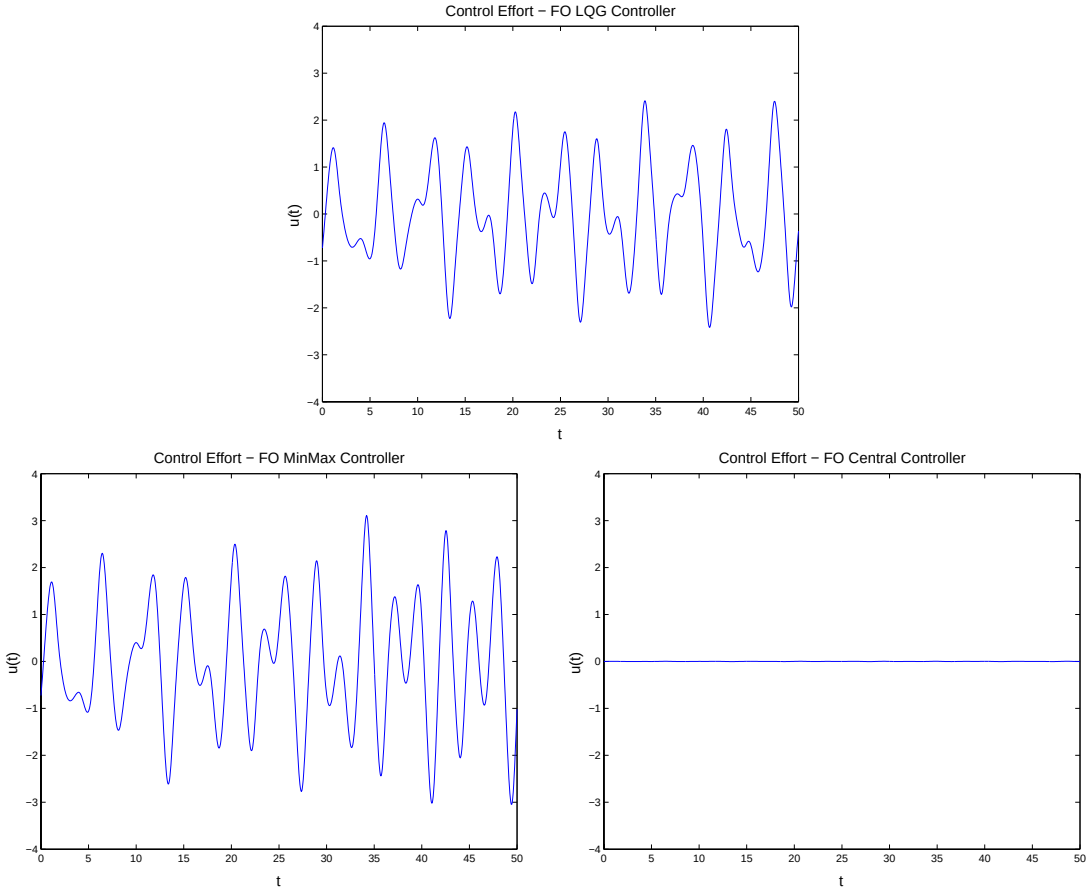

Figure 4.34: Control Effort: Full Order LQG (top), Full Order MinMax (bottom left), Full Order Central (bottom right)

Chapter 5

Linear Klein-Gordon Relativistic Wave Equation

To study the effects of regular and LQG balancing, the linear Klein-Gordon equation (KGL) is used as an example. Taking the constants velocity of light in a vacuum and $\hbar$ to be one and adding a viscous damping term, the KGL equation can be written as

$$\begin{aligned} \omega_{tt}(t,s) \; - \; \omega_{ss}(t,s) + \;\; m^2\omega(t,s) \;\; + \gamma\omega_t(t,s) = \; \sum_{i=1}^{m} b_i(s)u(t) \\ \omega(0,s) = \omega_{1_0}(s) \qquad\qquad \dot{\omega}(0,s) = \omega_{2_0}(s) \\ 0 \leq s \leq \ell \qquad\qquad t \geq 0 \\ \omega(t,0) \;\; = \;\; 0 \;\; = \;\; \omega(t,\ell) \end{aligned} \tag{5.1}$$

where m is the rest mass, ℓ is the length of the spatial domain, t is time, $u(t)$ is the control, and $b_i(s)$ are the control input functions which describe how the control is applied. The KGL equation is a relativistic wave equation which arises in quantum mechanics. It is a momentum equation used when there is a need to describe phenomena at high energies [23].

Using PDE framework, we can write (5.1) without the control term as a first order system $\dot{x} = Ax$. We take this time to define the A operator, the state space, and our choice of inner product on the state space. We will use this information to show A generates a C_0-semigroup and provide a Lyapunov argument that will guarantee exponential stability of the semigroup. We define the following: $w(t,s) = d(s)$ to be the displacement of the particle and $w_t(t,s) = v(s) = \dot{d}(s)$ to be the velocity of the particle. Making these substitutions,

(5.1) without the control term is transformed into

$$\begin{aligned} \frac{d}{dt}\begin{bmatrix} d \\ v \end{bmatrix} &= \begin{bmatrix} 0 & I \\ \left(\frac{\partial^2}{\partial s^2} - m^2 I\right) & (-\gamma I) \end{bmatrix}\begin{bmatrix} d \\ v \end{bmatrix} \\ &= \begin{bmatrix} v \\ d'' - m^2 d - \gamma v \end{bmatrix}. \end{aligned} \tag{5.2}$$

We take the state space to be the product space $X = H_0^1(0,\ell) \times L_2(0,\ell)$, and $[d,v]^T$ are elements from the domain of A which is given by

$$D(A) = \left\{ \begin{bmatrix} d \\ v \end{bmatrix} \in X \middle| \; d \in H^2(0,\ell) \cap H_0^1(0,\ell),\; v \in H_0^1(0,\ell) \right\}. \tag{5.3}$$

That is, $A : D(A) \subseteq X \to X$, and

$$A\begin{bmatrix} d \\ v \end{bmatrix} = \begin{bmatrix} v \\ d'' - m^2 d - \gamma v \end{bmatrix}. \tag{5.4}$$

We denote the natural norm on X as $\hat{X}$, and it is given by

$$\left|\left|\left|\begin{bmatrix} d \\ v \end{bmatrix}\right|\right|\right|_{\hat{X}} = \left(\int_0^\ell \left[|d(s)|^2 + |d'(s)|^2 + |v(s)|^2 + |v'(s)|^2\right] ds\right)^{\frac{1}{2}}. \tag{5.5}$$

However, we choose the norm on X to be

$$\left|\left|\left|\begin{bmatrix} d \\ v \end{bmatrix}\right|\right|\right|_{X} = \left(\int_0^\ell \left[|d'(s)|^2 + m^2|d(s)|^2 + |v(s)|^2\right] ds\right)^{\frac{1}{2}}, \tag{5.6}$$

which is induced by the inner product

$$\left\langle \begin{bmatrix} d \\ v \end{bmatrix}, \begin{bmatrix} \hat{d} \\ \hat{v} \end{bmatrix} \right\rangle_X = \int_0^\ell \left[d'(s)\hat{d}'(s) + m^2 d(s)\hat{d}(s) + v(s)\hat{v}(s)\right] ds. \tag{5.7}$$

Our choice for this norm is justified since it is equivalent to the above $\hat{X}$ norm. That is, for $\Phi = [d,v]^T \in D(A)$, we can find constants b and B such that

$$b||\Phi||_X \leq ||\Phi||_{\hat{X}} \leq B||\Phi||_X. \tag{5.8}$$

We can obviously take $b = 1$ to satisfy the lower bound, and we can use Poincare's inequality to guarantee the existence of B and satisfy the upper bound (see [35]). We will now show that A generates an exponentially stable C_0-semigroup.

Theorem 5.1. *The operator A, as defined in (5.3) and (5.4), generates an exponentially stable C_0-semigroup.*

Proof: Our approach to show that A generates a C_0-semigroup will be to show that A and A^* are both dissipative and then apply Theorem 2.10. We first need to show A is a closed, densely defined operator. Certainly A is densely defined, since $\overline{D(A)} = X$. The approach we will take to show that A is closed employs the following theorem.

Theorem 5.2. *Assume X is a Banach space and let A be a linear operator with $A : D(A) \subset X \to X$. If A is invertible with $A^{-1} : X \to X$ bounded, then A is a closed linear operator.*

Thus, we want to find a bounded linear operator $H : X \to X$ so that $HA \begin{bmatrix} d \\ v \end{bmatrix} = AH \begin{bmatrix} d \\ v \end{bmatrix} = \begin{bmatrix} d \\ v \end{bmatrix}$. Then $H = A^{-1}$. We now find A^{-1} formally. Let $H = \begin{bmatrix} \int_0^t \cdot \, dt & 0 \\ I & 0 \end{bmatrix}$. Then,

$$\begin{aligned} HA \begin{bmatrix} d \\ v \end{bmatrix} &= \begin{bmatrix} \int_0^t \cdot \, dt & 0 \\ I & 0 \end{bmatrix} \begin{bmatrix} v \\ d'' - m^2 d - \gamma I \end{bmatrix} \\ &= \begin{bmatrix} \int_0^t v \, dt \\ v \end{bmatrix} \qquad (5.9) \\ &= \begin{bmatrix} d \\ v \end{bmatrix}. \end{aligned}$$

This demonstrates that H is a left inverse for A, and we must now verify that H is a right inverse for A:

$$\begin{aligned} AH \begin{bmatrix} d \\ v \end{bmatrix} &= A \begin{bmatrix} \int_0^t d \, dt \\ d \end{bmatrix} \\ &= \begin{bmatrix} \frac{d}{dt} \int_0^t d \, dt \\ \frac{d}{dt} d \end{bmatrix} \qquad (5.10) \\ &= \begin{bmatrix} d \\ v \end{bmatrix}, \end{aligned}$$

since $A\begin{bmatrix} d \\ v \end{bmatrix} = \begin{bmatrix} \dot{d} \\ \dot{v} \end{bmatrix}$ by (5.2) and (5.4). This shows that H is a right inverse for A, and thus, $H = A^{-1}$. Note that I_X is bounded since X is a closed linear space, and the integral operator with respect to time is bounded on X. Thus formally, A^{-1} is bounded, and A is closed by Theorem 5.2.

We now calculate the adjoint of A, A^*. We will employ the Fundamental Lemma of the Calculus of Variations in order to determine the adjoint, and we state it here for completeness.

Theorem 5.3. *(Lemma 3 in [7])*
Part (A) *(also known as the Du Bois Reymond Lemma) If $\alpha(\cdot)$ is piecewise continuous on $[a, b]$ and*

$$\int_a^b \alpha(x)\eta'(x)\ dx = 0 \tag{5.11}$$

for all $\eta(\cdot) \in V_0 = \{\eta(\cdot)$ piecewise smooth on $(a, b) : \eta(a) = 0,\ \eta(b) = 0\}$, then there is a constant c such that $\alpha(x) = c$ on $[a, b]$ except at a finite number of points, and conversely.
Part (B) *If $\alpha(\cdot)$ and $\beta(\cdot)$ are piecewise continuous on $[a, b]$ and*

$$\int_a^b [\alpha(x)\eta(x) + \beta(x)\eta'(x)]\ dx = 0 \tag{5.12}$$

for all $\eta(\cdot) \in V_0$, then there is a constant c such that

$$\beta(x) = c + \int_a^x \alpha(s)\ ds \tag{5.13}$$

for all $x \in (a, b)$, and conversely.

Since we have multiple indefinite integrals in this argument, we carefully identify the independent variables of functions. We assume $[y(s), z(s)]^T \in D(A^*)$, which implies there is a $[\hat{y}(s), \hat{z}(s)]^T \in X$ such that

$$\left\langle A\begin{bmatrix} d(s) \\ v(s) \end{bmatrix}, \begin{bmatrix} y(s) \\ z(s) \end{bmatrix} \right\rangle_X - \left\langle \begin{bmatrix} d(s) \\ v(s) \end{bmatrix}, \begin{bmatrix} \hat{y}(s) \\ \hat{z}(s) \end{bmatrix} \right\rangle_X = 0 \tag{5.14}$$

$$\text{for all } [d(s), v(s)]^T \in D(A).$$

Now consider

$$\left\langle A\begin{bmatrix} d(s) \\ v(s) \end{bmatrix}, \begin{bmatrix} y(s) \\ z(s) \end{bmatrix} \right\rangle_X - \left\langle \begin{bmatrix} v(s) \\ d''(s) - m^2 d(s) - \gamma v(s) \end{bmatrix}, \begin{bmatrix} y(s) \\ z(s) \end{bmatrix} \right\rangle_X = 0$$

$$\Rightarrow \quad \int_{s=0}^{s=\ell} \left[d''(s)z(s) - d'(s)\hat{y}'(s) - m^2 d(s)(z(s) + \hat{y}(s)) \right] \, ds$$

$$+ \int_{s=0}^{s=\ell} \left[v'(s)y'(s) + v(s)(m^2 y(s) - \gamma z(s) - \hat{z}(s)) \right] \, ds = 0$$

$$\Rightarrow \quad \int_{s=0}^{s=\ell} d''(s) \left[z(s) + \hat{y}(s) - \int_{\beta=0}^{\beta=s} \int_{\alpha=0}^{\alpha=\beta} m^2 (z(\alpha) + \hat{y}(\alpha)) \, d\alpha \, d\beta \right] \, ds$$

$$+ \int_{s=0}^{s=\ell} v'(s) \left[y'(s) - \int_{\alpha=0}^{\alpha=s} (m^2 y(\alpha) - \gamma z(\alpha) - \hat{z}(\alpha)) \, d\alpha \right] \, ds \tag{5.15}$$

$$-d'(s)\hat{y}(s)\Big|_{s=0}^{s=\ell} + \left[v(s) \int_{\alpha=0}^{\alpha=s} (m^2 y(s) - \gamma z(s) - \hat{z}(s)) \, d\alpha \right] \Big|_{s=0}^{s=\ell}$$

$$+ \left[d'(s) \int_{\beta=0}^{\beta=s} \int_{\alpha=0}^{\alpha=\beta} m^2 (z(s) + \hat{y}(s)) \, d\alpha \, d\beta \right] \Big|_{s=0}^{s=\ell}$$

$$- \left[d'(s) \int_{\alpha=0}^{\alpha=s} m^2 (z(s) + \hat{y}(s)) \, d\alpha \right] \Big|_{s=0}^{s=\ell} = 0.$$

Since this argument is true for all $[d(s), v(s)]^T \in D(A)$, we apply the boundary conditions on $D(A)$ to (5.15), which implies

$$\int_{s=0}^{s=\ell} d''(s) \left[z(s) + \hat{y}(s) - \int_{\beta=0}^{\beta=s} \int_{\alpha=0}^{\alpha=\beta} m^2 (z(\alpha) + \hat{y}(\alpha)) \, d\alpha \, d\beta \right] \, ds$$

$$+ \int_{s=0}^{s=\ell} v'(s) \left[y'(s) - \int_{\alpha=0}^{\alpha=s} (m^2 y(\alpha) - \gamma z(\alpha) - \hat{z}(\alpha)) \, d\alpha \right] \, ds \tag{5.16}$$

$$-d'(\ell)\hat{y}(\ell) + d'(0)\hat{y}(0) - d'(\ell) \int_{\alpha=0}^{\alpha=\ell} m^2 (z(\alpha) + \hat{y}(\alpha)) \, d\alpha$$

$$+d'(\ell) \int_{\beta=0}^{\beta=\ell} \int_{\alpha=0}^{\alpha=\beta} m^2 (z(\alpha) + \hat{y}(\alpha)) \, d\alpha d\beta = 0.$$

Since we desire for the boundary terms that arise in (5.16) to be eliminated, we need to enforce the following conditions on $D(A^*)$:

$$\hat{y}(0) = 0 \tag{5.17}$$

$$\hat{y}(\ell) = 0 \tag{5.18}$$

$$\int_{\alpha=0}^{\alpha=\ell} m^2(z(\alpha) + \hat{y}(\alpha))\ d\alpha = 0 \tag{5.19}$$

$$\int_{\beta=0}^{\beta=\ell} \int_{\alpha=0}^{\alpha=\beta} m^2(z(\alpha) + \hat{y}(\alpha))\ d\alpha\ d\beta = 0. \tag{5.20}$$

Assuming we do so, (5.16) is transformed into

$$\begin{aligned} &\int_{s=0}^{s=\ell} d''(s) \left[z(s) + \hat{y}(s) - \int_{\beta=0}^{\beta=s} \int_{\alpha=0}^{\alpha=\beta} m^2(z(\alpha) + \hat{y}(\alpha))\ d\alpha\ d\beta \right]\ ds \\ &+ \int_{s=0}^{s=\ell} v'(s) \left[y'(s) - \int_{\alpha=0}^{\alpha=s} (m^2 y(\alpha) - \gamma z(\alpha) - \hat{z}(\alpha))\ d\alpha \right]\ ds = 0. \end{aligned} \tag{5.21}$$

Since (5.21) holds for all $[d(s), v(s)]^T \in D(A)$, we know

$$\int_{s=0}^{s=\ell} d''(s) \left[z(s) + \hat{y}(s) - \int_{\beta=0}^{\beta=s} \int_{\alpha=0}^{\alpha=\beta} m^2(z(\alpha) + \hat{y}(\alpha))\ d\alpha\ d\beta \right]\ ds = 0 \tag{5.22}$$

and

$$\int_{s=0}^{s=\ell} v'(s) \left[y'(s) - \int_{\alpha=0}^{\alpha=s} (m^2 y(\alpha) - \gamma z(\alpha) - \hat{z}(\alpha))\ d\alpha \right]\ ds = 0. \tag{5.23}$$

We apply the Fundamental Lemma of the Calculus of Variations to (5.22) and (5.23), which yields

$$z(s) + \hat{y}(s) - \int_{\beta=0}^{\beta=s} \int_{\alpha=0}^{\alpha=\beta} m^2(z(\alpha) + \hat{y}(\alpha))\ d\alpha\ d\beta = c_1 s + c_2 \tag{5.24}$$

and

$$y'(s) - \int_{\alpha=0}^{\alpha=s} (m^2 y(\alpha) - \gamma z(\alpha) - \hat{z}(\alpha))\ d\alpha = c_3, \tag{5.25}$$

for $c_1, c_2, c_3 \in \mathbb{R}$. We can rewrite (5.25) as

$$y'(s) = c_3 + \int_{\alpha=0}^{\alpha=s} (m^2 y(\alpha) - \gamma z(\alpha) - \hat{z}(\alpha))\ d\alpha, \tag{5.26}$$

which represents $y'(s)$ as an indefinite integral. Therefore, $y'(s)$ is absolutely continuous and has a derivative almost everywhere, given by

$$\begin{aligned} & y''(s) = m^2 y(s) - \gamma z(s) - \hat{z}(s) \\ \Rightarrow \qquad & \hat{z}(s) = -y''(s) + m^2 y(s) - \gamma z(s). \end{aligned} \tag{5.27}$$

We not only demonstrate that $y''(s)$ exists but also the form $\hat{z}(s)$ must take. We now examine (5.24), which can be rewritten as

$$\hat{y}(s) = -z(s) + \int_{\beta=0}^{\beta=s} \int_{\alpha=0}^{\alpha=\beta} m^2 (z(\alpha) + \hat{y}(\alpha))\, d\alpha\, d\beta + c_1 s + c_2. \tag{5.28}$$

Since $\hat{y}(s) \in H_0^1(0,\ell)$, we know from (5.28) that $z'(s)$ exists. Due to the complexity of (5.28), we cannot readily identify if there is a simplified form of $\hat{y}(s)$ as we did with $\hat{z}(s)$. Therefore, we now work with a slightly different form of (5.14) in order to identify $\hat{y}(s)$. We remind the reader that we must still enforce the conditions in (5.17-5.20) on $D(A^*)$. Consider

$$\begin{aligned} \left\langle A \begin{bmatrix} d \\ v \end{bmatrix}, \begin{bmatrix} y \\ z \end{bmatrix} \right\rangle_X &= \left\langle \begin{bmatrix} v \\ d'' - m^2 d - \gamma v \end{bmatrix}, \begin{bmatrix} y \\ z \end{bmatrix} \right\rangle_X \\ &= \int_0^\ell \left[v'y' + m^2 vy + d''z - m^2 dz - \gamma vz \right] ds. \end{aligned} \tag{5.29}$$

We then integrate by parts to obtain

$$\begin{aligned} & \int_0^\ell \left[v'(s)y'(s) + m^2 v(s)y(s) + d''(s)z(s) - m^2 d(s)z(s) - \gamma v(s)z(s) \right] ds \\ &= \int_0^\ell \left[-v(s)y''(s) + m^2 v(s)y(s) - d'(s)z'(s) - m^2 d(s)z(s) - \gamma v(s)z(s) \right] ds \\ &\qquad + v(\ell)y'(\ell) - v(0)y'(0) + d'(\ell)z(\ell) - d'(0)z'(0) \\ &= \int_0^\ell \left[d'(s)(-z'(s)) + m^2 d(s)(-z(s)) + v(s)(-y''(s) + m^2 y(s) - \gamma z(s)) \right] ds \\ &\qquad + d'(\ell)z(\ell) - d'(0)z(0), \end{aligned} \tag{5.30}$$

due to boundary conditions on v and since we have already shown $y''(s)$ and $z'(s)$ exist. This means $\hat{y}' = -z' \Rightarrow \hat{y} = -z + c$, $\hat{y} = -z$, which implies $c = 0$. Additionally, (5.30) shows $\hat{z} = -y'' + m^2 y - \gamma z$, which we already obtained from (5.27). Since $\hat{y} = -z$, (5.19,5.20)

are satisfied trivially. We let $z \in H_0^1(0,\ell)$ since z has a first derivative and we must satisfy (5.17,5.18). Also, we must let $y \in H^2(0,\ell) \cap H_0^1(0,\ell)$. This tells us that $A^* : D(A^*) \subseteq X \to X$,

$$A^* \begin{bmatrix} d \\ v \end{bmatrix} = \begin{bmatrix} -v \\ -d'' + m^2 d - \gamma v \end{bmatrix} \qquad \text{for } [d,v]^T \in D(A^*), \tag{5.31}$$

and

$$D(A^*) = \left\{ \begin{bmatrix} d \\ v \end{bmatrix} \in X \middle| \; d \in H^2(0,\ell) \cap H_0^1(0,\ell),\; v \in H_0^1(0,\ell) \right\}. \tag{5.32}$$

Next we show that both A and A^* dissipative. We first consider

$$\begin{aligned} \left\langle A \begin{bmatrix} d \\ v \end{bmatrix}, \begin{bmatrix} d \\ v \end{bmatrix} \right\rangle_X &= \left\langle \begin{bmatrix} v \\ d'' - m^2 d - \gamma v \end{bmatrix}, \begin{bmatrix} d \\ v \end{bmatrix} \right\rangle_X \\ &= \int_0^\ell \left[d'(s)v'(s) + m^2 d(s)v(s) + v(s)d''(s) - m^2 d(s)v(s) - \gamma |v(s)|^2 \right] \, ds \qquad (5.33) \\ &= -\gamma \int_0^\ell |v(s)|^2 \, ds \leq 0, \end{aligned}$$

after integrating by parts and applying the boundary conditions on v. This shows that A is dissipative. Next we consider

$$\begin{aligned} \left\langle A^* \begin{bmatrix} d \\ v \end{bmatrix}, \begin{bmatrix} d \\ v \end{bmatrix} \right\rangle_X &= \left\langle \begin{bmatrix} -v \\ -d'' + m^2 d - \gamma v \end{bmatrix}, \begin{bmatrix} d \\ v \end{bmatrix} \right\rangle_X \\ &= \int_0^\ell \left[-d'(s)v'(s) - m^2 d(s)v(s) - v(s)d''(s) + m^2 d(s)v(s) - \gamma |v(s)|^2 \right] \, ds, \qquad (5.34) \\ &= -\gamma \int_0^\ell |v(s)|^2 \, ds \leq 0, \end{aligned}$$

after integrating by parts and applying the boundary conditions on v. This argument shows that A^* is also dissipative. Then by Theorem 2.10, A generates a C_0-semigroup.

We now focus our attention on the exponentially stable aspect. Considering $\Phi = [d,v]^T \in D(A)$, we define a new function

$$V(\Phi) = \int_0^\ell \left[|d'(s)|^2 + m^2 |d(s)|^2 + |v(s)|^2 \right] \, ds + \int_0^\ell \left[\gamma d(s)v(s) + \frac{\gamma^2}{2} |d(s)|^2 \right] \, ds. \tag{5.35}$$

We will show that $V(\Phi)$ is a Lyapunov function. The choice of this candidate for a Lyapunov function is based on discussion in [48]. We can readily note that $V(\Phi)$ is a continuous

function, but it is not obvious that $V(\Phi)$ is positive for all $\Phi \neq 0$. However, with some algebraic manipulation, we can show this straightforwardly. After completing the square with the terms $|v|^2$ and γdv, we can write $V(\Phi)$ as

$$V(\Phi) = \int_0^\ell \left[|d'(s)|^2 + \left(v(s) + \frac{\gamma}{2} d(s) \right)^2 - \frac{\gamma^2}{4} |d(s)|^2 + \left(m^2 + \frac{\gamma^2}{2} \right) |d(s)|^2 \right] ds. \tag{5.36}$$

Combining the last two terms in the integrand yields

$$V(\Phi) = \int_0^\ell \left[|d'(s)|^2 + \left(v(s) + \frac{\gamma}{2} d(s) \right)^2 + \left(m^2 + \frac{\gamma^2}{4} \right) |d(s)|^2 \right] ds, \tag{5.37}$$

which is obviously non-negative. Therefore, $V(\Phi) > 0$ for all $\Phi \neq 0$.

We will now show that $\dot{V}(\Phi) < 0$ for all $\Phi \neq 0$. We compute $\dot{V}(\Phi)$ as

$$\begin{aligned} \dot{V}(\Phi) &= \int_0^\ell \Big[2d'(s)v'(s) + 2v(s)(d''(s) - m^2 d(s) - \gamma v(s)) + \gamma d(s)(d''(s) \\ &\quad - m^2 d(s) - \gamma v(s)) + \gamma |v(s)|^2 + 2 \left(m^2 + \frac{\gamma^2}{2} \right) d(s)v(s) \Big] ds. \end{aligned} \tag{5.38}$$

Integrating by parts and rearranging terms yields

$$\dot{V}(\Phi) = -\gamma ||\Phi||_X^2 \leq 0 \tag{5.39}$$

for all $\Phi \in D(A)$. In particular, $-\gamma ||\Phi||_X^2 < 0$ if $\Phi \neq 0$. Therefore, $V(\Phi)$ is a Lyapunov function. We will now apply Theorem 2.15 to show we are guaranteed exponential stability.

We first note that the equilibrium is $\Phi_e = [0, 0]^T$ and $V(\Phi_e) = 0$. Additionally, $V(\Phi)$ is defined on the open ball $\mathcal{S}_r(\Phi_e)$, for some $r > 0$. We now need to show $V(\Phi) \geq f(||\Phi||_X)$ for all $\Phi \in \mathcal{S}_r(\Phi_e)$ and some monotone function $f : ([0, r]) \subset \mathbb{R} \to \mathbb{R}$ with $f(0) = 0$, $f(\eta) > 0$ for all $\eta \in (0, r)$. We now derive our choice for the monotone function f. We can rewrite $V(\Phi)$ as

$$\begin{aligned} V(\Phi) &= \int_0^\ell \Big[(2) \left(\frac{1}{2} \right) |d'(s)|^2 + \frac{1}{2} |v(s)|^2 + \frac{1}{2} |v(s)|^2 \\ &\quad + \gamma d(s)v(s) + \left(m^2 + \frac{\gamma^2}{2} \right) |d(s)|^2 \Big] ds. \end{aligned} \tag{5.40}$$

Then completing the square on the third and fourth terms in the integrand and rearranging

terms yields

$$\begin{aligned} V(\Phi) &= \int_0^\ell \left[\frac{1}{2}|d'(s)|^2 + \frac{1}{2}|v(s)|^2\right]\, ds + \\ &\quad \int_0^\ell \left[\frac{1}{2}|d'(s)|^2 + \frac{1}{2}\left(v + \frac{\gamma}{2}d\right)^2 + \left(m^2 + \frac{3\gamma^2}{8}\right)|d(s)|^2\right]\, ds \\ &\geq \int_0^\ell \left[\frac{1}{2}|d'(s)|^2 + \frac{1}{2}m^2|d(s)|^2 + \frac{1}{2}|v(s)|^2\right]\, ds \\ &= \frac{1}{2}||\Phi||_X^2. \end{aligned} \tag{5.41}$$

Based on this argument, we define our monotone function to be $f(||\Phi||_X) = \frac{1}{2}||\Phi||_X^2$. Also note $f(0) = 0$ and $f(\eta) > 0$ for all $\eta \in (0, r)$. This shows that Φ_e is stable. To guarantee asymptotic stability, we want to define a monotone function g such that $\dot{V}(\Phi) \leq -g(||\Phi - \Phi_e||_X)$ for all $\Phi \in \mathcal{S}_r(\Phi_e)$ and $g : ([0, r]) \subset \mathbb{R} \to \mathbb{R}$ with $g(0) = 0$ and $g(\eta) > 0$ for all $\eta \in (0, r)$. As shown above in equations (5.38) and (5.39), we could let $g(||\Phi||_X) = \gamma||\Phi||_X^2$. Then $g(0) = 0$ and $g(\eta) > 0$ for all $\eta \in (0, r)$, and we have shown that Φ_e is asymptotically stable. To be assured of exponential stability we need to find real numbers $c_2 \geq c_1 > 0,\ \mu > 0,\ k > 0$, such that $\dot{V}(\Phi) \leq -\mu V(\Phi)$ and $c_1||\Phi||_X^k \leq V(\Phi) \leq c_2||\Phi||_X^k$ for all $\Phi \in \mathcal{S}_r(\Phi_e)$. If we choose $k = 2$, and rewrite $V(\Phi)$ as in (5.41), then we want to find c_1 and c_2 such that the following holds

$$\begin{aligned} c_1||\Phi||_X^2 &\leq \frac{1}{2}||\Phi||_X^2 + \int_0^\ell \left[\frac{1}{2}|d'(s)|^2 + \frac{1}{2}\left(v(s) + \frac{\gamma}{2}d(s)\right)^2\right. \\ &\quad \left. + \frac{3\gamma^2}{8}|d(s)|^2\right]\, ds \leq c_2||\Phi||_X^2, \end{aligned} \tag{5.42}$$

or, equivalently,

$$\begin{aligned} c_1 &\leq \frac{1}{2} + \frac{1}{||\Phi||_X^2}\int_0^\ell \left[\frac{1}{2}|d'(s)|^2 + \frac{1}{2}\left(v(s) + \frac{\gamma}{2}d(s)\right)^2\right. \\ &\quad \left. + \frac{3\gamma^2}{8}|d(s)|^2\right]\, ds \leq c_2. \end{aligned} \tag{5.43}$$

Note that the integral term is non-negative. So we can choose $c_1 \in \left(0, \frac{1}{2}\right)$ such that the lower bound will be satisfied and a sufficiently large choice for c_2 will allow the upper

bound to be satisfied. Therefore, there exist real numbers c_1, c_2, and k such that $c_1||\Phi||_X^k \leq V(\Phi) \leq c_2||\Phi||_X^k$ for all $\Phi \in \mathcal{S}_r(\Phi_e)$. We now want to find μ such that $\dot{V}(\Phi) \leq -\mu V(\Phi)$. After algebraic manipulation, we find this is equivalent to desiring

$$\begin{aligned}(\gamma-\mu)\int_0^\ell |d'(s)|^2\,ds \;\; + \;\; \int_0^\ell \left[(\gamma-\mu)|v(s)|^2 - \mu\gamma d(s)v(s)\right]\,ds + \\ \left(\gamma m^2 - \mu m^2 - \frac{\gamma^2\mu}{2}\right)\int_0^\ell |d(s)|^2\,ds \quad \geq \;\; 0.\end{aligned} \tag{5.44}$$

We now complete the square on the $|v|^2$ and dv terms, thereby yielding the following inequality we would like to achieve:

$$\begin{aligned}(\gamma-\mu)\int_0^\ell |d'(s)|^2\,ds + (\gamma-\mu)\int_0^\ell \left(v(s) - \frac{\mu\gamma}{2(\gamma-\mu)}d(s)\right)^2\,ds + \\ \left(\gamma m^2 - \mu m^2 - \frac{\gamma^2\mu}{2}\right)\int_0^\ell |d(s)|^2\,ds \geq \frac{\mu^2\gamma^2}{4\,(\gamma-\mu)}\int_0^\ell |d(s)|^2\,ds.\end{aligned} \tag{5.45}$$

Since the first two terms are non-negative, and we have parameters values $m = .001$ and $\gamma = .05$, if we can show

$$\begin{aligned}\left(\left(5\times 10^{-8}\right) - (1\times 10^{-6})\mu - (1.25\times 10^{-3})\mu\right)\int_0^\ell |d(s)|^2\,ds \geq \\ \left(\frac{(6.25\times 10^{-4})\mu^2}{.05-\mu}\right)\int_0^\ell |d(s)|^2\,ds,\end{aligned} \tag{5.46}$$

then this will be enough to guarantee $\dot{V}(\Phi) \leq -\mu V(\Phi)$ for some $\mu > 0$. We note that this inequality is satisfied, non-uniquely, if we take $\mu = .01$. Therefore, by Theorem 2.15, Φ_e is exponentially stable with exponent $-\frac{1}{2}(\gamma\times 10^{-9})t$, and A generates an exponentially stable C_0-semigroup. $\boxtimes$

We can now use distributed parameter control theory to design a control for the system. To write a finite dimensional approximation of the PDE, we use a Galerkin finite element scheme. To determine the finite element approximation to the KGL equation, we first write the weak form of the PDE. Considering the weak form of the problem, we want to find an $\omega(s) \in S = H_0^1(0,\ell)$ such that

$$\begin{aligned}\int_0^\ell \ddot{\omega}(t,s)y(s)\,ds - \int_0^\ell \omega''(t,s)y(s)\,ds + \int_0^\ell m^2\omega(t,s)y(s)\,ds \\ + \int_0^\ell \gamma\dot{\omega}(t,s)y(s)\,ds = \int_0^\ell u(t)\sum_{i=1}^m b_i(s)y(s)\,ds\end{aligned} \tag{5.47}$$

for all $y(s) \in Y \subseteq H_0^1(0,\ell)$. After integrating by parts, we arrive at

$$\begin{aligned}\int_0^\ell \ddot{\omega}(t,s)y(s)\ ds + \int_0^\ell \omega'(t,s)y'(s)\ ds + \int_0^\ell m^2\omega(t,s)y(s)\ ds \\ + \int_0^\ell \gamma\dot{\omega}(t,s)y(s)\ ds = \int_0^\ell u(t)\sum_{i=1}^m b_i(s)y(s)\ ds.\end{aligned} \tag{5.48}$$

In order to develop a finite dimensional problem using a Galerkin finite element approximation, we divide the spatial domain $[0,\ell]$ into N equidistant subintervals. Then approximate $\omega(t,s)$ by $\omega^N(t,s) = \sum_{i=1}^N c_i(t)\varphi_i(s)$, where $\varphi_i(s)$ are piecewise linear basis functions and $c_i(t)$ are their coefficients. After making this substitution for $\omega(t,s)$ in (5.48), we have

$$\begin{aligned}\int_0^\ell \ddot{\omega}^N(t,s)y(s)\ ds + \int_0^\ell \omega'^N(t,s)y'(s)\ ds + \int_0^\ell m^2\omega^N(t,s)y(s)\ ds \\ + \int_0^\ell \gamma\dot{\omega}^N(t,s)y(s)\ ds = \int_0^\ell u(t)\sum_{i=1}^m b_i(s)y(s)\ ds,\end{aligned} \tag{5.49}$$

or equivalently,

$$\begin{aligned}\int_0^\ell \sum_{i=1}^N \ddot{c}_i(t)\varphi_i(s)y(s)\ ds + \int_0^\ell \sum_{i=1}^N c_i(t)\varphi_i'(s)y'(s)\ ds \\ + \int_0^\ell m^2\sum_{i=1}^N c_i(t)\varphi_i(s)y(s)\ ds + \int_0^\ell \gamma\sum_{i=1}^N \dot{c}_i(t)\varphi_i(s)y(s)\ ds = \\ \int_0^\ell u(t)\sum_{i=1}^m b_i(s)y(s)\ ds.\end{aligned} \tag{5.50}$$

We let $y(s)$ range over the basis functions, $\varphi_i(s)$ for $i = 1,\ldots,N$, to obtain

$$M\begin{bmatrix}\ddot{c}_1(t)\\ \vdots \\ \ddot{c}_N(t)\end{bmatrix} + K\begin{bmatrix}c_1(t)\\ \vdots \\ c_N(t)\end{bmatrix} + m^2M\begin{bmatrix}c_1(t)\\ \vdots \\ c_N(t)\end{bmatrix} + \gamma M\begin{bmatrix}\dot{c}_1(t)\\ \vdots \\ \dot{c}_N(t)\end{bmatrix} = u(t)B_0, \tag{5.51}$$

where $M = \left[\int_0^\ell \varphi_i(s)\varphi_j(s)\ ds\right]_{i,j=1}^N$ and $K = \left[\int_0^\ell \varphi_i'(s)\varphi_j'(s)\ ds\right]_{i,j=1}^N$ are the mass and

stiffness matrices, respectively, and $B_0 = \left[\int_0^\ell \sum_{i=1}^{m} b_i(s)\varphi_j(s)\, ds\right]_{j=1}^{N}$. Then

$$\begin{bmatrix} \ddot{c}_1(t) \\ \vdots \\ \ddot{c}_N(t) \end{bmatrix} = (-M^{-1}K - m^2 I)\begin{bmatrix} c_1(t) \\ \vdots \\ c_N(t) \end{bmatrix} - \gamma I \begin{bmatrix} \dot{c}_1(t) \\ \vdots \\ \dot{c}_N(t) \end{bmatrix} + u(t)M^{-1}B_0. \tag{5.52}$$

We desire to convert this into a first order system of differential equations, so we define $x_1(t) = c(t)$ and $x_2(t) = \dot{x}_1(t) = \dot{c}(t)$ and (5.52) becomes

$$\begin{bmatrix} \dot{x}_1(t) \\ \dot{x}_2(t) \end{bmatrix} = \begin{bmatrix} 0 & I \\ (-M^{-1}K - m^2 I) & -\gamma I \end{bmatrix}\begin{bmatrix} x_1(t) \\ x_2(t) \end{bmatrix} + \begin{bmatrix} 0 \\ M^{-1}B_0 \end{bmatrix} u(t). \tag{5.53}$$

We still desire a measurement equation as in (2.3), and in this framework, the measurement equation will be

$$y(t) = C\begin{bmatrix} x_1(t) \\ x_2(t) \end{bmatrix}. \tag{5.54}$$

In particular, for all KGL simulations, four averaging measurements of both position and velocity are taken, and this creates the $8 \times (2N-2)$ dimensional matrix C, given by

$$C = \begin{bmatrix} \left[\frac{4}{\ell}\int_0^{\frac{\ell}{4}} \varphi_i^N(s)ds\right]_{i=1}^{N-1} & 0 \\ \left[\frac{4}{\ell}\int_{\frac{\ell}{4}}^{\frac{\ell}{2}} \varphi_i^N(s)ds\right]_{i=1}^{N-1} & 0 \\ \left[\frac{4}{\ell}\int_{\frac{\ell}{2}}^{\frac{3\ell}{4}} \varphi_i^N(s)ds\right]_{i=1}^{N-1} & 0 \\ \left[\frac{4}{\ell}\int_{\frac{3\ell}{4}}^{\ell} \varphi_i^N(s)ds\right]_{i=1}^{N-1} & 0 \\ 0 & \left[\frac{4}{\ell}\int_0^{\frac{\ell}{4}} \varphi_i^N(s)ds\right]_{i=1}^{N-1} \\ 0 & \left[\frac{4}{\ell}\int_{\frac{\ell}{4}}^{\frac{\ell}{2}} \varphi N_i(s)ds\right]_{i=1}^{N-1} \\ 0 & \left[\frac{4}{\ell}\int_{\frac{\ell}{2}}^{\frac{3\ell}{4}} \varphi_i^N(s)ds\right]_{i=1}^{N-1} \\ 0 & \left[\frac{4}{\ell}\int_{\frac{3\ell}{4}}^{\ell} \varphi_i^N(s)ds\right]_{i=1}^{N-1} \end{bmatrix}. \tag{5.55}$$

For the purpose of defining $\{b_i\}_{i=1}^m$, we create a partition of $[0, \ell]$ as $\{s_i\}_{i=1}^m$ where $s_i = i*\ell/m$. We then choose the functions b_i to be defined by $b_i(s) = e^{-(s-s_i^*)^2}$ for $s_{i-1} \leq s \leq s_i$, where $s_i^* = \dfrac{s_{i-1}+s_i}{2} = 1.25, 3.75, 6.25, 8.75$ in this problem since we take $m = 4$. These functions are depicted in Figure 5.1. We define $B_i = \displaystyle\int_0^\ell b_i(s)\varphi_j(s)\, ds$ for $i = 1, \ldots, m$, $j = 1, \ldots, N-1$,

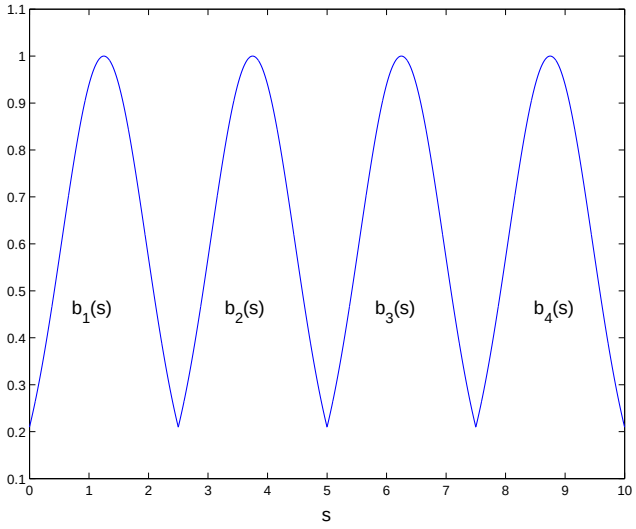

Figure 5.1: Control Input Functions, $b_i(s)$

and thus

$$B_0 = \begin{bmatrix} 0 & \cdots & 0 \\ B_1 & \cdots & B_m \end{bmatrix}. \tag{5.56}$$

We note that (5.53) and (5.54) are precisely of the form in (3.23), and we can apply the ideas from Chapter 3 for control design. We now turn our attention to numerical results. Similar numerical results can be found in [9, 10].

5.1 Numerical Results with $R = .001 * I$

For all simulations in this section we take $N = 80$ since we will typically obtain convergence of a Galerkin finite element scheme at a lower value of N. Additionally, we take the MinMax parameter to be as large as possible: $\theta = .81$. In this section, we will present results

regarding singular values, uncontrolled simulations, functional gains, controlled simulations, and finally, controller robustness.

5.1.1 Uncontrolled Results

We begin by displaying the Hankel singular values and the LQG characteristic values, respectively, in Figure 5.2. Table 5.1 provides the corresponding number of states needed to retain 95% and 99% information about the system, which is contained in the singular values.

The information in this table is quite similar to that which we found for the cable mass

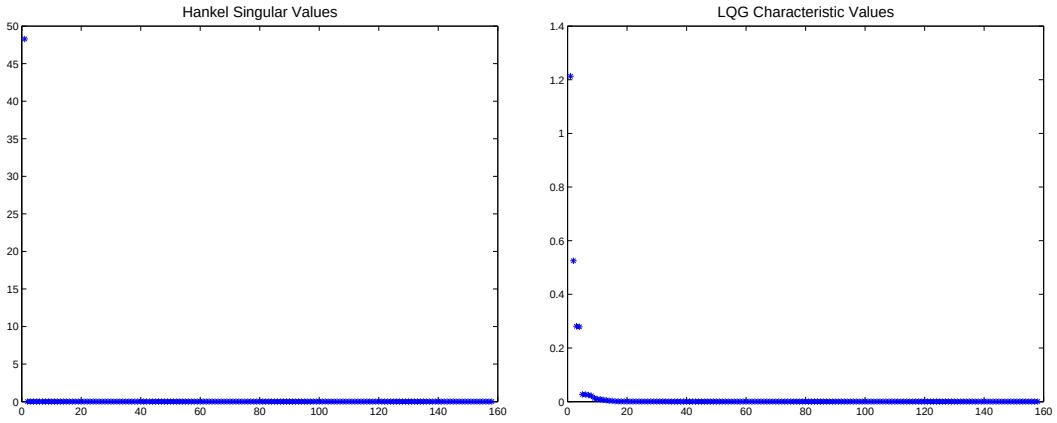

Figure 5.2: Hankel Singular Values (left), LQG Characteristic Values (right)

	Values needed for	
	95% significance	99% significance
Hankel singular values	1	1
LQG characteristic values	6	15

Table 5.1: Values needed to retain 95% and 99% information.

system in Table 4.2. We again demonstrate that the low order controller performance seems to be more dependent on the control design used as opposed to the number of states retained in the low order state estimate. However, we continue to provide this information since those who typically use POD for low order controller design often refer to values of this nature in order to determine the order of the controller.

We choose initial conditions of the form

$$x_0 = \left[x(0,s), \frac{\partial}{\partial t}x(0,s)\right] = [\sin s, \cos s], \qquad \left[x_c(0,s), \frac{\partial}{\partial t}x_c(0,s)\right] = [x_0, .75x_0], \tag{5.57}$$

in order to simulate and obtain a solution.

We begin with the uncontrolled position state in Figure 5.3. We have chosen sinusoidal initial conditions that generate much oscillation. Once we apply a control, we hope to see the position state tend to zero since $[d, v]^T = [0, 0]^T$ is an exponentially stable equilibrium for the equation.

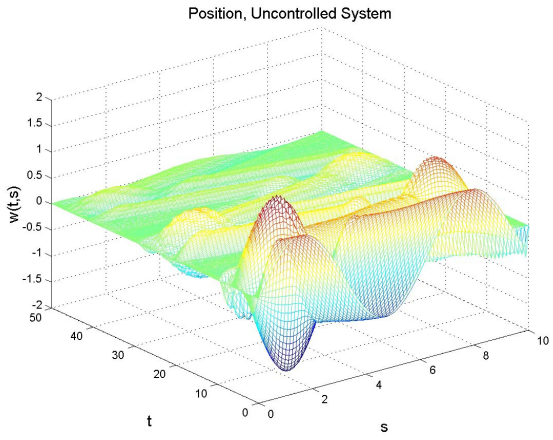

Figure 5.3: Uncontrolled Position State

5.1.2 Controlled Results

Before applying the different controllers to KGL, we look at the functional gains plots in order to visually verify that we have gain convergence. We examine the full order and reduced order functional gains for the LQG, MinMax, and central controllers in Figures 5.4, 5.5, and 5.6, respectively. Since there are four actuators in the system, there will be four position and four velocity gains for each controller type. For all three sets of plots, the color legend is as follows: $N = 10$ cyan, $N = 20$ blue, $N = 40$ green, $N = 80$ red, and $N = 160$ black. The figures appear to show the functional gains are converging to zero.

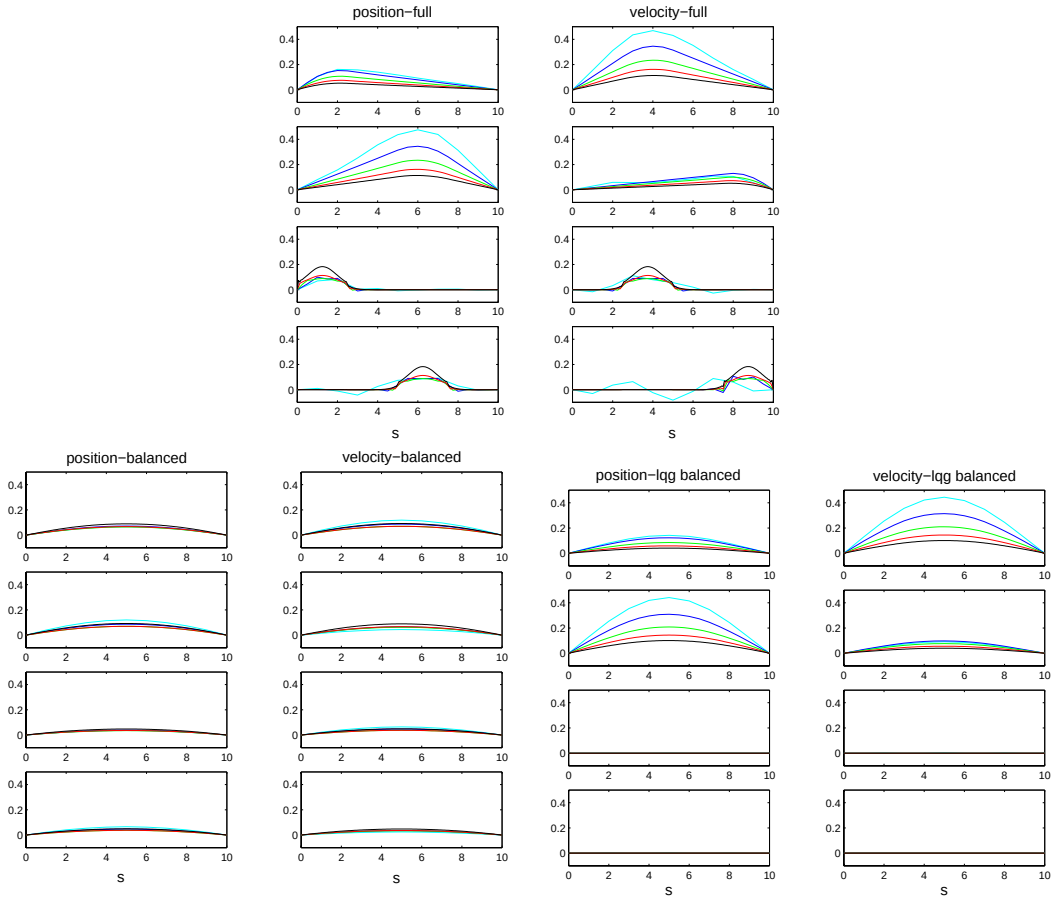

Figure 5.4: LQG Controller: Full Order Functional Gains (top), Reduced Order Balanced Gains (bottom left), Reduced Order LQG Balanced Gains (bottom right)

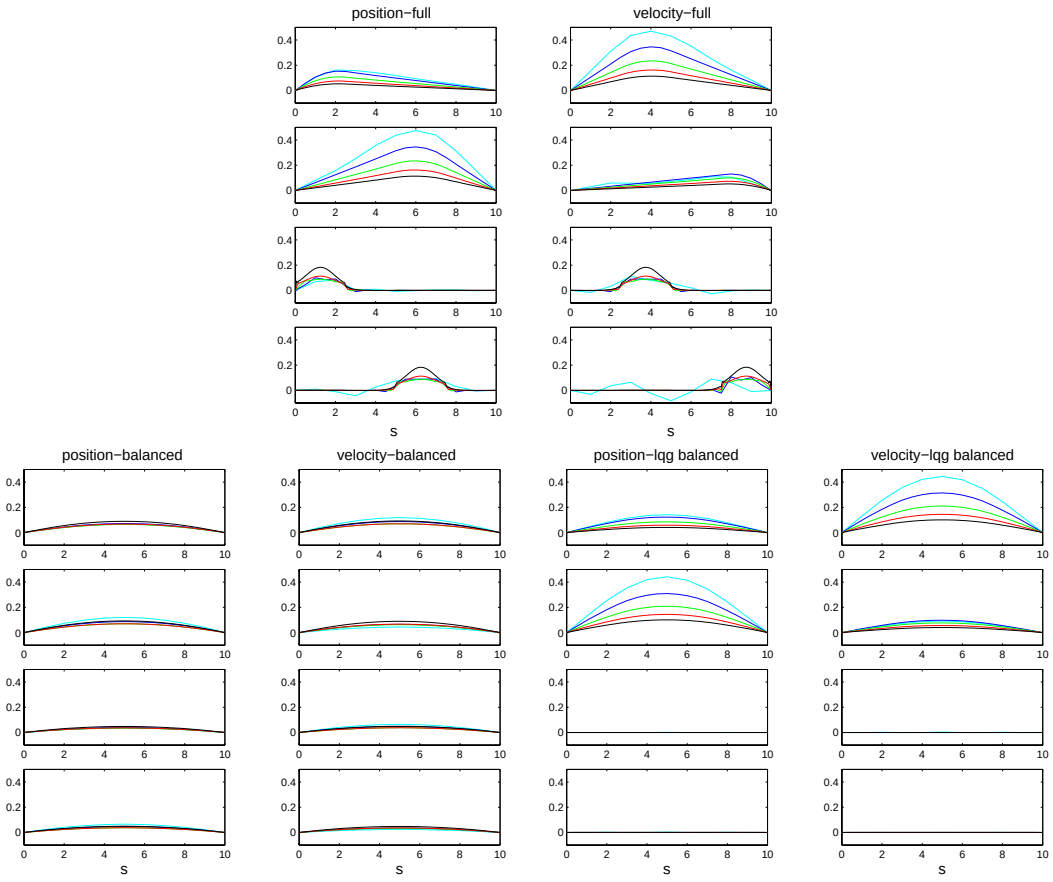

Figure 5.5: MinMax Controller: Full Order Functional Gains (top), Reduced Order Balanced Gains (bottom left), Reduced Order LQG Balanced Gains (bottom right)

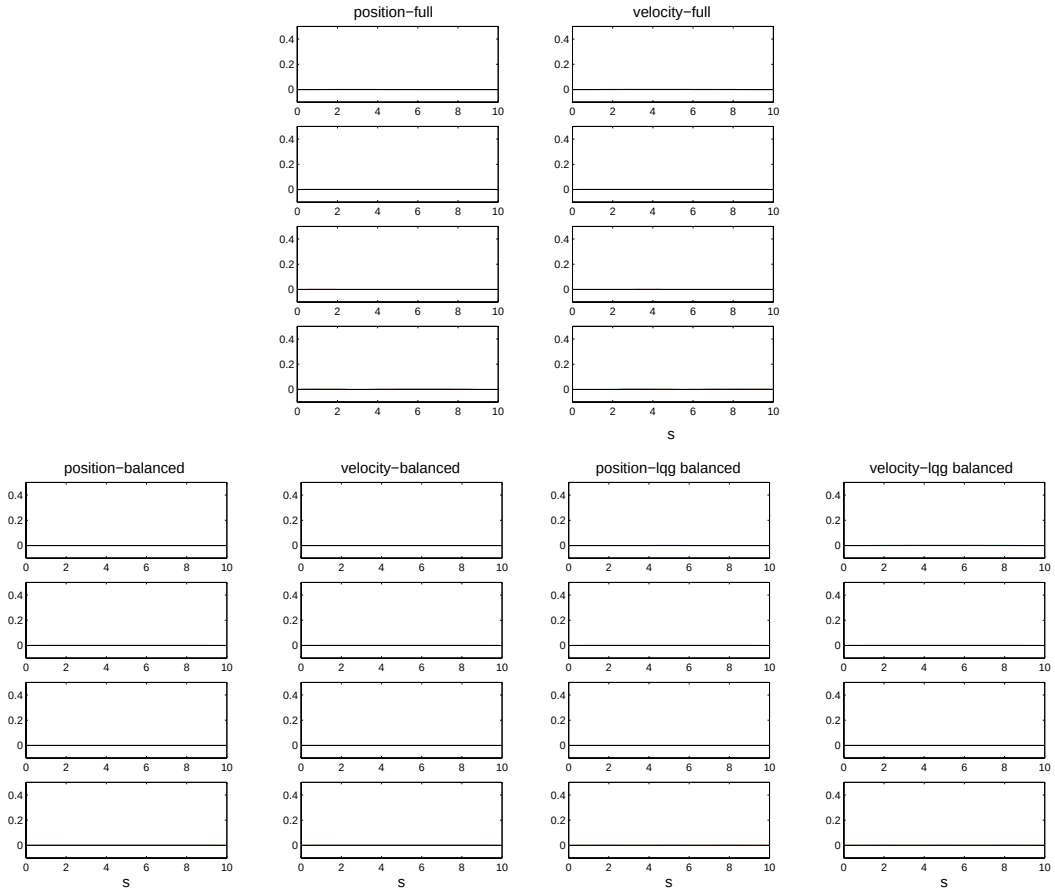

Figure 5.6: Central Controller: Full Order Functional Gains (top), Reduced Order Balanced Gains (bottom left), Reduced Order LQG Balanced Gains (bottom right)

We now look at simulations where the control is a full order compensator. The application of the LQG, MinMax, and central controllers are contained in Figure 5.7. All three controllers do a nice job at driving the position state toward zero, including decreasing the amplitude of waves occurring early in time caused by the initial conditions. We note there appears to be no visual difference in the performance of the controllers.

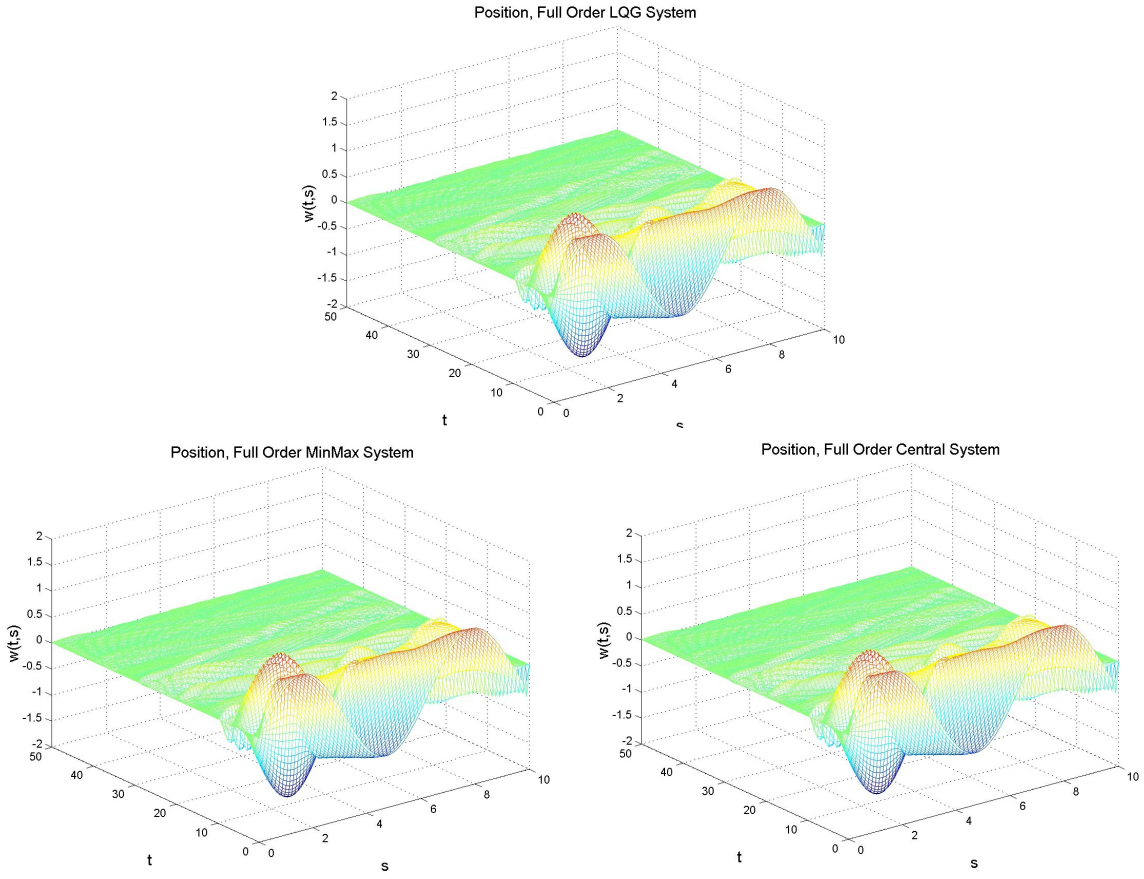

Figure 5.7: Full Order Position State: LQG controller (top), MinMax controller (bottom left), and Central controller (bottom right)

Figure 5.8 displays the full order LQG, MinMax, and central controllers. The LQG and MinMax controllers require several orders of magnitude more effort than the central controller, which is not identically zero, but on the order of 10^{-4}. As discussed in Section 4.2, this is not a surprising observation based on the control weight being used in these results, i.e., $R = .001 * I$. Note the small scale, indicating that even the LQG and MinMax controllers do not need much control effort.

We now focus our attention on low order controllers designed using balanced truncation and

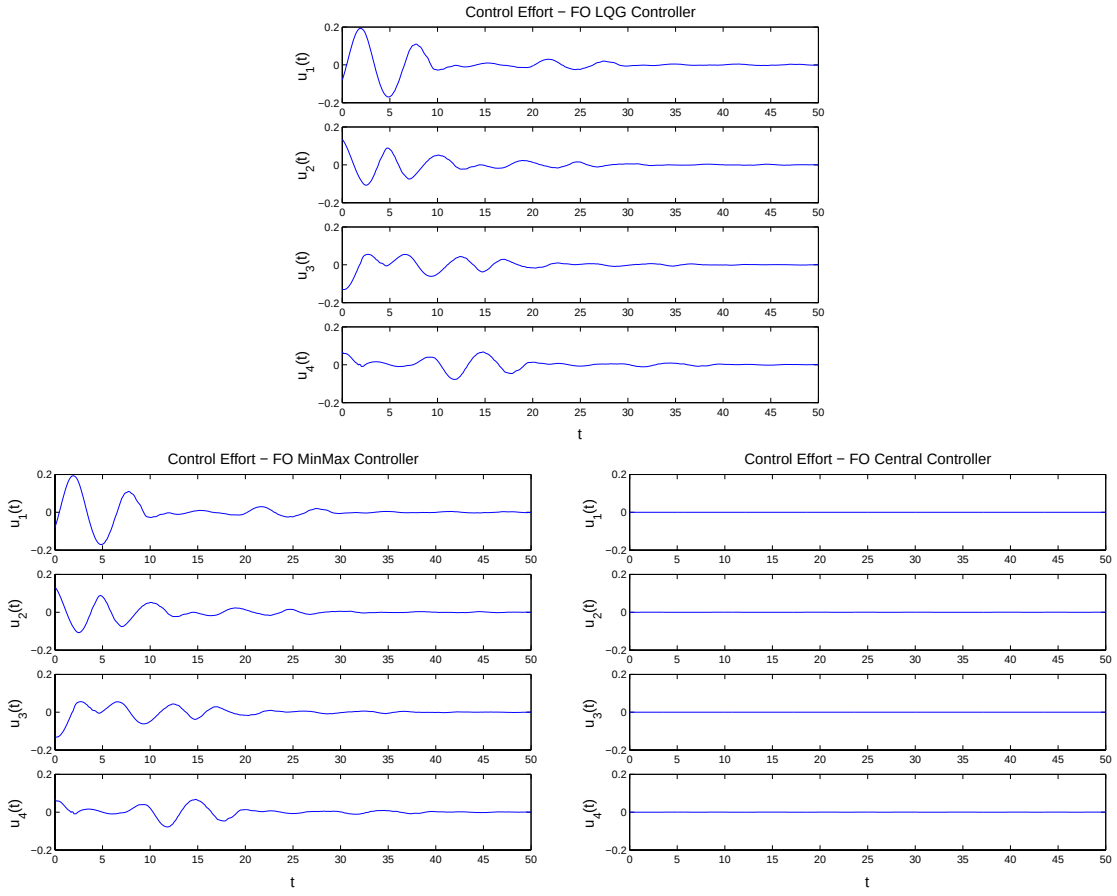

Figure 5.8: Control Effort: Full Order LQG (top), Full Order MinMax (bottom left), Full Order Central (bottom right)

LQG balanced truncation. In particular, we design first order controllers, i.e., $q = 1$ in (3.28). We will continue in our approach to compare low order LQG controllers obtained through these two reduction methods, low order MinMax controllers, and low order central controllers and then compare the performance of each control design.

First Order Controllers

Figures 5.9, 5.10, and 5.11 provide the behavior of the system when low order LQG, MinMax, and central controllers are applied, respectively. We see no real difference between the two LQG controllers, the two MinMax controllers, and the two central controllers. All three sets of position states resemble the uncontrolled position more than the full order controlled simulations. Although this is certainly not favorable, we can at least note that all three controllers perform comparably; that is, there is no visible difference between the first order LQG, MinMax, or central controllers.

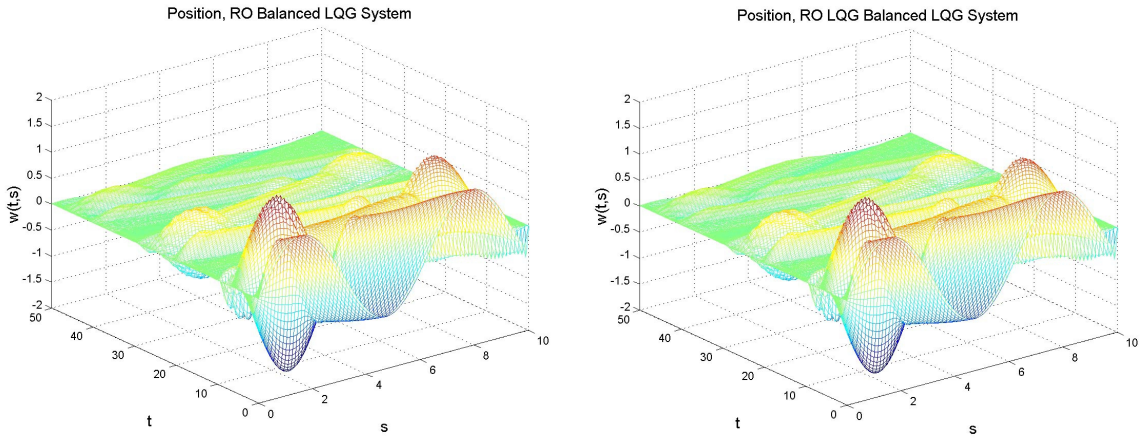

Figure 5.9: Reduced Order Position State: Balanced LQG Controller (left) and LQG Balanced LQG Controller (right)

The poor performance of all the low order controllers prompts us to examine the control effort of each. Figures 5.12, 5.13, and 5.14 show the reduced order LQG, MinMax, and central controllers, respectively. We quickly identify that all of the low order controllers are essentially requiring no effort, so it is not surprising that the controlled simulations do not yield favorable results. However, the LQG balanced controllers appear to be identically zero, while we can observe this is not true of the balanced controllers. In fact, the LQG balanced controllers are not identically zero, but there are orders of magnitude difference between the balanced and LQG balanced controllers. Additionally, the vertical axis scale, which is kept

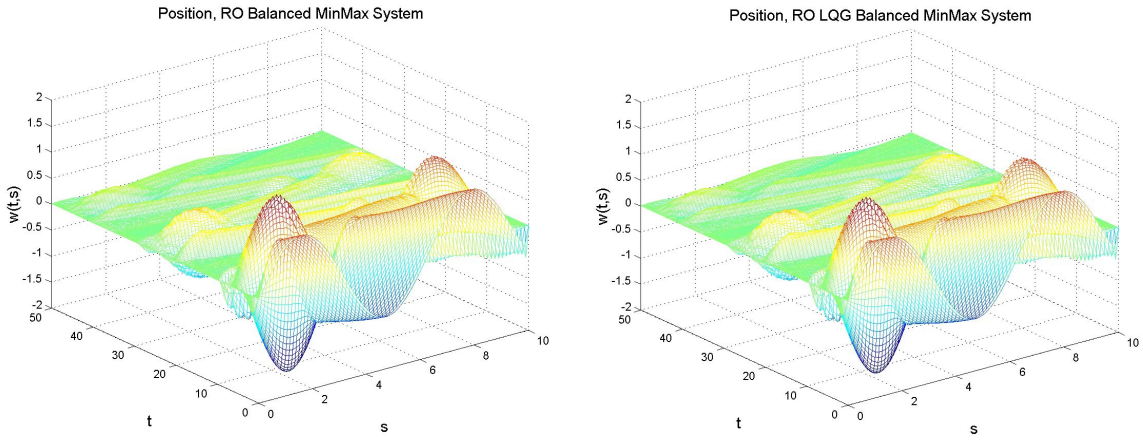

Figure 5.10: Reduced Order Position State: Balanced MinMax Controller (left) and LQG Balanced MinMax Controller (right)

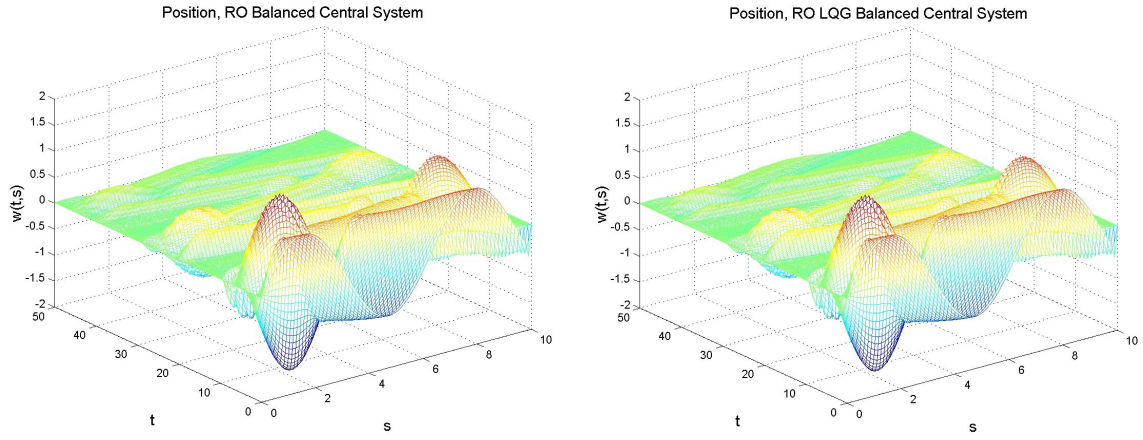

Figure 5.11: Reduced Order Position State: Balanced Central Controller (left) and LQG Balanced Central Controller (right)

consistent with the full order controllers for comparison sake, enhances the impression that the LQG balanced controllers are zero.

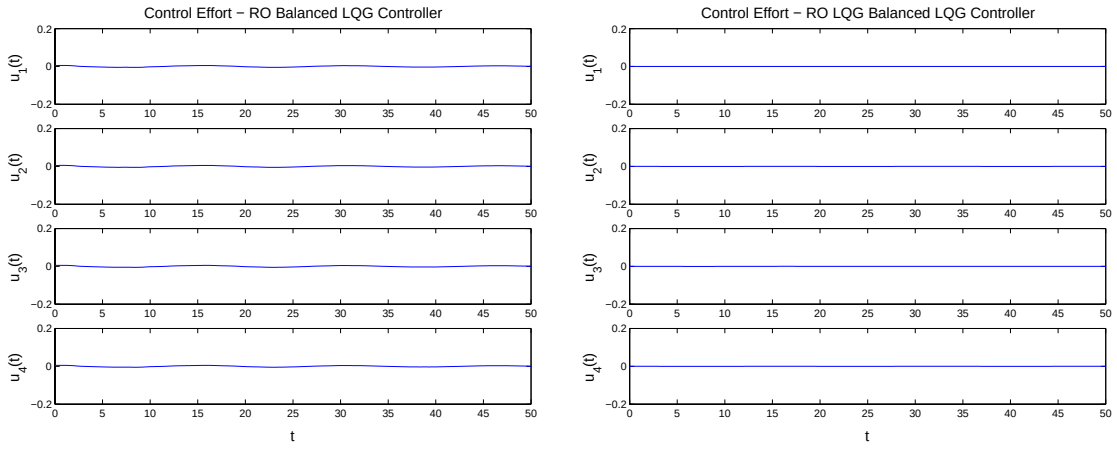

Figure 5.12: Control Effort: Reduced Order Balanced LQG (left), Reduced Order LQG Balanced LQG (right)

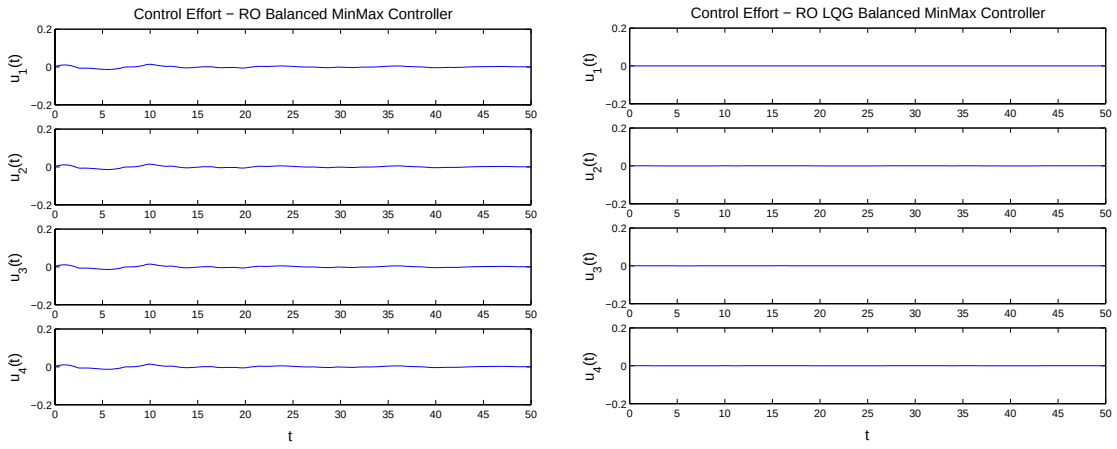

Figure 5.13: Control Effort: Reduced Order Balanced MinMax (left), Reduced Order LQG Balanced MinMax (right)

Controllers of Other Orders

In an attempt to see if we can enhance the performance of our low order controllers, we consider controllers of slightly higher order. Therefore, we now explore the possibility of

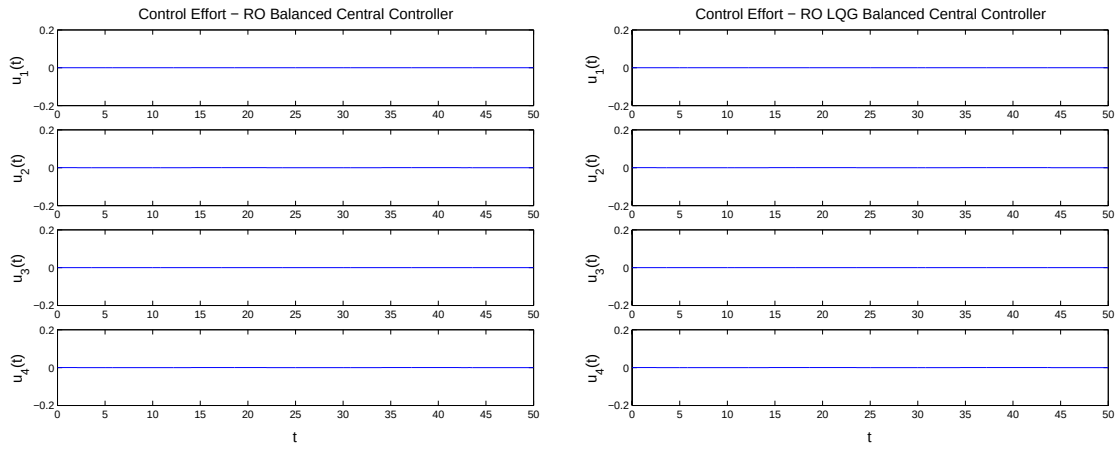

Figure 5.14: Control Effort: Reduced Order Balanced Central (left), Reduced Order LQG Balanced Central (right)

using a second, third, fourth, or fifth order controller.

If we use a second or third order controller, there is no visible difference in the performances of any of the low order controllers. It is not until we use a fourth order controller that we see any difference. We note that the difference is minute, but we now present the fourth order controller simulations. Additionally, note that a fifth order controller results in the balanced central controller being unstable.

Figures 5.15, 5.16, and 5.17 provide the fourth order LQG, MinMax, and central controlled systems, respectively. If we compare the first and fourth order LQG controlled systems, in Figures 5.9 and 5.15, respectively, we see there is only a shift in the fourth order balanced controller, with no real change in the amplitude of waves, while the fourth order LQG balanced controller experiences an increase in wave amplitude and performs *worse*. This would seem to indicate that even though we include more information in the fourth order controller, perhaps it is irrelevant, or bad, information.

Comparing the first and fourth order MinMax controlled systems, in Figures 5.10 and 5.16, respectively, we again see there is only a shift in the fourth order balanced controller, while the fourth order LQG balanced controller actually performs *worse* by seeing an increase in the amplitude of the waves. It appears that we are including unnecessary information, almost comparable to including a disturbance, and causing the LQG balanced controller to attempt to attenuate this "noise." We note there is no difference in the first and fourth order central controlled systems in Figures 5.11 and 5.17, respectively.

To summarize, on the whole, our first order controllers perform better than our fourth order

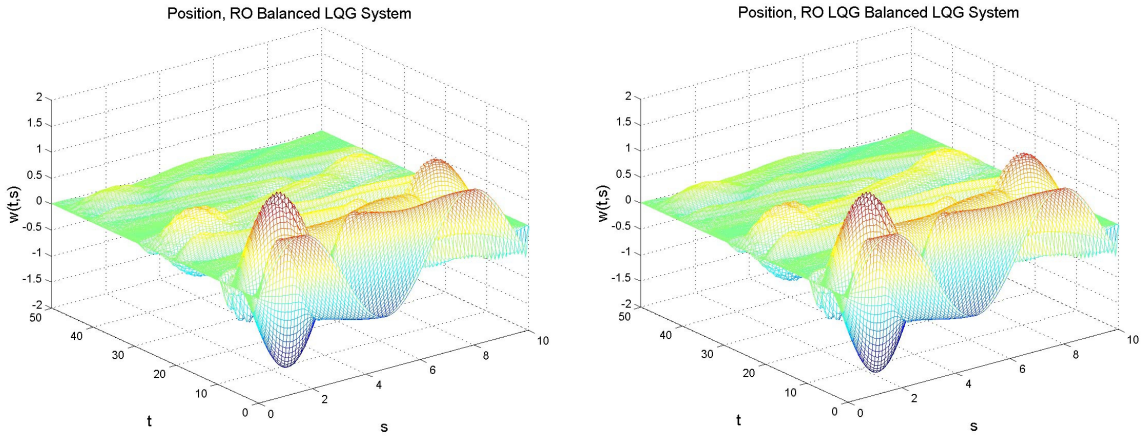

Figure 5.15: Reduced Order Position State: Balanced LQG Controller (left) and LQG Balanced LQG Controller (right)

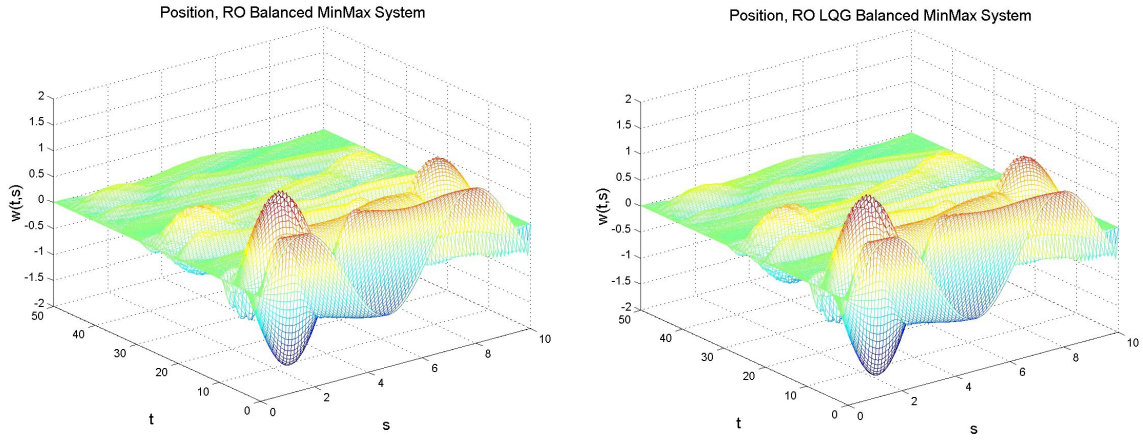

Figure 5.16: Reduced Order Position State: Balanced MinMax Controller (left) and LQG Balanced MinMax Controller (right)

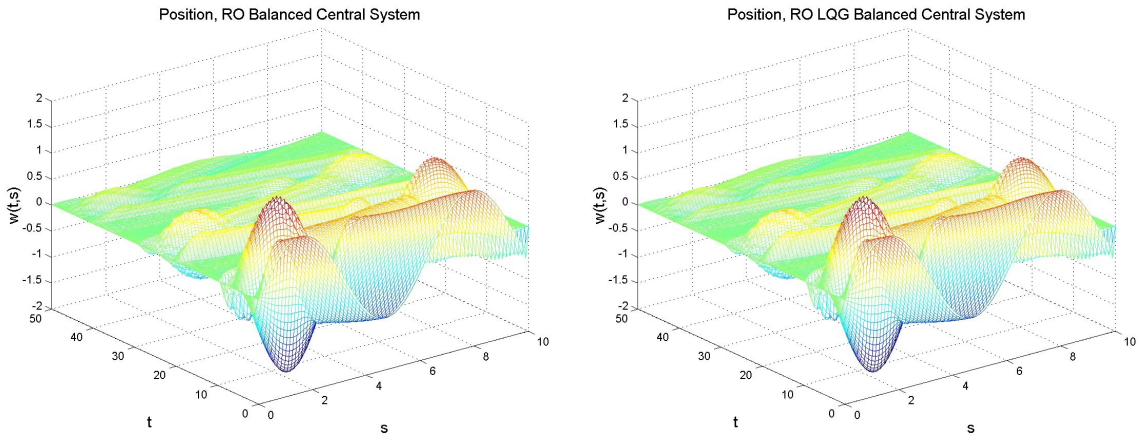

Figure 5.17: Reduced Order Position State: Balanced Central Controller (left) and LQG Balanced Central Controller (right)

controllers. Additionally, there is no distinguishing the performance of the LQG, MinMax, and central controllers based on our simulations thus far. Consequently, we look at robustness measures of the controllers in order to get a better idea which controller is more desirable for implementation.

5.1.3 Robustness of Low Order Controllers

First Order Controllers

We first look at the eigenvalues of all systems being examined in Figure 5.18, paying particular attention to those eigenvalues closest to the imaginary axis since they will likely impact the stability margin the greatest.

From the zoomed in views of the eigenvalues, we can identify there is a shift to the right of eigenvalues corresponding to the low order balanced and LQG balanced LQG and balanced MinMax controllers, as compared with the eigenvalues of the full order controlled systems. Thus, we expect decreased stability margins for the low order LQG controllers, which will result in a slower decay of solution and decreased performance.

The stability margins for all systems we consider are on the same order of magnitude, with the balanced and LQG balanced central controller values being the largest. The stability radii for these systems paint a different picture. The three full order controlled systems are on the same order of magnitude and within 7.75×10^{-3} of each other. Interestingly, the

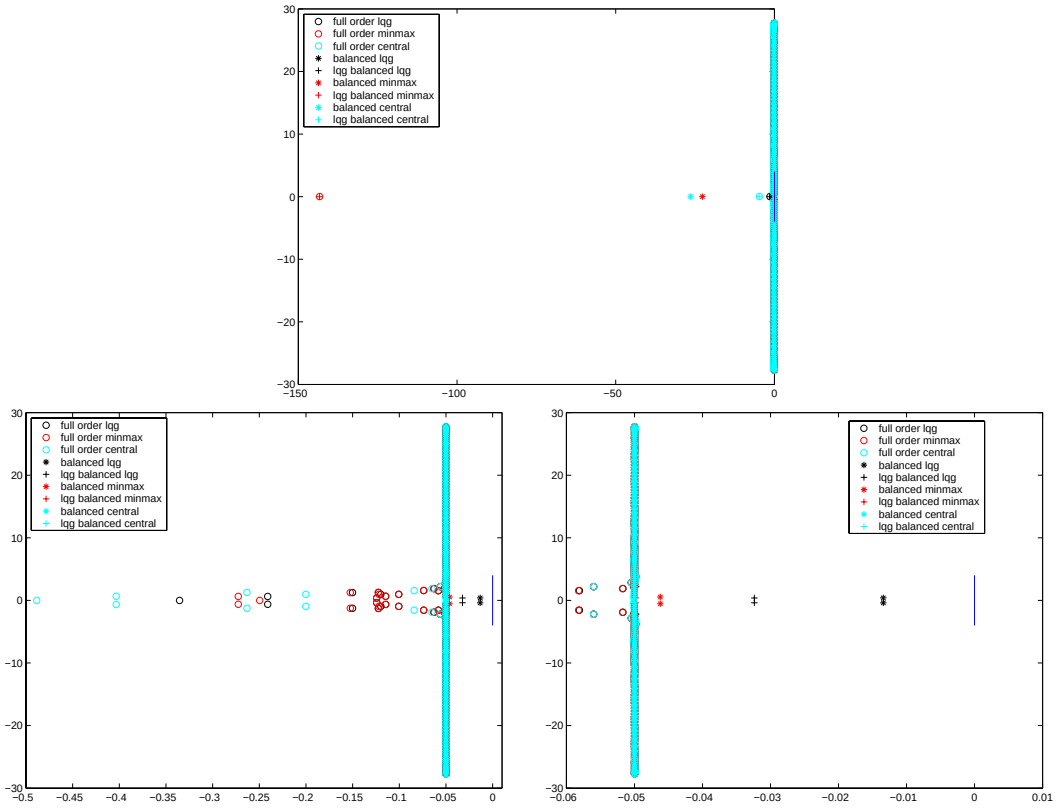

Figure 5.18: Eigenvalues (top), Zoomed In Views (bottom)

Matrix	Stability Margin	Stability Radius	Guaranteed Robustness Margin
Full order LQG	0.04981	0.06678	n/a
Full order MinMax	0.04981	0.05903	n/a
Full order central	0.04982	0.06650	0.63610
Balanced LQG	0.01341	0.00176	n/a
LQG balanced LQG	0.03237	0.04974	n/a
Balanced MinMax	0.04621	0.00283	n/a
LQG balanced MinMax	0.04983	0.04943	n/a
Balanced central	0.05000	0.00109	0.92609
LQG balanced central	0.04999	0.03213	0.63610

Table 5.2: Stability Margins and Radii for Full and Reduced Order Compensators.

stability radii of all three LQG balanced controllers are on the same order of magnitude as the full order controllers. Additionally, the stability radii of all three balanced controllers are an order of magnitude less than those of the full order and LQG balanced controllers. The robustness margins guaranteed by the central controller indicate that the balanced central controller should stabilize much larger perturbations than the full order or LQG balanced central controllers.

We now show parameter study results similar to those we provided for the cable mass system. We design first order controllers based on a low order system with $N = 10$. Due to this change in our discretization, we must modify the value of the MinMax parameter, θ, used. In particular, the largest we may take the parameter is $\theta = .77$. We then take these low order controllers and apply them to a high order system with $N = 80$. We denote these systems with diamond shapes in Figures 5.19, 5.20, and 5.21. We also apply these low order controllers to high order systems where we vary the values of the mass and damping parameters. If the low order controller stabilizes the high order system, then there is a dot on the graph for the corresponding mass and damping pair. If the low order controller does not stabilize the high order system, there is a square on the plot for the related mass and damping.

The balanced MinMax controller has a slightly smaller stabilizing region than that of the LQG balanced MinMax controller. The other balanced controllers designed stabilize comparably to their LQG balanced counterparts. Additionally, both central controllers stabilize all systems considered in the parameter studies, while both LQG and MinMax controllers fail to stabilize at least some of the parameter pairings considered.

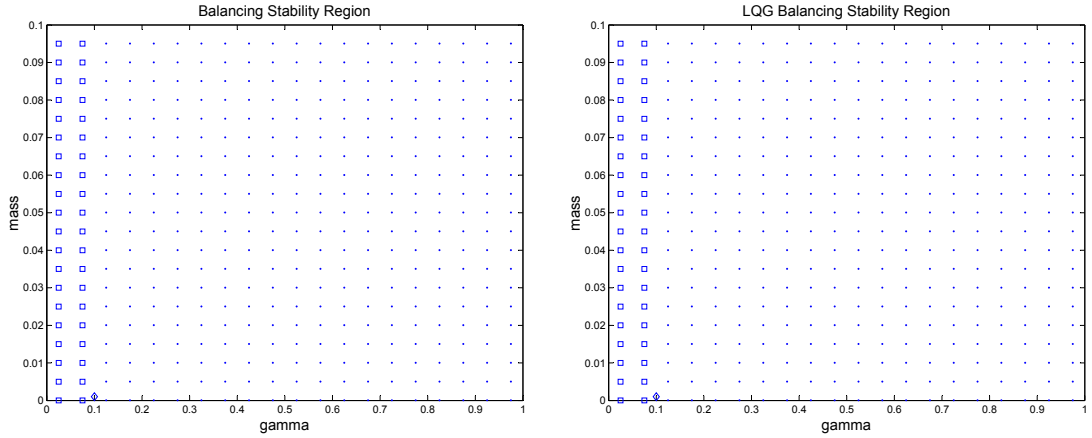

Figure 5.19: Parameter Studies: Reduced Order Balanced LQG Controller (left), Reduced Order LQG Balanced LQG Controller (right)

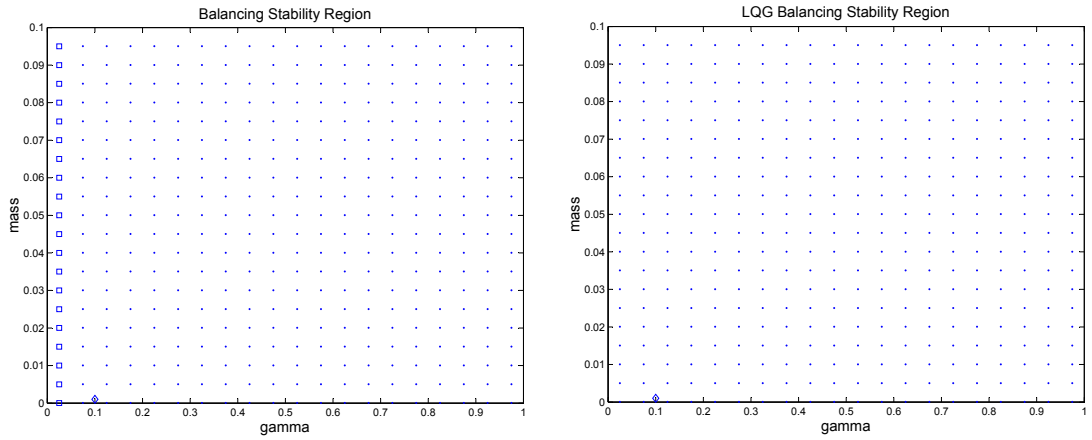

Figure 5.20: Parameter Studies: Reduced Order Balanced MinMax Controller (left), Reduced Order LQG Balanced MinMax Controller (right)

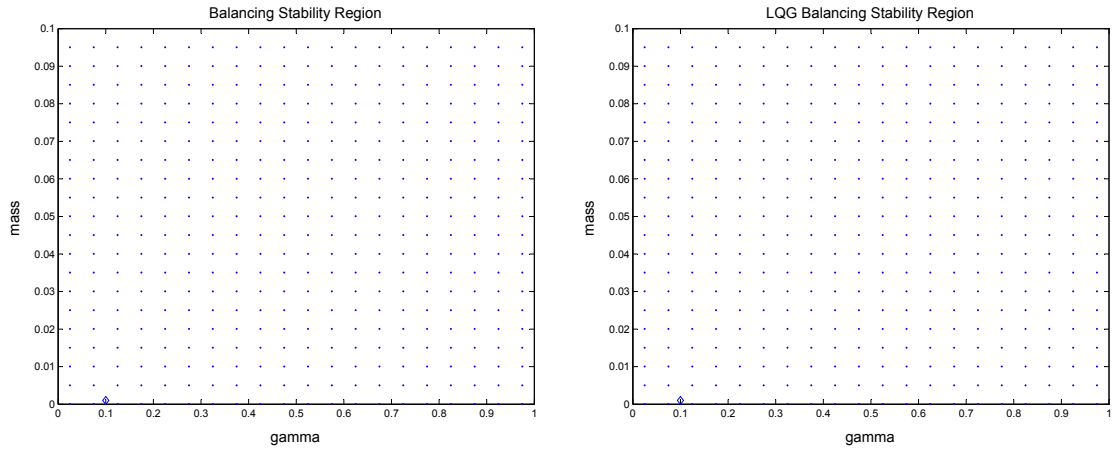

Figure 5.21: Parameter Studies: Reduced Order Balanced Central Controller (left), Reduced Order LQG Balanced Central Controller (right)

Fourth Order Controllers

We have already seen that the fourth order controllers do not perform as well as the first order controllers, but we desire to look at their stability margins and radii in order to examine how the additional three states affect robustness. We first look at the eigenvalues of all relevant systems in Figure 5.22.

We identify a shift to the right of eigenvalues for the balanced and LQG balanced MinMax and LQG balanced LQG controllers. This observation is quantified in Table 5.3, where we compute the stability margins. We note that there is little difference in any of the stability margins, with all of the values falling within 1.38×10^{-2} of each other.

The stability radii of all three balanced controllers are *two* orders of magnitude less than the radii of the full order controllers. The radii of all three LQG balanced controllers are on the same order of magnitude as the full order controllers, thus creating two orders of magnitude difference between the balanced and LQG balanced controllers. The guaranteed robustness margins of the central controller tell us that the balanced central controller will stabilize slightly larger perturbations than the full order and LQG balanced central controllers.

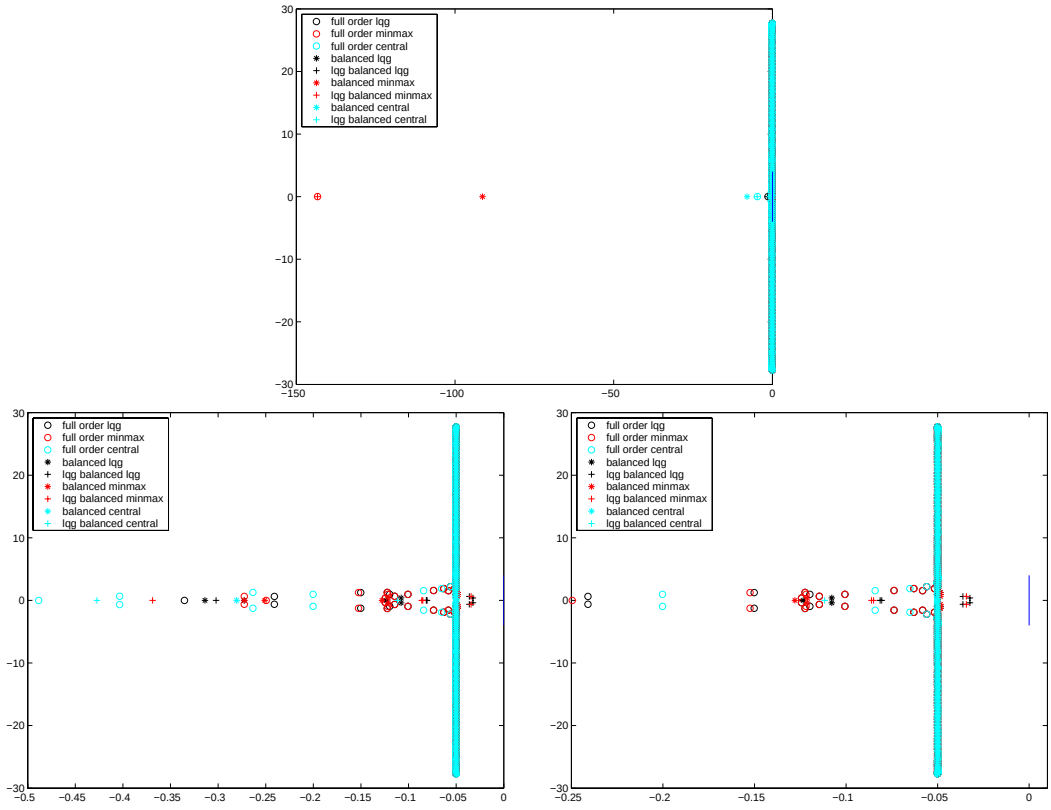

Figure 5.22: Eigenvalues (top), Zoomed In Views (bottom)

Matrix	Stability Margin	Stability Radius	Guaranteed Robustness Margin
Full order LQG	0.04981	0.06678	n/a
Full order MinMax	0.04981	0.05903	n/a
Full order central	0.04982	0.06650	0.63610
Balanced LQG	0.04854	0.00070	n/a
LQG balanced LQG	0.03237	0.04937	n/a
Balanced MinMax	0.04838	0.00057	n/a
LQG balanced MinMax	0.03430	0.04943	n/a
Balanced central	0.05000	0.00050	0.75453
LQG balanced central	0.04998	0.03213	0.63610

Table 5.3: Stability Margins and Radii for Full and Reduced Order Compensators.

5.2 Numerical Results with $R = I$

In this section, we change the value of the control weighting so that $R = I$, which should offer the LQG and MinMax controllers less authority. We let $\theta = .52$, which is as large as possible. However, we cannot identify any visible difference in the performance of the full order controllers. We only display the full order simulation plots in Figure 5.23.

Figure 5.24 provides the full order LQG, MinMax, and central controllers. The LQG and MinMax controllers require less effort than when the control weight was taken to be $R = .001 * I$, while the central controller needs more effort than it did with the previous control weight. These comments are consistent with the observations made about the cable mass system. There is a large difference in the control efforts of these three controllers with $R = I$.

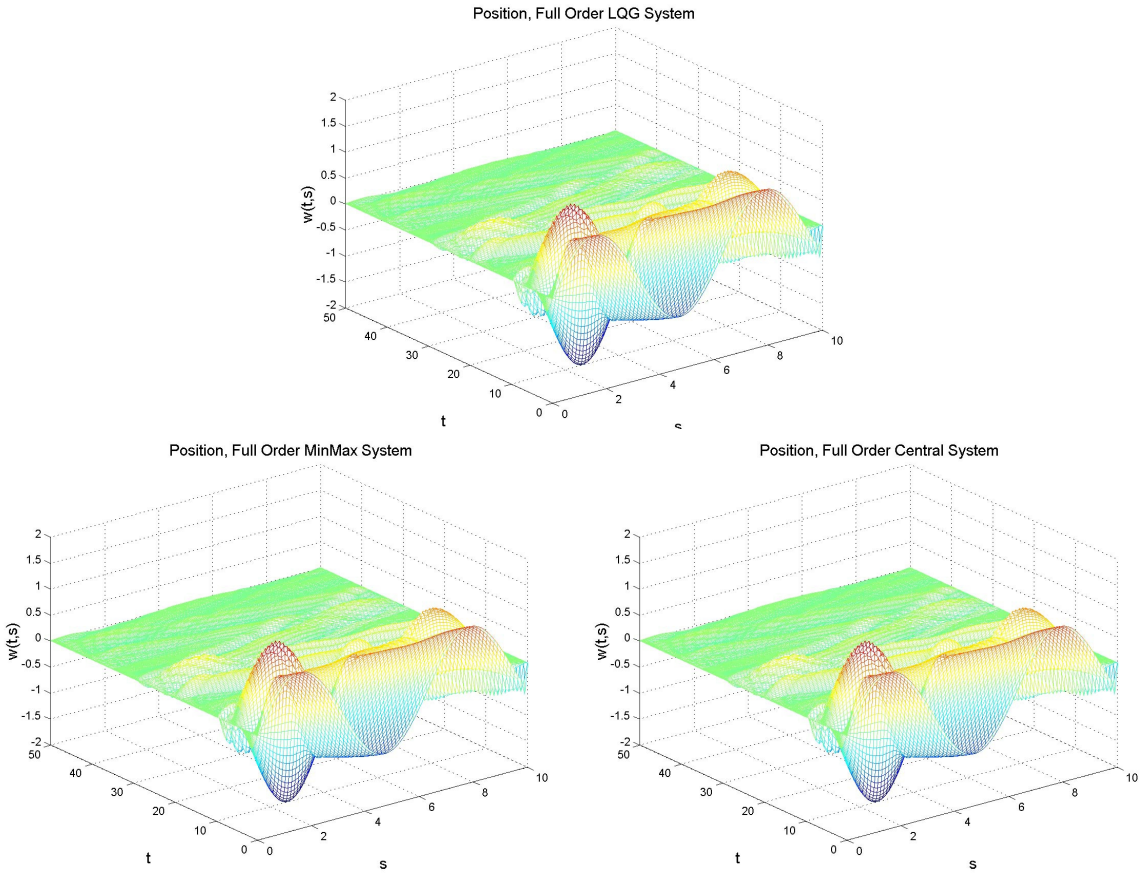

Figure 5.23: Full Order Position State: LQG Controller (top), MinMax Controller (bottom left), and Central Controller (bottom right)

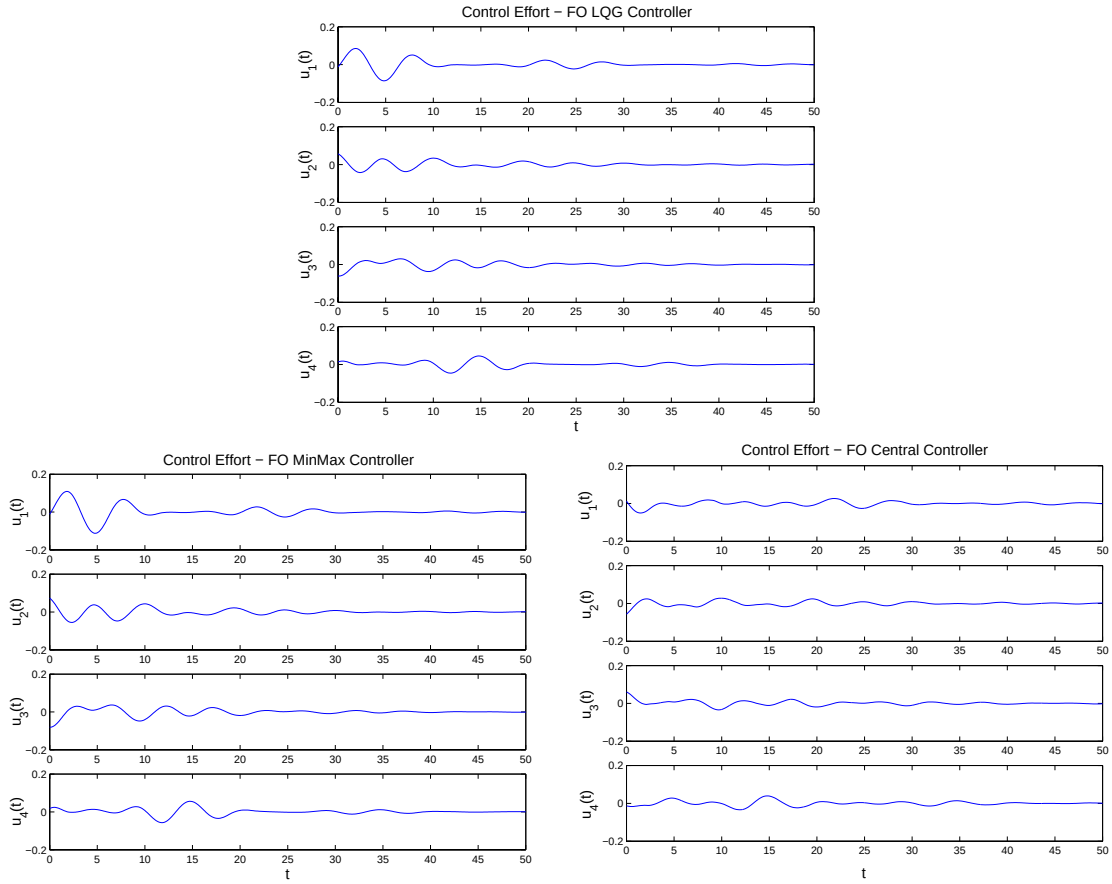

Figure 5.24: Control Effort: Full Order LQG (top), Full Order MinMax (bottom left), Full Order Central (bottom right)

Chapter 6

Linear Cantilevered Euler-Bernoulli Beam Equation

Continuing to examine the effects of regular and LQG balancing, we take the cantilevered Euler-Bernoulli beam (CEB) as our next example. Including both viscous and Kelvin-Voigt damping, using sine and cosine initial conditions and taking our spatial domain to be of length $\ell = 30$, CEB can be written as

$$\begin{gathered}
\rho a\omega_{tt}(t,s) + EI\omega_{ssss}(t,s) + \gamma_1\omega_t(t,s) + \gamma_2\omega_{tssss}(t,s) = \sum_{i=1}^{m} b_i(s)u(t) \\
\omega(t,0) = \omega_s(t,0) = 0 \\
EI\omega_{ss}(t,\ell) + \gamma_2\omega_{tss}(t,\ell) = 0 \\
EI\omega_{sss}(t,\ell) + \gamma_2\omega_{tsss}(t,\ell) = 0 \\
\omega(0,s) = \sin(s/4) \qquad \omega_t(0,s) = .25\cos(s/4) \\
t > 0 \qquad 0 < s < \ell
\end{gathered} \tag{6.1}$$

where the parameters are chosen to fit the physics for this particular beam and are taken as follows:

ρ	=	5.24 : density	a	=	1/48 : cross-sectional area
E	=	1.44e9 : Young's modulus	I	=	1/1327104 : moment of inertia.

To formulate a full order approximation, a Galerkin finite element scheme is applied with cubic splines. We take the functions $b_i(s)$ to be defined as $b_i(s) = e^{-(s-s_i^*)^2}$ where $s_i^* =$

$3, 9, 15, 21, 27$ since $m = 5$ in this example. Additionally, we assume there are eight averaged measurements—four each of position and velocity.

Using PDE framework, we can write (6.1) without the control term as a first order system $\dot{x} = Ax$. We take this time to give the state space, our choice of inner product on the state space, and the domain of A. We will use this information to show A generates a C_0 semigroup and provide a Lyapunov argument that will guarantee exponential stability of the semigroup. For simplicity, we consider (6.1) without the Kelvin-Voigt damping term. We note that our semigroup and Lyapunov arguments will still apply when Kelvin-Voigt damping is included in our model since it is a stronger type of damping than viscous damping. We define the following: $\omega(t,s) = d(s)$ to be the displacement of the particle and $\omega_t(t,s) = v(s) = \dot{d}(s)$ to be the velocity of the particle. Making these substitutions, (6.1) without the control term is transformed into

$$\frac{d}{dt}\begin{bmatrix} d \\ v \end{bmatrix} = \begin{bmatrix} 0 & I \\ \dfrac{-EI}{\rho A}\dfrac{\partial^4}{\partial x^4} & -\dfrac{\gamma_1}{\rho A}I \end{bmatrix}\begin{bmatrix} d \\ v \end{bmatrix} = \begin{bmatrix} v \\ \dfrac{-EI}{\rho A}d'''' - \dfrac{\gamma_1}{\rho A}v \end{bmatrix}. \tag{6.2}$$

That is,

$$A\begin{bmatrix} d \\ v \end{bmatrix} = \begin{bmatrix} v \\ \dfrac{-EI}{\rho a}d'''' - \dfrac{\gamma_1}{\rho a}v \end{bmatrix}. \tag{6.3}$$

We take the state space to be the product space $X = H_L^2(0,\ell) \times L_2(0,\ell)$, and $[d, v]^T$ are elements from the domain of A which is given by

$$\begin{aligned} D(A) = \Bigg\{ \begin{bmatrix} d \\ v \end{bmatrix} \in X \Bigg| \; & d \in H^4(0,\ell) \cap H_L^2(0,\ell),\ v \in H_L^2(0,\ell), \\ & d''(\ell) = 0,\ d'''(\ell) = 0 \Bigg\}. \end{aligned} \tag{6.4}$$

We denote the natural norm on X as $\hat{X}$, and it is given by

$$\begin{aligned} \left\| \begin{bmatrix} d \\ v \end{bmatrix} \right\|_{\hat{X}} = \Bigg(\int_0^\ell \Big[& |d(s)|^2 + |d'(s)|^2 + |d''(s)|^2 + |v(s)|^2 \\ & + |v'(s)|^2 + |v''(s)|^2 \Big]\, ds \Bigg)^{\frac{1}{2}}. \end{aligned} \tag{6.5}$$

However, we make use of Poincare's inequality and choose the norm on X to be

$$\left\| \begin{bmatrix} d \\ v \end{bmatrix} \right\|_X = \left(\int_0^\ell \left[\frac{EI}{\rho a}|d''(s)|^2 + |v(s)|^2 \right] ds \right)^{\frac{1}{2}}, \tag{6.6}$$

which is induced by the inner product

$$\left\langle \begin{bmatrix} d \\ v \end{bmatrix}, \begin{bmatrix} \hat{d} \\ \hat{v} \end{bmatrix} \right\rangle_X = \int_0^\ell \left[\frac{EI}{\rho a} d''(s)\hat{d}''(s) + v(s)\hat{v}(s) \right] ds. \tag{6.7}$$

In order to guarantee that the Hankel operator for this problem is nuclear, we need to know that A generates an exponentially stable C_0-semigroup. We note that [5] provides the arguments showing A is the infinitesimal generator or an exponentially stable C_0-semigroup.

We now consider the weak form of the CEB in order to develop a Galerkin finite element approximation of the problem. We want to find an $\omega(s) \in Y \subseteq S = H_L^2(0,\ell) \cap H^4(0,\ell)$ such that

$$\begin{aligned} \int_0^\ell \rho a \ddot{\omega}(t,s)y(s)\ ds + \int_0^\ell EI\omega''''(t,s)y(s)\ ds + \int_0^\ell \gamma_1 \dot{\omega}(t,s)y(s)\ ds \\ + \int_0^\ell \gamma_2 \dot{\omega}''''(t,s)y(s)\ ds = \int_0^\ell u(t) \sum_{i=1}^m b_i(s)y(s)\ ds \end{aligned} \tag{6.8}$$

for all $y(s) \in Y \subseteq H_L^2(0,\ell)$. After integrating by parts twice, we arrive at

$$\begin{aligned} \int_0^\ell \rho a \ddot{\omega}(t,s)y(s)\ ds + \int_0^\ell EI\omega''(t,s)y''(s)\ ds + \int_0^\ell \gamma_1 \dot{\omega}(t,s)y(s)\ ds \\ + \int_0^\ell \gamma_2 \dot{\omega}''(t,s)y''(s)\ ds = \int_0^\ell u(t) \sum_{i=1}^m b_i(s)y(s)\ ds. \end{aligned} \tag{6.9}$$

We now divide the spatial domain $[0,\ell]$ into N equidistant subintervals and approximate $\omega(t,s)$ by $\omega^N(t,s) = \sum_{i=1}^N c_i(t)\varphi_i(s)$, where $\varphi_i(s)$ are cubic spline basis functions and $c_i(t)$ are their coefficients. After making this substitution for $\omega(t,s)$ in (6.9), we have

$$\begin{aligned} \int_0^\ell \rho a \ddot{\omega}^N(t,s)y(s)\ ds + \int_0^\ell EI\omega''^N(t,s)y''(s)\ ds + \int_0^\ell \gamma_1 \dot{\omega}^N(t,s)y(s)\ ds \\ + \int_0^\ell \gamma_2 \dot{\omega}''^N(t,s)y''(s)\ ds = \int_0^\ell u(t) \sum_{i=1}^m b_i(s)y(s)\ ds, \end{aligned} \tag{6.10}$$

or equivalently,

$$\begin{aligned}\int_0^\ell \rho a \sum_{i=1}^N \ddot{c}_i(t)\varphi_i(s)y(s)\ ds + \int_0^\ell EI \sum_{i=1}^N c_i(t)\varphi_i''(s)y''(s)\ ds + \\ + \int_0^\ell \gamma_1 \sum_{i=1}^N \dot{c}_i(t)\varphi_i(s)y(s)\ ds + \int_0^\ell \gamma_2 \sum_{i=1}^N \dot{c}_i(t)\varphi_i''(s)y''(s)\ ds \\ = \int_0^\ell u(t) \sum_{i=1}^m b_i(s)y(s)\ ds.\end{aligned} \tag{6.11}$$

We let $y(s)$ range over the basis functions, $\varphi_i(s)$ for $i = 1, \ldots, N$, to obtain

$$\begin{aligned}\rho a\ M \begin{bmatrix} \ddot{c}_1(t) \\ \vdots \\ \ddot{c}_N(t) \end{bmatrix} + EI\ K \begin{bmatrix} c_1(t) \\ \vdots \\ c_N(t) \end{bmatrix} + \gamma_1 M \begin{bmatrix} \dot{c}_1(t) \\ \vdots \\ \dot{c}_N(t) \end{bmatrix} \\ + \gamma_2 K \begin{bmatrix} \dot{c}_1(t) \\ \vdots \\ \dot{c}_N(t) \end{bmatrix} = u(t)B_0,\end{aligned} \tag{6.12}$$

where $M = \left[\int_0^\ell \varphi_i(s)\varphi_j(s)\ ds\right]_{i,j=1}^N$ and $K = \left[\int_0^\ell \varphi_i''(s)\varphi_j''(s)\ ds\right]_{i,j=1}^N$ are the mass and stiffness matrices, respectively, and $B_0 = \left[\int_0^\ell \sum_{i=1}^M b_i(s)\varphi_j(s)\ ds\right]_{j=1}^N$. Then

$$\begin{aligned}\begin{bmatrix} \ddot{c}_1(t) \\ \vdots \\ \ddot{c}_N(t) \end{bmatrix} &= \left(-\frac{EI}{\rho a} M^{-1}K\right) \begin{bmatrix} c_1(t) \\ \vdots \\ c_N(t) \end{bmatrix} \\ &\quad - \left(\frac{\gamma_1}{\rho a} I + \frac{\gamma_2}{\rho a} M^{-1}K\right) \begin{bmatrix} \dot{c}_1(t) \\ \vdots \\ \dot{c}_N(t) \end{bmatrix} + \frac{1}{\rho a} u(t) M^{-1}B_0.\end{aligned} \tag{6.13}$$

We now want to convert this into a first order system of differential equations, so we define $x_1(t) = c(t)$ and $x_2(t) = \dot{x}_1(t) = \dot{c}(t)$ and (6.13) becomes

$$\begin{aligned} \begin{bmatrix} \dot{x}_1(t) \\ \dot{x}_2(t) \end{bmatrix} &= \begin{bmatrix} 0 & I \\ \left(-\frac{EI}{\rho a} M^{-1}K\right) & -\left(\frac{\gamma_1}{\rho a} I + \frac{\gamma_2}{\rho a} M^{-1}K\right) \end{bmatrix} \begin{bmatrix} x_1(t) \\ x_2(t) \end{bmatrix} \\ &+ \frac{1}{\rho a} \begin{bmatrix} 0 \\ M^{-1}B_0 \end{bmatrix} u(t). \end{aligned} \tag{6.14}$$

Just as with the KGL equation, we will have a measurement equation of the form

$$y(s) = C \begin{bmatrix} x_1(t) \\ x_2(t) \end{bmatrix}. \tag{6.15}$$

By taking four averaging measurements of both position and velocity, we arrive at the $8 \times (2N-2)$ dimensional matrix C, given by (5.55). Now (6.14,6.15) is of the form in (3.23), and we are ready to apply the ideas from Chapter 3 for control design. We now turn our attention to numerical results.

6.1 Numerical Results with $R = I$

We take $N = 40$ for the beam simulations since we achieve gain convergence at the value for N, and we experience convergence of our Galerkin finite element approximation scheme. We again take the MinMax parameter to be as large as possible such that the conditions described in Section 3.2.2 are satisfied: $\theta = .81$. We will present results on singular values, uncontrolled simulations, functional gains, controlled simulations, and controller robustness.

6.1.1 Uncontrolled Results

Figure 6.1 shows the Hankel singular values and the LQG characteristic values, while Table 6.1 displays the corresponding number of singular values needed to retain 95% and 99% of the system information that is embodied in the singular values.

As we have also observed with the cable mass system and the Klein-Gordon equation, the performance of the low order controllers seems to be more dependent on the control design as opposed to the number of states retained in the low order state estimate.

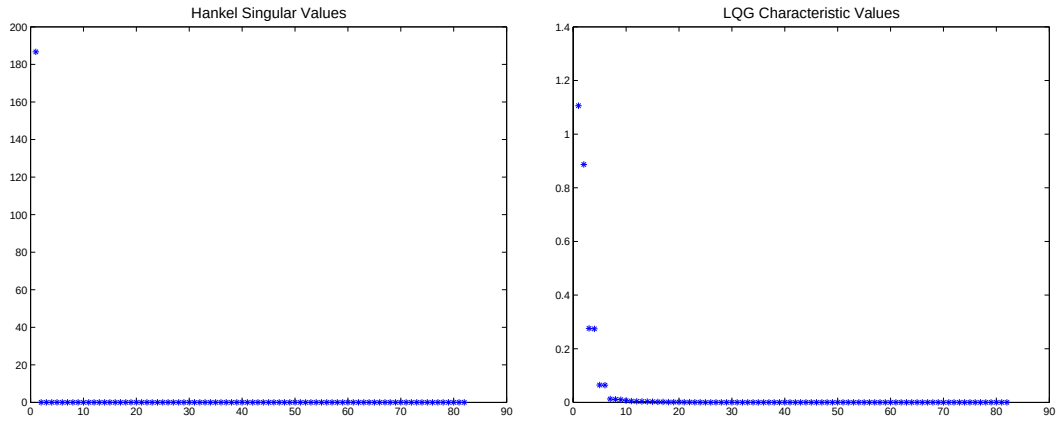

Figure 6.1: Hankel Singular Values (left), LQG Characteristic Values (right)

	Values needed for	
	95% significance	99% significance
Hankel singular values	1	1
LQG characteristic values	5	11

Table 6.1: Values needed to retain 95% and 99% information.

We choose initial conditions of the form

$$\begin{aligned} x_0 = \left[x(0,s), \frac{\partial}{\partial t}x(0,s)\right] &= \left[\sin\frac{s}{4}, \frac{1}{4}\cos\frac{s}{4}\right], \\ \left[x_c(0,s), \frac{\partial}{\partial t}x_c(0,s)\right] &= [x_0, .75x_0], \end{aligned} \tag{6.16}$$

in order to simulate and obtain a solution.

The uncontrolled position state is found in Figure 6.2. By choosing sinusoidal initial conditions, we generate a great deal of vibration in the beam. Ideally, we hope to see the position state tend to zero once a control is applied since $[0,0]^T$ is an exponentially stable equilibrium for the beam.

6.1.2 Controlled Results

Before applying the controllers to the beam, we want to look at the functional gains plots in order to visually verify that we have gain convergence. Figures 6.3, 6.4, and 6.5 show the

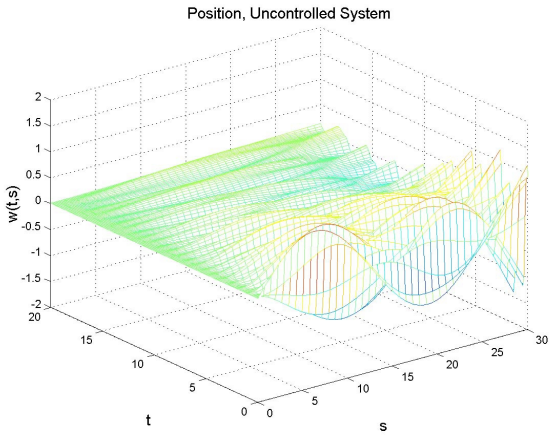

Figure 6.2: Uncontrolled Position State

full order and reduced order functional gains for the LQG, MinMax, and central controllers, respectively. Since there are five actuators in the system, there will be five position and five velocity gains for each controller type. As we can see from these plots, it appears that we have functional gain convergence for all three controllers with both balanced truncation methods. For all three sets of plots, the color legend is as follows: $N = 10$ cyan, $N = 20$ blue, $N = 40$ green, and $N = 80$ red.

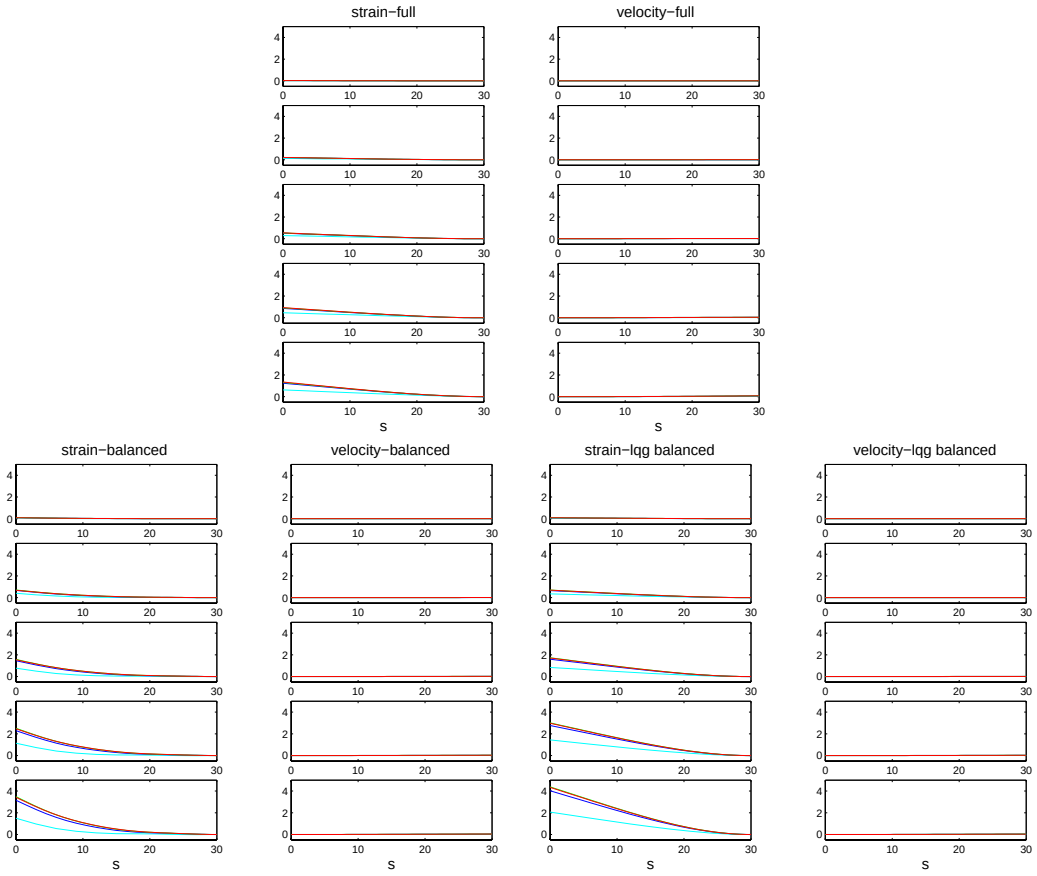

Figure 6.3: LQG Controller: Full Order Functional Gains (top), Reduced Order Balanced Gains (bottom left), Reduced Order LQG Balanced Gains (bottom right)

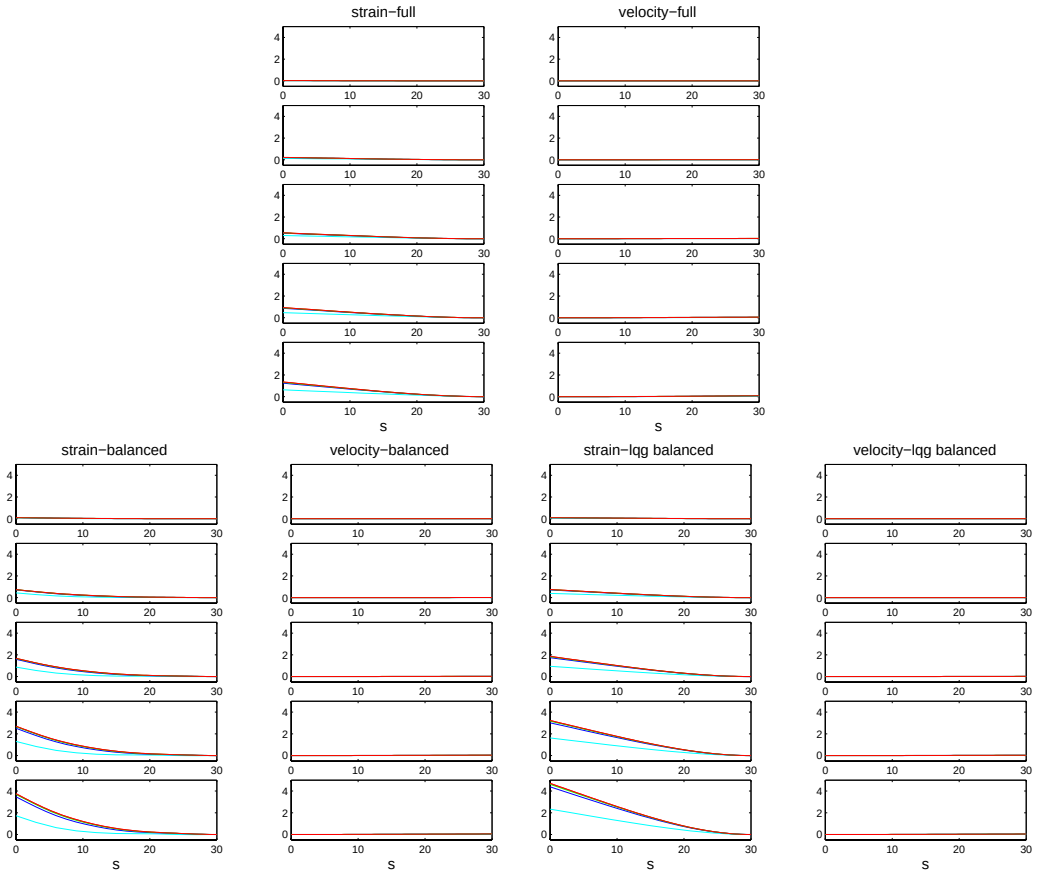

Figure 6.4: MinMax Controller: Full Order Functional Gains (top), Reduced Order Balanced Gains (bottom left), Reduced Order LQG Balanced Gains (bottom right)

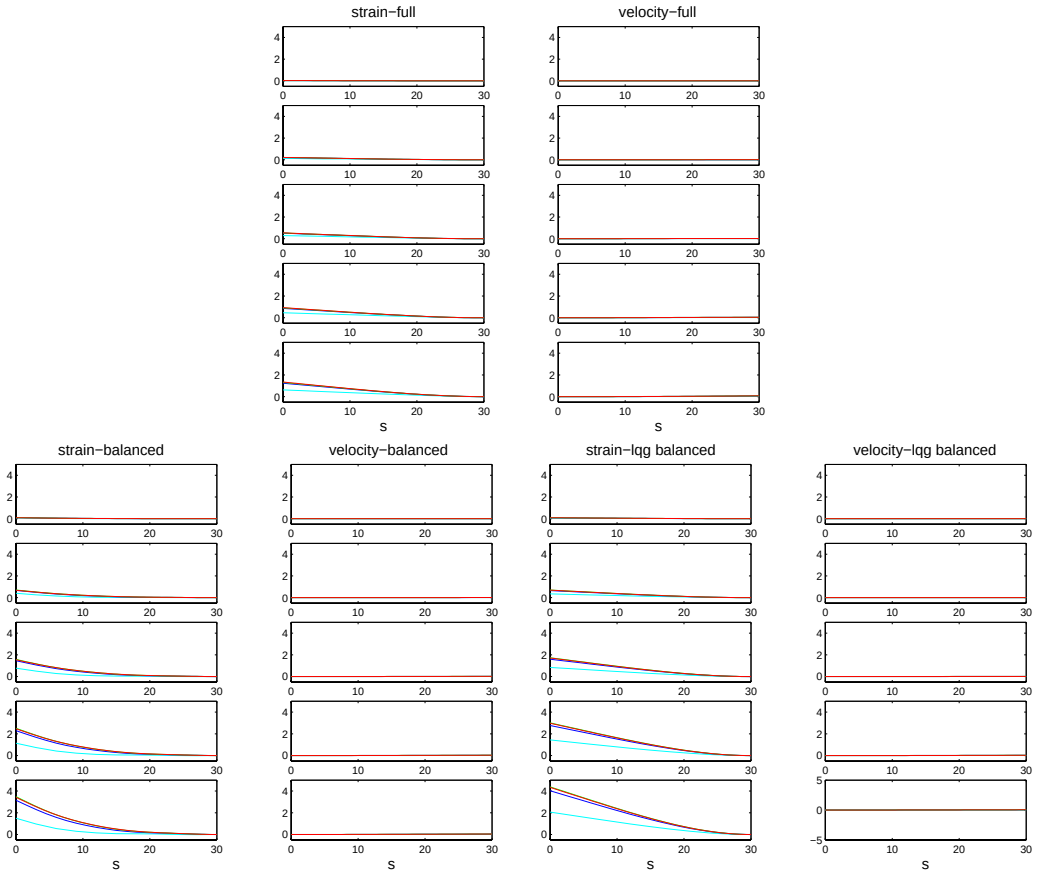

Figure 6.5: Central Controller: Full Order Functional Gains (top), Reduced Order Balanced Gains (bottom left), Reduced Order LQG Balanced Gains (bottom right)

We now look at simulations where the control is provided by a full order compensator. We recognize in advance that this beam may be difficult to regulate given that it is rather long and thing. The application of the LQG, MinMax, and central controllers are contained in Figure 6.6.

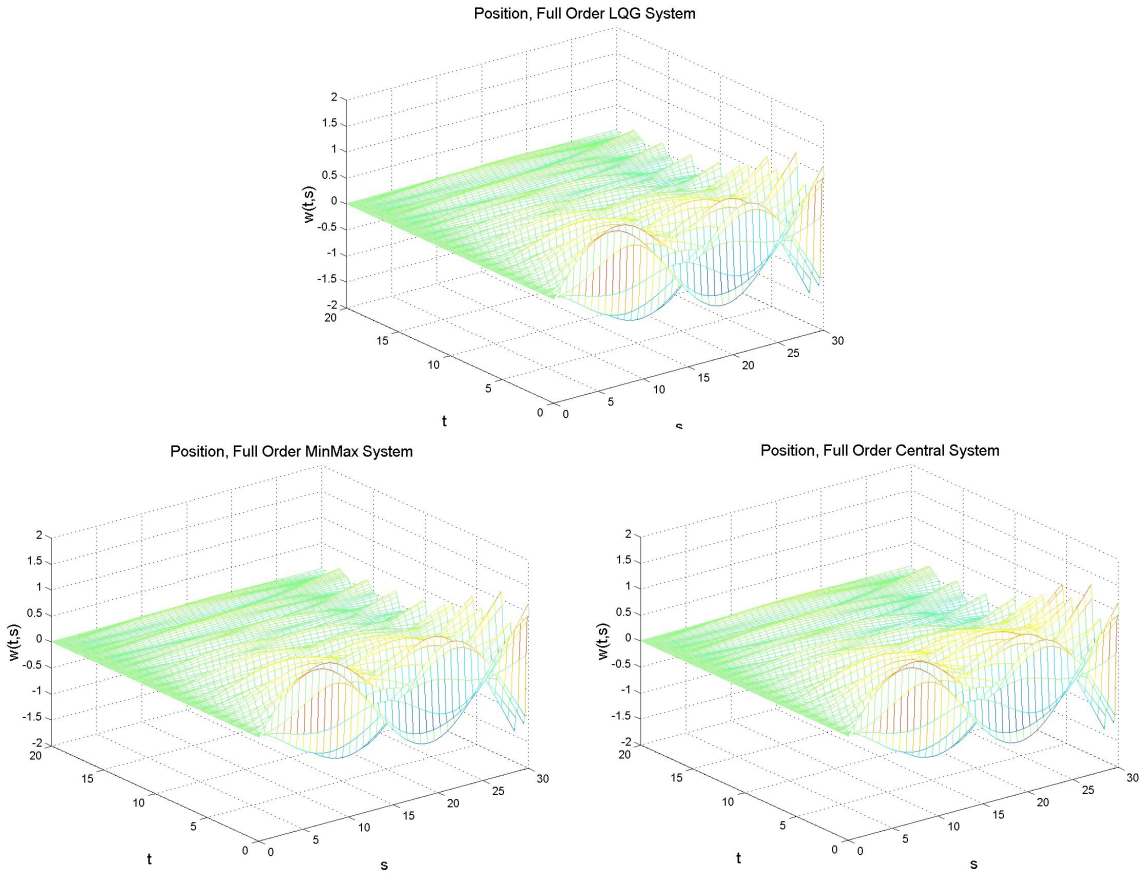

Figure 6.6: Full Order Position State: LQG controller (top), MinMax controller (bottom left), and Central controller (bottom right)

The full order MinMax controller does a better job at regulating the beam position than the LQG or central controllers, even though the difference between the LQG and MinMax controllers is minute. There is little difference between the uncontrolled system and the full order central controlled system.

The full order LQG, MinMax, and central controllers are provided in Figure 6.7. All three controllers require comparable effort.

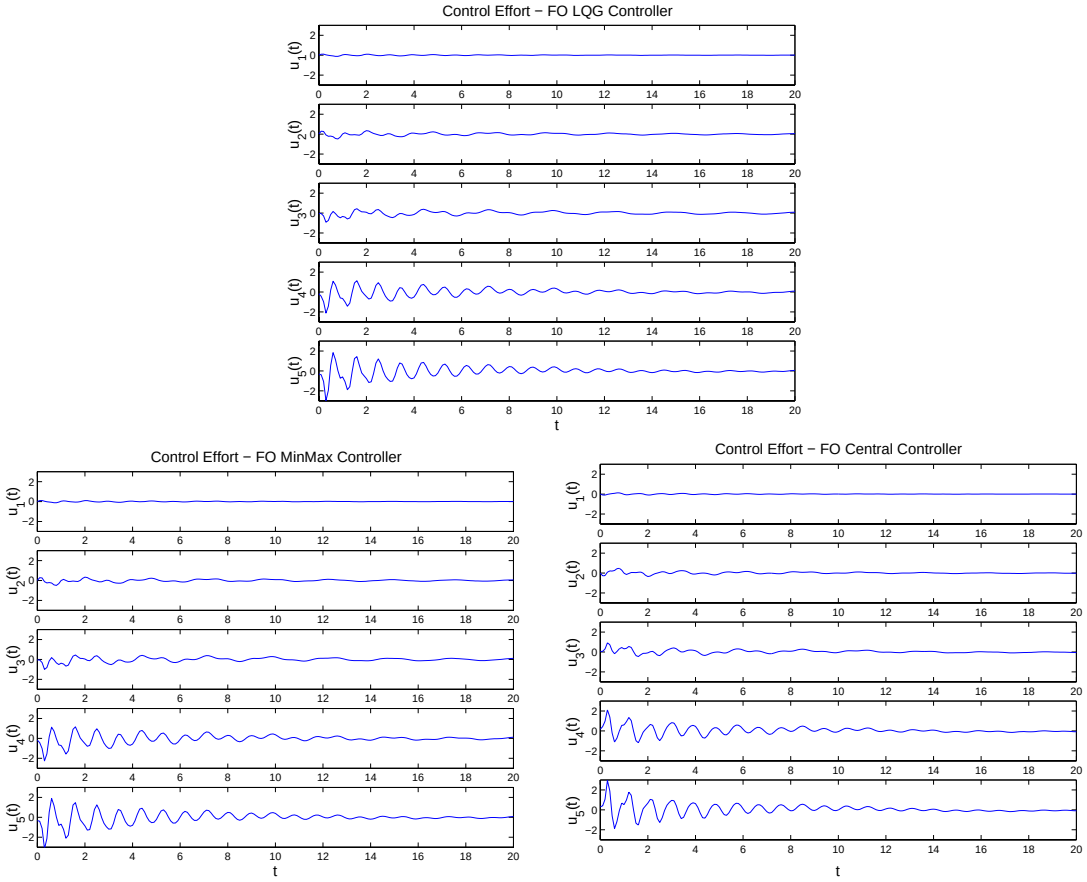

Figure 6.7: Control Effort: Full Order LQG (top), Full Order MinMax (bottom left), Full Order Central (bottom right)

First Order Controllers

In order to achieve real time control, we now focus our attention on low order controllers designed using balanced truncation and LQG balanced truncation. In particular, we design first order controllers, i.e., $q = 1$ in (3.28). Figure 6.8 provides the behavior after applying balanced and LQG balanced LQG controllers. There is little difference between these two low order controllers, rather only a shift. Additionally, the position states corresponding to both of these controllers are only slightly closer to zero than the uncontrolled position state.

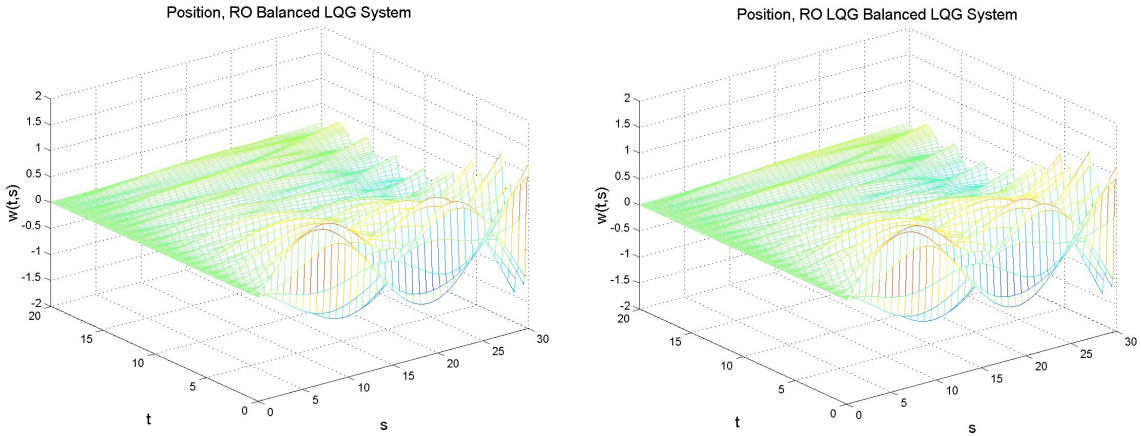

Figure 6.8: Reduced Order Position State: Balanced LQG Controller (left) and LQG Balanced LQG Controller (right)

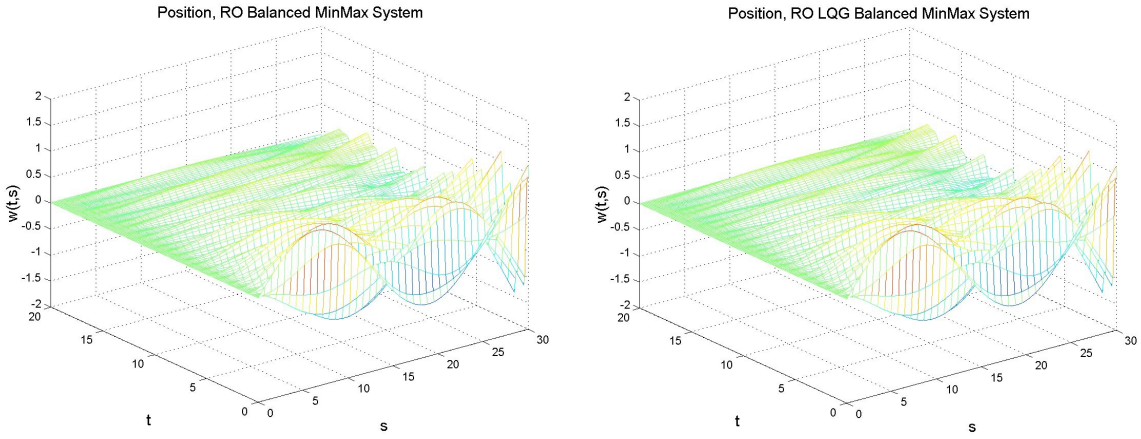

Figure 6.9: Reduced Order Position State: Balanced MinMax Controller (left) and LQG Balanced MinMax Controller (right)

Figure 6.9 displays the balanced and LQG balanced MinMax controlled systems. Both of the MinMax controllers perform well, and there is little difference between them. Finally of the first order controllers, we consider central control design. Figure 6.10 provides the central controlled systems obtained through balanced truncation and LQG balanced truncation. The LQG balanced central controller regulates slightly better than the balanced central controller. Overall, the MinMax controllers outperform the LQG controllers which outperform the central controllers.

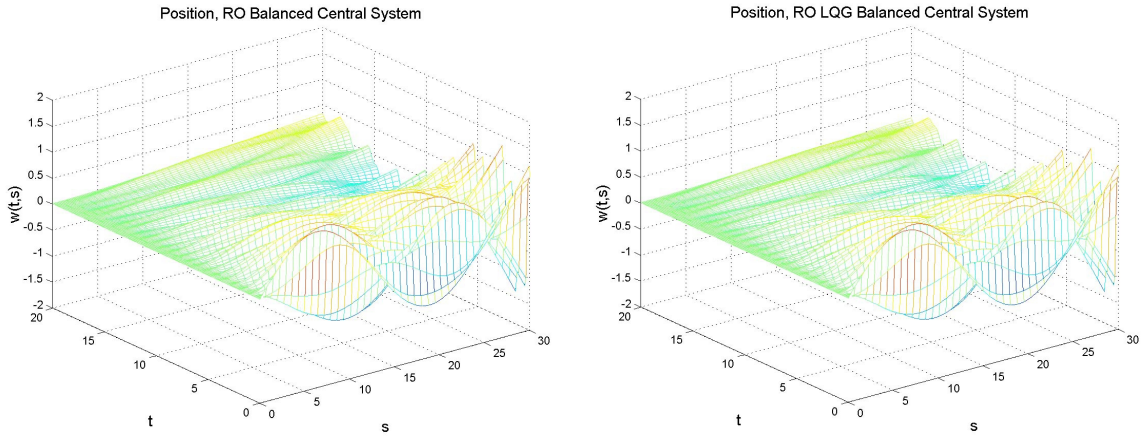

Figure 6.10: Reduced Order Position State: Balanced Central Controller (left) and LQG Balanced Central Controller (right)

In addition to examining the system performance when all six of the low order controllers are applied, we also look at the control effort of each. Figures 6.11, 6.12, and 6.13 show the reduced order LQG, MinMax, and central controllers, respectively. All of the low order controllers require close to no effort. However, with the vertical axis scale, the LQG balanced controllers appear to be identically zero, while we observe there is at least visible movement from zero for the balanced controllers. In fact, the LQG balanced controllers are not identically zero, and there is at least two orders of magnitude difference between the balanced and LQG balanced controllers. A different scale on the vertical axis would demonstrate this comment, but, for the purpose of comparison, we maintain the same scale for the full and reduced order controllers.

Controllers of Other Orders

Similar to our treatment of the cable mass system and the Klein-Gordon equation, we consider the use of a larger order controller. We find that when using a second, third, fourth, or fifth order controller, between one and three of the possible six low order controllers do

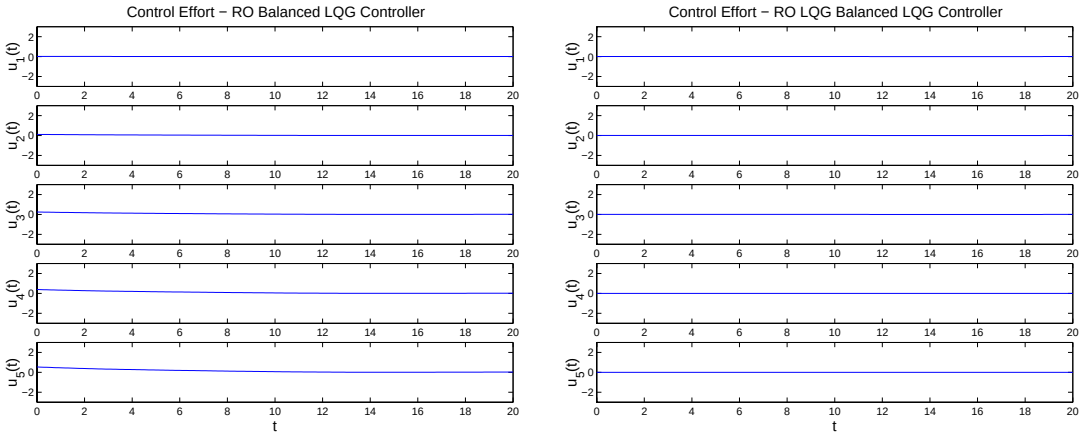

Figure 6.11: Control Effort: Reduced Order Balanced LQG (left), Reduced Order LQG Balanced LQG (right)

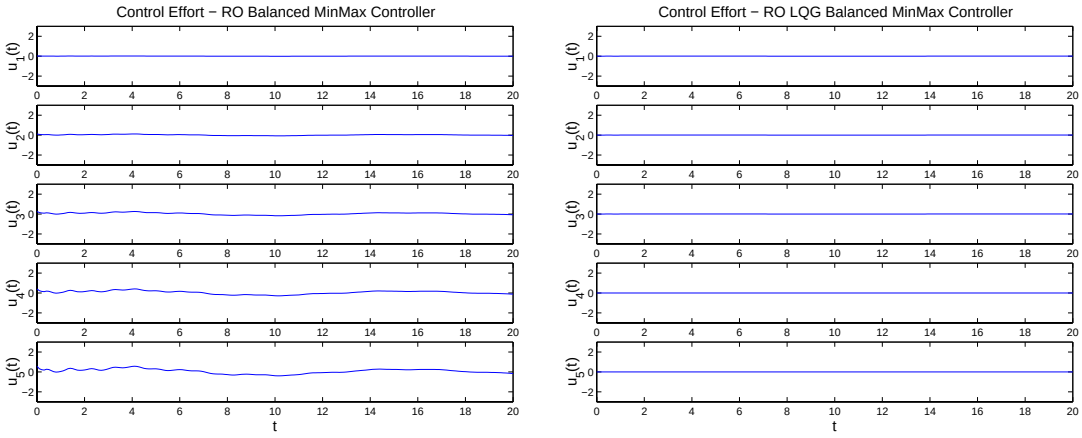

Figure 6.12: Control Effort: Reduced Order Balanced MinMax (left), Reduced Order LQG Balanced MinMax (right)

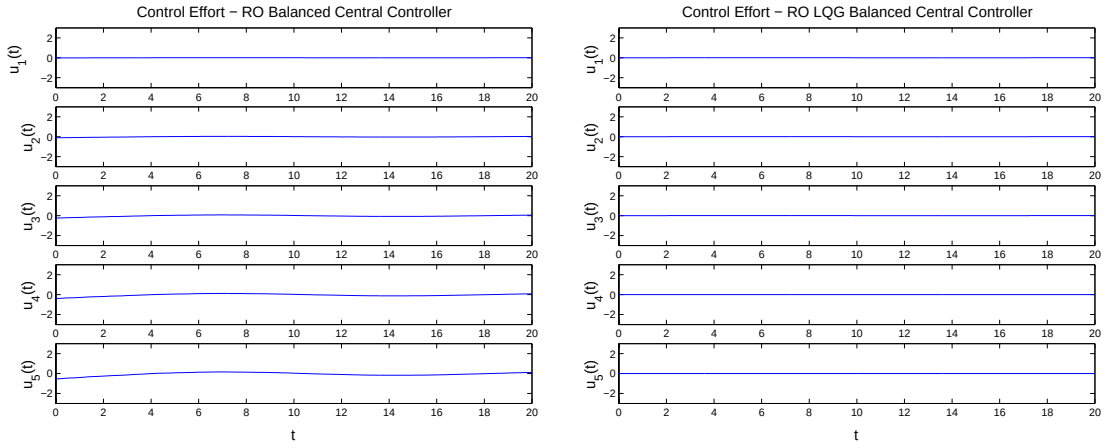

Figure 6.13: Control Effort: Reduced Order Balanced Central (left), Reduced Order LQG Balanced Central (right)

no stabilize the beam. For this reason, we do not display any of the higher order simulation plots.

6.1.3 Robustness of First Order Controllers with $R = I$

In Chapter 2, two measures of robustness are discussed: the stability margin and the stability radius. To gain some insight into the stability margin, we first look at the eigenvalues of all relevant systems in Figure 6.14. There is an apparent shift to the right of the eigenvalues for the balanced LQG, MinMax, and central controlled systems. In Table 6.2 we compute the stability margins, along with the stability radii.

The stability margins for all systems of consideration are on the same order of magnitude. The stability radii are as consistent as what we have observed with the cable mass system and the Klein-Gordon equation. The stability radii of all LQG balanced controllers and the full order LQG controller are on the same order of magnitude. The full order MinMax and central controllers are one order less and on the same order, while the balanced controllers are another order of magnitude less. Based on the guaranteed robustness margins of the central controllers, the balanced central controller should stabilize slightly larger perturbations than the full or LQG balanced central controllers.

We now turn our attention to parameter studies. These parameter variations do not provide a numerical measure of robustness, but they perhaps offer some insight into the robustness of the controllers. We again design first order controllers based on a low order system with

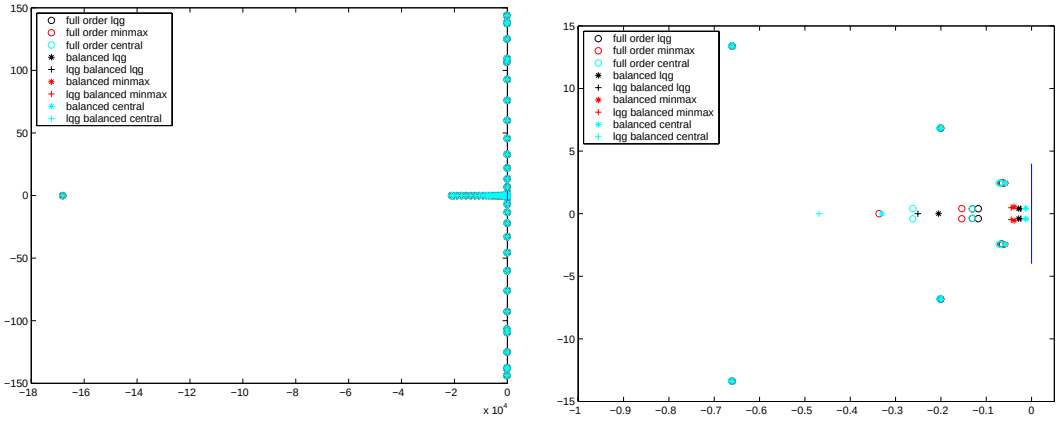

Figure 6.14: Eigenvalues (left), Zoomed In View (right)

Matrix	Stability Margin	Stability Radius	Guaranteed Robustness Margin
Full order LQG	0.06703	0.10730	n/a
Full order MinMax	0.06428	0.06669	n/a
Full order central	0.06715	0.09029	0.67067
Balanced LQG	0.02848	0.00189	n/a
LQG balanced LQG	0.02365	0.19583	n/a
Balanced MinMax	0.03854	0.00379	n/a
LQG balanced MinMax	0.04501	0.20164	n/a
Balanced central	0.01282	0.00249	0.72116
LQG balanced central	0.01305	0.19861	0.67067

Table 6.2: Stability Margins and Radii for Full and Reduced Order Compensators.

$N = 10$. We then take these low order controllers and apply them to a higher order system with $N = 40$. We denote these low order controlled systems with diamonds in Figures 6.15, 6.16, and 6.17. We also apply these low order controllers to high order systems where we vary the values of the beam density and beam thickness parameters. If the low order controller stabilizes the high order system, then there is a dot on the graph for the corresponding density and thickness pair. If the low order controller does not stabilize the high order system, there is a square on the plot for the related density and thickness.

Both LQG and central controllers are able to stabilize all nearby systems we examined in these studies. Only the LQG balanced MinMax controller has a slightly smaller stabilizing region as compared with the balanced MinMax controller.

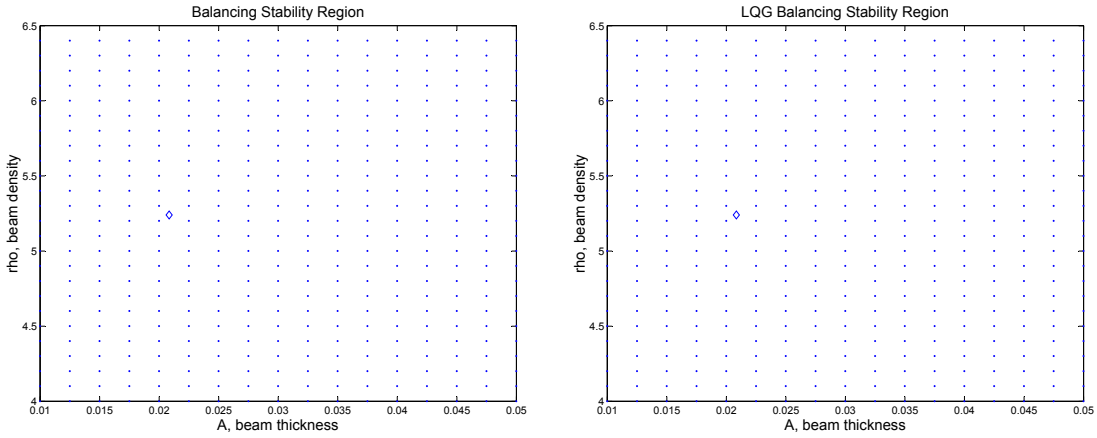

Figure 6.15: Parameter Studies: Reduced Order Balanced LQG Controller (left), Reduced Order LQG Balanced LQG Controller (right)

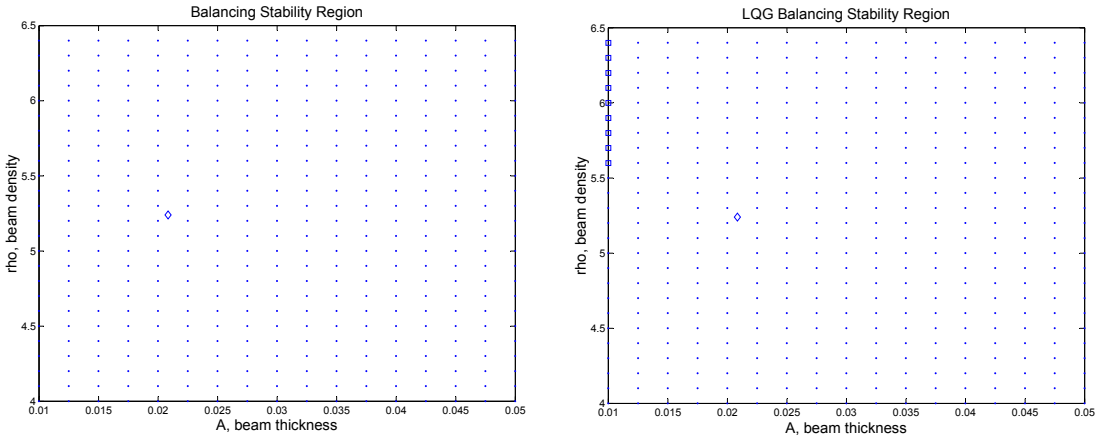

Figure 6.16: Parameter Studies: Reduced Order Balanced MinMax Controller (left), Reduced Order LQG Balanced MinMax Controller (right)

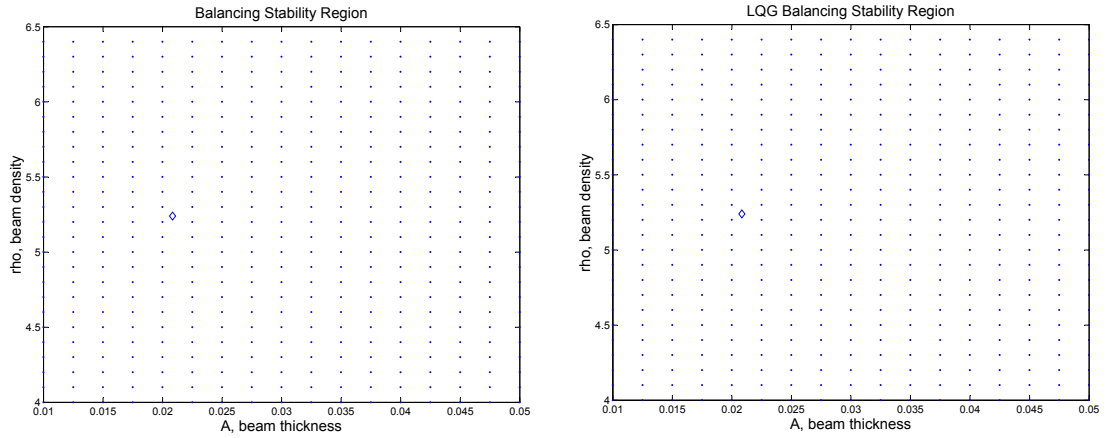

Figure 6.17: Parameter Studies: Reduced Order Balanced Central Controller (left), Reduced Order LQG Balanced Central Controller (right)

6.2 Numerical Results with $R = .001 * I$

In this section, we consider a control weighting so that $R = .001 * I$ to offer more control authority. We take $\theta = 31.33$, which is as large as possible while still satisfying the MinMax conditions in Section 3.2.2. We recognize this is a rather large θ value; however, to find it, we tested all values $\theta = 0 : .01 : k$ in order to find the largest possible k. The LQG controller with this new weighting performs noticeably better the LQG controller with $R = I$. The new MinMax controller performs terribly. In particular, we draw attention to the fact that the scale on the MinMax simulation plot is larger than the scales of the LQG and central controllers. The MinMax position gets large quickly but then stabilizes. We could take a smaller value for θ and achieve different results, but in the usual way, we choose the largest θ possible. It must also be remembered that the MinMax controller is a stabilizing one, even though it does not drive the position to zero. This new central controller performs just slightly worse than the full order central controller with $R = I$. Due to this unimpressive performance, we only display the full order simulation plots. Figure 6.18 shows the full order LQG, MinMax, and central controlled simulation plots.

The full order LQG, MinMax, and central controllers are provided in Figure 6.19. We expressly use different scales for the three controllers to draw attention to the drastic differences in the control efforts. When the control weight was taken to be the identity, i.e., $R = I$, the effort required of the three full order controllers were comparable. Now with the control weight being $R = .001 * I$, the three full order controllers all require more effort. In particular, the MinMax controller requires significantly more effort than the LQG controller, which requires more effort than the central controller. The scale of the central controller indicates

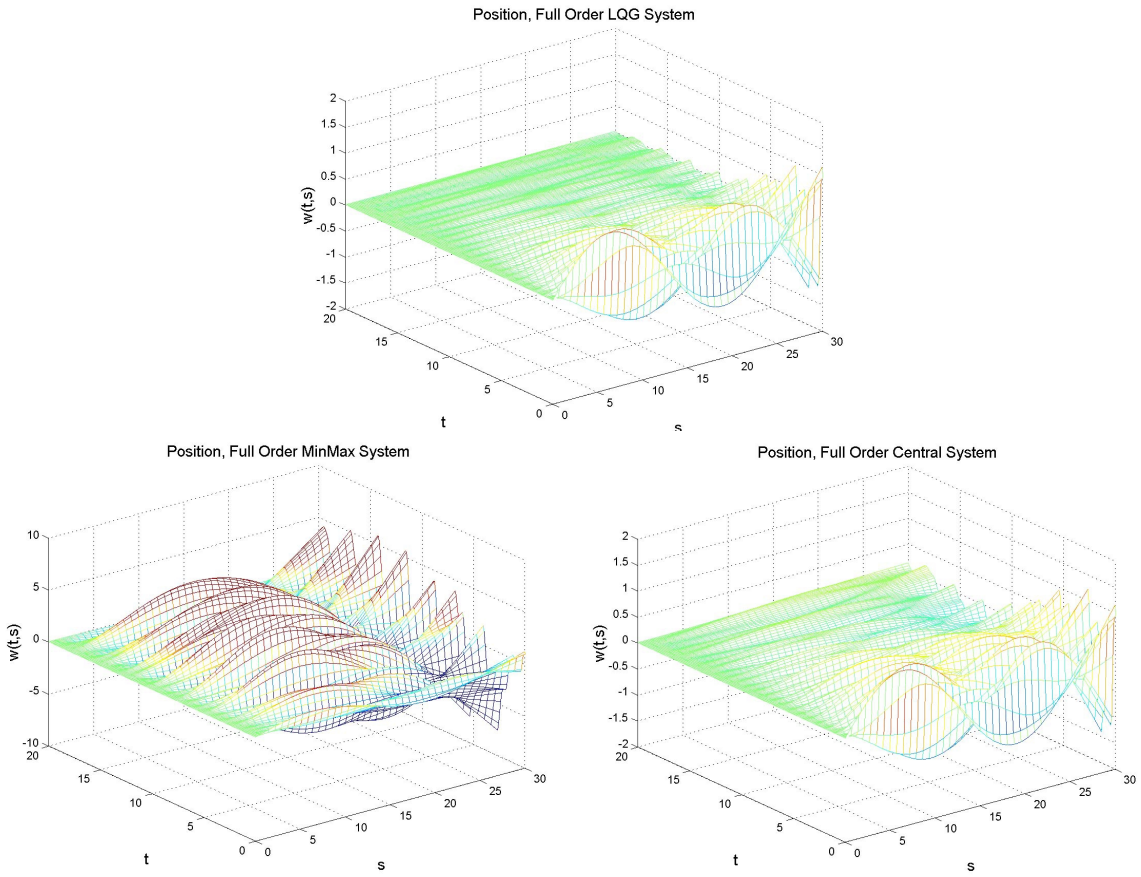

Figure 6.18: Full Order Position State: LQG Controller (top), MinMax Controller (bottom left), and Central Controller (bottom right)

that this controller still requires very little effort.

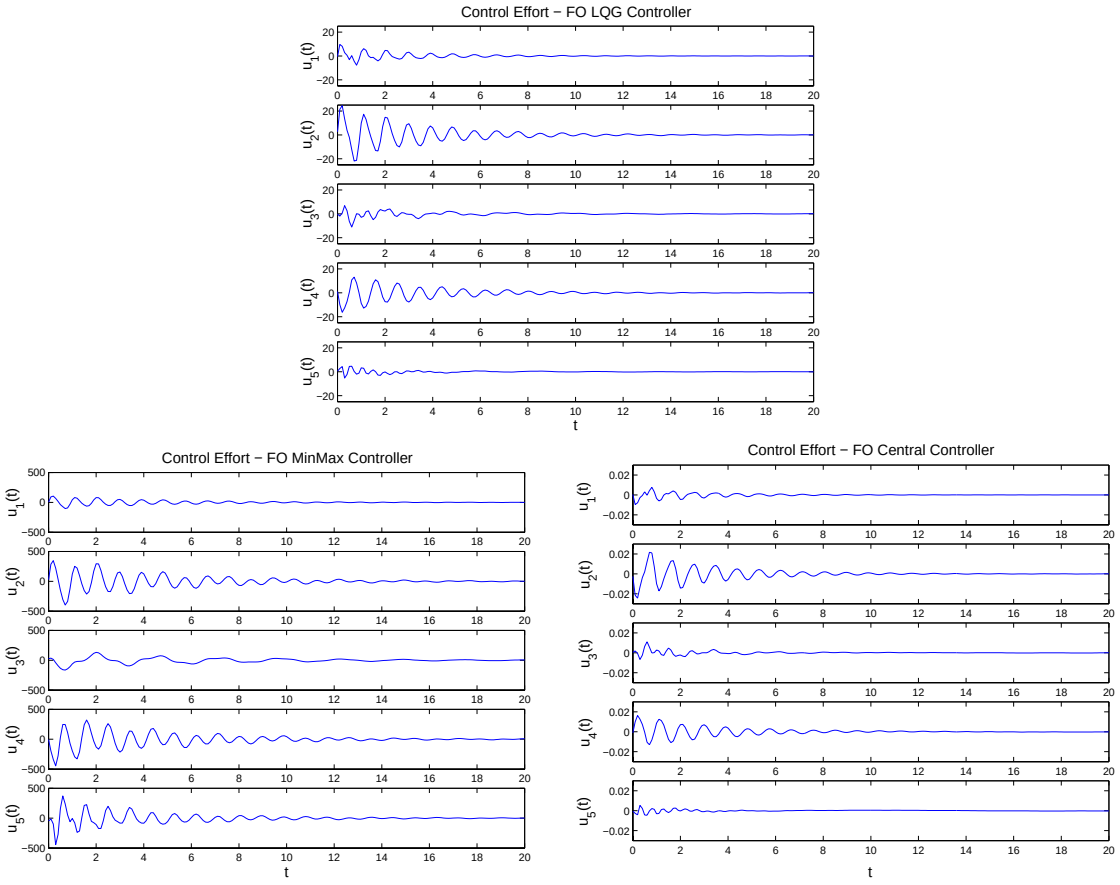

Figure 6.19: Control Effort: Full Order LQG (top), Full Order MinMax (bottom left), Full Order Central (bottom right)

Chapter 7

Conclusions and Future Work

The primary focus of this research has been to numerically explore the viability of LQG balanced truncation as a means for low order control design of PDE systems. Since balanced truncation is a commonly used method for low order control design in the distributed parameter setting, our approach was to apply both balanced reduction methods to several PDE systems and examine the performance and robustness properties of the controllers. To compare controller performance we considered the ability of the low order controller to stabilize the high order finite dimensional approximation of the PDE and regulate the states toward the exponential stable equilibrium of the system. We also examined the effort required be the controllers since this is a serious constraint in a real, live physical situation. We looked at these issues after applying three different control designs for the low order controllers: LQG, MinMax, and central. To consider the issue of robustness, we calculated the stability margins and radii of all systems to gauge the distance of the system from instability. We also calculated the guaranteed robustness margins of the central controllers to gain insight into the size of perturbations the controllers could reject. Additionally, we conducted parameter studies in order to examine the ability of the low order controllers to stabilize high order, nearby systems.

Based on our numerical findings, we observed that the full order controller performance seems to be application dependent. The one consistent observation is that the MinMax controller either outperforms or matches the performances of the LQG and central controllers. However, it must be remembered that there is no explicit formula for the optimal value of θ such that the MinMax conditions are satisfied. The process of finding an appropriate value for θ can add computational expense. Additionally, the full order MinMax controllers sometimes required more control effort than the full order LQG or central controllers. In regard to reduced order controller performance, we observed that again the MinMax controller either outperforms or matches the performances of the low order LQG and central controllers. It

was observed that the LQG balanced controllers require less control effort than the balanced controllers. We also found that it is sufficient to use a first order controller, as opposed to a second, third, fourth, or fifth order, since the higher order controllers either make little difference in terms of performance or are not able to stabilize the higher order system. The robustness results for all three problems of interest were consistent. The stability margins of all full and reduced order controlled systems were on the same order of magnitude. Additionally, the stability radii of the LQG balanced controllers were one (KGL) to two (CM, CEB) orders of magnitude more than the radii for the balanced controllers. Summarizing the performance and robustness results, we conclude that regardless of the control methodology implemented, the low order controllers obtained through LQG balanced truncation perform comparably to the low order controllers obtained through balanced truncation, while achieving enhanced robustness and requiring less control effort.

In this research, we offered a way of computing the balanced solutions of Riccati equations, without actually re-solving the Riccati equations for the balanced system. Instead, speaking from the perspective of numerical implementation in finite dimensions, we determined how to multiply the original Riccati equation solutions, by the similarity transformation in an appropriate way. This is advantageous from a computational perspective since it is cheaper to multiply matrices than to solve Riccati equations. We also demonstrated that balancing is indeed only a change of basis, even for the MinMax and central control designs, where this was not obviously true due to inverted quantities in the control design operators.

The numerical results of this research have led to further questions. Based on the good performance and robustness we observed of the MinMax controllers, it seems reasonable to explore the possibility of developing the theory of MinMax balancing for distributed parameter systems. Additionally, we observed that the low order MinMax controllers obtained through LQG balanced truncation perform well, while still maintaining the robustness properties of the other LQG balanced controllers. For this reason, theory guaranteeing that the low order LQG balanced MinMax controller would stabilize the PDE system, much like the theory now in place for the low order LQG balanced central controller, would be useful and should be considered. Another avenue to be explored is the possibility of coupling a robust low order controller, e.g. the LQG balanced central controller, with an adaptive element to enhance performance. Yet another question to be examined is why the low order LQG balanced controllers consistently require less effort than the low order balanced controllers.

Bibliography

[1] J. A. Atwell. *Proper Orthogonal Decomposition for Reduced Order Control of Partial Differential Equations*. PhD thesis, Virginia Polytechnic Institute and State University, April 2000.

[2] J. A. Atwell and B. B. King. Reduced order controllers for spatially distributed systems via proper orthogonal decomposition. *SIAM J. Sci. Comput., accepted*.

[3] J. A. Atwell and B. B. King. Proper orthogonal decomposition for reduced basis feedback controllers for parabolic equations. *Math. and Comput. Model.*, pages 1–19, Jan 2001.

[4] H. T. Banks, R. C. H del Rosario, and R. C. Smith. Reduced order model feedback control design: numerical implementation in a thin shell model. *CRSC Technical Report CSRC-TR98-27, N. C. State Univ., July 1998. IEEE Trans. Auto. Contr., submitted*.

[5] H. T. Banks, R. C. Smith, and Y. Wang. *Smart Material Structures*. Masson and Wiley, Paris, 1996.

[6] A. Bensoussan, G. Da Prato, M. Delfour, and S. Mitter. *Representation and Control of Infinite Dimensional Systems, Volume I*. Birkhauser, Boston, 1992.

[7] J. A. Burns. Lecture notes on modern calculus of variations with applications to control theory, numerical methods, and differential equations. 2000.

[8] J. A. Burns and B. B. King. A reduced basis approach to the design of low order feedback controllers for nonlinear continuous systems. *Journal of Vibration and Control*, 4:297–323, 1998.

[9] K. A. E. Camp. The search for a reduced order controller: Comparison of balanced reduction techniques. Master's thesis, Virginia Polytechnic Institute and State University, May 2001.

[10] K. A. E. Camp and B. B. King. A comparison of balanced truncation techniques for reduced order controllers. *Proc. MTNS 2002, South Bend IN*, 2002. 23323_2.pdf.

[11] K. A. E. Camp and B. B. King. A comparison of linear quadratic gaussian and central compensators for a structural control. *Proc. ACC 2003, Denver CO*, 2003. TA04-3.pdf.

[12] S. Chen and R. Triggiani. Proof of extensions of two conjectures on structural damping for elastic systems. *Pacific Journal of Mathematics*, 136:15–55, 1989.

[13] R. F. Curtain. A new approach to model reduction in finite-dimensional control design for distributed parameter systems. *preprint*, 2001.

[14] R. F. Curtain and K. Glover. Balanced realisations for infinite-dimensional systems. *Operator Theory and Systems: Proc. Workshop Amsterdam*, pages 87–104, 1985.

[15] R. F. Curtain and H. J. Zwart. *An Introduction to Infinite-Dimensional Linear Systems Theory*. Springer-Verlag, New York, 1995.

[16] P. Dorato, C. Abdallah, and V. Cerone. *Linear-Quadratic Control, An Introduction*. Prentice Hall, Englewood Cliffs, 1995.

[17] J. C. Doyle. Guaranteed margins for lqg regulators. *IEEE Trans. AC*, 23:756–767, 1978.

[18] A. L. Faulds and B. B. King. Centroidal voronoi tesselations for sensor placement. *Proc. IEEE CCA/CACSD 2000, Anchorage AK*, pages 536–541, 2000.

[19] J. S. Gibson and A. Adamian. Approximation theory for linear quadratic gaussian control of flexible structures. *SIAM J. Contr. Opt.*, 29:1–37, 1991.

[20] K. Glover, R. F. Curtain, and J. R. Partington. Realization and approximation of linear infinite-dimensional systems with error bounds. *SIAM Journal on Control and Optimization*, 26:863–898, 1988.

[21] K. Glover, J. Lam, and J. R. Partington. Rational approximation of a class of infinite-dimensional systems, i: Singular values of hankel operators. *Mathematics of Control, Signals, and Systems*, 3:325–344, 1990.

[22] K. Glover and D. C. McFarlane. Robust stabilization of normalized coprime factor plant descriptions with $\mathcal{H}_\infty$ bounded uncertainty. *IEEE Trans. AC*, 34(8):821–830, 1989.

[23] W. Greiner. *Relativistic Quantum Mechanics*. Springer-Verlag, Berlin, 1997.

[24] D. Hinrichsen and A. J. Pritchard. Stability radii of linear systems. *Systems Control Lett.*, 7(1):1–10, 1986.

[25] E. A. Jonckheere and L. M. Silverman. A new set of invariants for linear systems—application to reduced order compensator design. *IEEE Trans. AC*, 28:953–964, 1983.

[26] G. M. Kepler, H. T. Tran, and H. T. Banks. Reduced order model compensator control of species transport in a cvd reactor. *Optimal Control Application & Methods*, 21:143–160, April 2000.

[27] B. B. King. Nonuniform grids for reduced basis design of low order feedback controllers for nonlinear continuous systems. *Mathematical Models and Methods in Applied Sciences*, 8(7):1223–1241, 1998.

[28] B. B. King. Representation of feedback operators for parabolic control problems. *Proc. of the AMS*, 128:1339–1346, 2000.

[29] B. B. King and E. W. Sachs. Semidefinite programming techniques for reduced order systems with guaranteed stability margins: a numerical study. *Comput. Optim. Appl.*, 17(1):37–59, 2000.

[30] K. Kunisch and S. Volkwein. Control of burgers' equation by a reduced order approach using proper orthogonal decomposition. *In press, J. Opt. Theor. & Apps.*

[31] H. Kwakernaak and R. Sivan. *Linear Optimal Control Systems*. John Wiley & Sons, New York, 1972.

[32] S. Lall, J. E. Marsden, and S. Glavaski. Empirical model reduction of controlled nonlinear systems. *Proceedings of the IFAC World Congress*, pages 473–478.

[33] J. L. Lions. *Optimal Control of Systems Governed by Partial Differential Equations*. Springer-Verlag, Berlin, 1971.

[34] H. V. Ly and H. T. Tran. Modeling and control of physical processes using proper orthogonal decomposition. *Mathematical and Computer Modeling*, 33:223–236, 2001.

[35] J. T. Marti. *Introduction to Sobolev Spaces and Finite Element Solution of Elliptic Boundary Value Problems*. Academic Press Inc., Orlando, 1986.

[36] D. C. McFarlane and K. Glover. *Robust Controller Design Using Normalized Coprime Factor Plant Descriptions*, volume 138 of *Lecture Notes in Control and Information Sciences*. Springer-Verlag, Berlin, 1990.

[37] B. C. Moore. Principal component analysis in linear systems: controllability, observability, and model reduction. *IEEE Trans. on Auto. Control*, 26(1):17–32, 1981.

[38] A. H. Nayfeh, J. F. Nayfeh, and D. T. Mook. On methods for continuous systems with quadratic and cubic nonlinearities. *Nonlinear Dynamics*, 3:145–162, 1992.

[39] K. Oh. *A Theoretical and Experimental Study of Modal Interactions in Metallic and Laminated Composite Plates*. PhD thesis, Virginia Polytechnic Institute and State University, 1994.

[40] A. Pazy. *Semigroups of Linear Operators and Applications to Partial Differential Equations*. Springer-Verlag, New York, 1983.

[41] L. Pernebo and L. M. Silverman. Model reduction via balanced state space representations. *IEEE Trans. on Auto. Control*, 27(2):382–387, 1982.

[42] I. Rhee and J. Speyer. A game theoretic controller and its relationship to h_∞ and linear-exponential-gaussian synthesis. *Proceedings of the 28th Conference on Decision and Control*, pages 909–915, 1989.

[43] A. Sasane. *Hankel Norm Approximation for Infinite Dimensional Systems*. PhD thesis, University of Groningen, January 2001.

[44] S. Skogestad and I. Postlethwaite. *Multivariable Feedback Control*. John Wiley & Sons, Chichester, 1996.

[45] S. van Mourik. Lqg balancing in controller design. Master's thesis, University of Groningen, June 2003.

[46] E. I. Verriest. Low sensitivity design and optimal order reduction for the lqg-problem. *24th Midwest Symposium on Circuits and Systems*, pages 365–369, 1981.

[47] E. I. Verriest. Suboptimal lqg-design via balanced realizations. *20th IEEE Conference on Decision and Control*, pages 686–687, 1981.

[48] J. L. Walker. *Dynamical Systems and Evolution Equations*. Plenum Press, New York, 1980.

[49] J. Wloka. *Partial Differential Equations*. Cambridge University Press, Cambridge, 1987.

[50] A. Yousuff and R. E. Skelton. A note on balanced controller reduction. *IEEE Trans. AC*, 29(3):254–257, 1984.

[51] G. Zames. Feedback and optimal sensitivity: model reference transformations, multiplicative seminorms and approximate inverses. *IEEE Trans. Auto. Control*, 26(2):301–320, 1981.

Vita

Katie Allison Evans was born in Ashland, Kentucky on May 22, 1977. She graduated co-valedictorian from Boyd County High School in 1995 and received a full academic scholarship to attend Morehead State University in Morehead, Kentucky. After undergraduate research experiences at Los Alamos National Laboratory, Louisiana State University, and University of Kentucky, she decided her interest was in applied mathematics. Katie graduated summa cum laude with a Bachelor of Science in Mathematics in May 1999. She then began her graduate studies at Virginia Polytechnic Institute and State University in Blacksburg, Virginia. Katie received her Masters of Science in Mathematics in May 2001, and her Doctor of Philosophy in Mathematics in December 2003. Katie has accepted a Research Associate position with the Department of Mechanical Engineering at Oregon State University.